



University of Calabria

**DEPARTMENT OF
ENGINEERING FOR THE ENVIRONMENT AND THE TERRITORY
AND CHEMICAL ENGINEERING**

PH.D. COURSE

SCIENCE AND ENGINEERING OF THE ENVIRONMENT, THE STRUCTURES AND THE ENERGY

**TECHNIQUES AND FACILITIES FOR NEUTRON IRRADIATION
TESTING OF POWER ELECTRONICS DEVICES**

SDD
ING-INF/01
ING-IND/20

Coordinator
Prof. Salvatore CRITELLI

Ph.D. Candidate
Ing. Nicolò Marchese

Supervisors
Prof. Felice Crupi

Prof. Elio Angelo Tomarchio

*To Rino, my PhD supervisor, but much more than this for me.
I will never forget him.*



List of Publications

Cazzaniga C., Bhuva B., Bagatin M., Gerardin S., **Marchese N.** and Frost C. D., "Atmospheric-Like Neutron Attenuation During Accelerated Neutron Testing With Multiple Printed Circuit Boards," in *IEEE Transactions on Nuclear Science*, vol. 65, no. 8, pp. 1830-1834, Aug. 2018; doi: 10.1109/TNS.2018.2825644

Cannuli A., Caccamo M. T., **Marchese N.**, Tomarchio E. A., Pace C. and Magazù S., «Indoor Fast Neutron Generator for Biophysical and Electronic Applications», *Journal of Physics: Conference Series*, vol. 1014, pag. 012001, mag. 2018.

Pace C., Fragomeni L., Parlato A., Solano A., **Marchese N.** and Fiore D., "Low Dose-Rate, High Total Dose Set-Up for Rad-Hard CMOS I/O Circuits Testing", in *Applications in Electronics Pervading Industry, Environment and Society: APPEPIES 2016*, A. De Gloria, A c. di Cham: Springer International Publishing, 2017, pagg. 27–33.

Chillura Martino S., Di Chiara G., Fiore D., **Marchese N.**, Pace C., Parlato A., Tomarchio E. A., "Progettazione di un irradiatore autocontenuto per la calibrazione di dosimetri personali a termoluminescenza", conference proceedings in *AIRP Workshop: Tecniche Speciali e Avanzate di Dosimetria e Radioprotezione, Palermo (IT)*, 2016.

Marchese N., Cannuli A., Caccamo M. T., Pace C., "New Generation Non-Stationary Portable Neutron Generators for Biophysical Applications of Neutron Activation Analysis", *Biochimica et Biophysica Acta (BBA) - General Subjects*, 2016.

Fiore D., Guagliardo S., **Marchese N.**, Parlato A., Tomarchio E. A. G., "Ottimizzazione della protezione di un irradiatore neutronico per test di componenti elettronici", conference proceedings in *XXXVI Congresso Nazionale di Radioprotezione, Matera (IT)*, 28-30/10/2015.

Fiore D., **Marchese N.**, Parlato A., Tomarchio E. A. G., "Le facilities di irraggiamento del DEIM per il testing di componenti rad-hard", *Antipodes s.a.s.*, 2015.

Guagliardo S., **Marchese N.**, Parrinello V., Tomarchio E., "Application of ALARA method in the Periodic Safety Review for a zero-power research nuclear reactor". *Safe Application of Radiation and radionuclides SARA, Final Report on the ALARA Workshop*, 2014.

Consentino G., Laudani M., Privitera G., Parlato A., **Marchese N.**, Tomarchio E., Pace C., Giordano C., Mazzeo M., Hernandez Ambato J.L., "Dangerous Effects Induced on Power MOSFETs by Terrestrial Neutrons - A theoretical study and an empirical approach based on accelerated experimental analysis". *AEIT 2013*.

Contents

Chapter 1 - Power Electronics and Reliability	9
1.1 Power electronics: Definition, History and Mission	9
1.2 Power electronic systems and Power Electronic Devices	11
1.3 Power systems in renewable applications	14
1.4 PV plant reliability.....	15
1.5 Power MOSFETs.....	18
1.6 Electronic Devices Reliability	21
Bibliography	25
Chapter 2 – Neutron effects on power MOSFET devices.....	27
2.1 Cosmic rays	27
2.2 Characteristics of neutron component of terrestrial cosmic rays	30
2.3 Radiation effects on electronic devices.....	33
2.4 SEEs in power MOSFET devices	36
Bibliography	40
Chapter 3 – Standard for accelerated neutron testing	43
3.1 Accelerated tests for power electronic devices	43
3.2 JEP151 – Test Procedure for the Measurement of Terrestrial Cosmic Ray Induced Destructive Effects in Power Semiconductor Devices	45
3.2.1 Beam requirements	46
3.2.2 Test Set Up	48
3.2.3 Test Procedure	50
3.3 JEDEC STANDARD – JESD89A.....	51
3.3.1 Test equipment – ATE hardware	51
3.3.2 Determination of terrestrial neutron flux	52
3.4 MIL-STD-750E - Test Methods for Semiconductor Devices	56
3.4.1 METHOD 1017.1 – Neutron Irradiation	57
3.4.2 METHOD 1080 – SEB and SEGR.....	58
3.4.3 Method 3407.1 – Breakdown Voltage, Drain-To-Source	60
Bibliography	61
Chapter 4 – Investigation on the Single Event Burnout of Power MOSFETs under atmospheric-like neutron spectrum irradiation.....	62
4.1 Test Facility	63
4.2 Test equipment	65
4.3 Devices characterisation procedures.....	69
4.4 SEE threshold evaluation.....	71
4.5 Failure parameters evaluation.....	75
Bibliography	80
Chapter 5 – Neutron irradiation facilities	81
5.1 D-D Neutron Generator for accelerated test on power devices	81
5.2 Design of a quasi-monoenergetic neutron source for accelerated testing on power devices	89
Bibliography	95
Conclusions	97

List of Figures

Figure 1.1: The figure represents the main milestones in power devices evolution.....	10
Figure 1.2: Figure shows a schematic representation of a Power Electronic System in which energy is adequately handled in order to satisfy load characteristics.	12
Figure 1.3: Power electronic devices groups with respect to the terminal number, on the right, and with respect to the carrier type, on the left.	14
Figure 1.4: Figure shows a simplified diagram of a power system for the conversion of renewable sources of power [7].....	15
Figure 1.5: Figures show results of the large residential PV Program in Germany and Japan, presented by type of failure and failure frequency per 100 systems; data underline that the main failure source in PV plants is represented by inverter systems [19].	17
Figure 1.6: The figure illustrates Schematic diagram for (a) n-channel lateral MOSFET and (b) n-channel Power MOSFET [11; 16].	19
Figure 1.7: The figure shows the structure of the parasitic components in a power MOSFET device.	20
Figure 2.1: The figure shows the schematic diagram of a cosmic ray cascade, in which an incident cosmic ray particle interacts with the atoms at the top of the atmosphere producing a cascade of electromagnetic radiation, of muons and nucleons [17].	28
Figure 2.2: In figure are presented the mechanisms of radiation interactions; ionisation (a), in which Coulomb force due to energetic charged particles acts on the electrons surrounding atomic nuclei, and displacement (b), in which a charged particle or a neutron interact with atomic nuclei.	29
Figure 2.3: In figure (a) the comparison of neutron energy spectra in units of lethargy on three different days, July 12 (high flux), September 6 (medium flux) and May 12 (low flux) in 2002, while in figure (b) are showed cosmic-ray neutron energy spectra in units of lethargy at different atmospheric depths (altitudes) [13].	32
Figure 2.4: Figure shows the schematic energy band diagram for MOS structure with the major physical processes generating radiation-induced traps in Si-SiO ₂ interface.	34
Figure 2.5: Figure describes the sequence of processes leading to the failure of the transistor due to the plasma filament generated by the passage of a heavy ion; electrons flow through the filament from the source n ⁺ region to the substrate n ⁺ region, while holes flow out of the plasma filament through the body p-region to the body contact; if the filament is located near the channel of the MOSFET, the voltage drop along the p-region tends to forward-bias the junction between the p-region and the source. This forward bias is highest near the filament, and there it most strongly turns on the parasitic bipolar npn transistor [9].	37
Figure 2.6: Figure describes the schematic mechanism inducing SEGR for an n-channel power MOSFET; ion strikes the device in the neck region below the gate oxide and the electric field, due to the applied positive drain bias, causes the generated holes in the silicon to move toward the interface and the electrons to move toward the drain contact. The holes diffuse toward the p-body at a slower rate than the holes drifting toward the interface resulting in a hole pile-up condition at the interface around the strike area. This hole accumulation effect at the Si-SiO ₂ interface creates a pool of positive charge, which results in a transient field increase across the oxide at the track position. If this transient field increases above a critical value, oxide breakdown occurs and the collected holes discharge through the oxide, heating the structure locally; if the breakdown current lasts long enough, a permanent short-circuit through the oxide results [1].	38
Figure 3.1: The differential flux of cosmic-ray-induced neutrons under reference conditions (sea level, New York City, mid-level solar activity, outdoors); the data points are	

the reference spectrum, the solid curve is the analytic fit to the reference spectrum, and the dashed curve is the model from the previous version of this standard [4].	54
Figure 3.2: Figure shows the SEB/SEGR test circuit (a) and SEB circumvention and monitoring circuit (b) supplied by Method 1080 of MIL-STD-750E [2].	59
Figure 3.3: Figure represents the test circuit configurations for breakdown voltage characterisation suggested by Method 3407.1 of MIL-STD-750E [2].	60
Figure 4.1: Figures shows ChipIr Neutron Irradiation Facility layout (a) and the ChipIr neutron spectrum in units of energy in comparison with the JESD89A atmospheric and LANSCE spectra (b) [1].	63
Figure 4.2: Figure shows a map of the neutron beam measured with a diamond detector [3].	64
Figure 4.3: In figure are presented the block diagram of the experimental apparatus used during SEEs investigation.	66
Figure 4.4: The figure represents the electronic layout of the capacitor board and op amp buffers (on left) and DUTs Board (on right).	67
Figure 4.5: In figure the test equipment, from left, SMU, Beam monitor Board DC Supply and Capacitor Board.	68
Figure 4.6: Figure shows the structure of DUTs Board.	69
Figure 4.7: Figures show the gate-to-source short-circuit configuration used in DUTs characterisation (a) and the corresponding setup (b).	70
Figure 4.8: Figures shows the DUTs board fixed on the sliding holder inside the experimental room (a) and a detail of the laser alignment system (b).	71
Figure 4.9: Figure summarises the SEEs thresholds evaluation in which symbols represent the devices V_{Burnout} while dashed lines represent the mean V_{Burnout} obtained for each type of device.	73
Figure 4.10: In figure is showed the correlation between the V_{Burnout} and the Rated and Measured values of $V_{(\text{BR})\text{DSS}}$ for each type of tested device and relative fit curves that underline the exponential trend.	74
Figure 4.11: Failure parameters trend for a STW20N95K5 power MOSFET.	78
Figure 4.12: Failure parameters trend for a STW15N80K5 power MOSFET.	78
Figure 4.13: Failure parameters trend for a STW18NM60ND power MOSFET.	79
Figure 4.14: Failure parameters trend for a STW19NM50N power MOSFET.	79
Figure 5.1: Figure shows the schematic design of a sealed-tube neutron generator with a Penning ion source.	82
Figure 5.2: In figure the ThermoScientific MP 320 Neutron Generator.	83
Figure 5.3: Figures represent the shielding thicknesses (a), the shielding section view (b) and the shielding whole structure (c); green is the 30% Borated PE, while grey is the Barite Concrete.	86
Figure 5.4: Figures show the D-D neutron spectrum (a) and the D-T neutron spectrum (b); the spectra have been evaluated using tally F4 in MCNP simulation in order to obtain the average neutron spectrum in a little spherical volume.	89
Figure 5.5: Figure shows the experimental setup with Li target and siloxane organic scintillator positioned at 26° with respect to the protons beam line; yellow disk is the beam stopper.	90
Figure 5.6: Figures shows experimental setup with lead bricks placed between the target and the neutron counter.	91
Figure 5.7: Figure represents the MCNP preliminary model of the experimental setup.	92
Figure 5.8: In figure is summarised the neutrons attenuation profile in function of lead thickness for different energy ranges.	93
Figure 5.9: In figure is summarised the neutrons attenuation profile in function of lead thickness for different energy threshold.	94

List of Tables

Table 2.1: Q-Values and energy thresholds for neutrons interactions with silicon isotopes from literature and from Q-value Calculator of National Nuclear Data Centre	39
Table 3.1: Cosmic ray induced neutron differential flux for reference conditions (sea level, New York City, mid-level solar activity, outdoors) [4].....	53
Table 3.2: Relative neutron flux at sea level vs. geomagnetic vertical cutoff rigidity [4].....	55
Table 4.1: Summary of devices characterisation results	70
Table 4.2: Summary of V_{Burnout} Fitting Parameters	74
Table 4.3: Summary of bias conditions for failure rate evaluation procedures	76
Table 4.4: Summary of fitting parameters.....	77
Table 5.1: Removal cross section for some shielding materials.....	84
Table 5.2: Neutron flux attenuation due to the different materials.....	86
Table 5.3: Summary of neutron flux values obtained via Monte Carlo simulation.....	87
Table 5.4: Neutron dose rate values outside the shielding	88
Table 5.5: Summary of neutron attenuation coefficients from MCNP simulations.	94

Abstract

Il percorso dottorale ha avuto fin dal suo inizio il chiaro obiettivo di formare una figura altamente specializzata nell'ambito della ricerca industriale.

Tema centrale del percorso di dottorato è stato quello del test con neutroni di dispositivi elettronici di potenza. Tali dispositivi, oggi largamente impiegati nei sistemi per la generazione, trasporto e trasformazione dell'energia (PV Plants, Wind Farms, Power Systems), rappresentano il fulcro dei moderni sistemi di elettronica di potenza e ne caratterizzano drasticamente l'affidabilità. I dispositivi elettronici di potenza, oltre ad essere soggetti alle normali sollecitazioni operative, sono sottoposti agli stress derivanti dall'ambiente in cui operano. Negli ultimi decenni è divenuto sempre più rilevante l'effetto che i neutroni atmosferici hanno su tali dispositivi (Single Event Effects, SEEs) e quanto tale effetto possa compromettere irrimediabilmente il funzionamento dei dispositivi stessi e l'affidabilità dei sistemi in cui vengono impiegati.

Nell'ottica più ampia dettata dalla stipula del Protocollo di Kyoto (1997), che pone in primo piano la tematica dell'efficienza energetica nei settori più rilevanti nelle economie nazionali, il tema dell'affidabilità dei sistemi di generazione, trasformazione e trasporto dell'energia ricopre un ruolo fondamentale, e ha sostenuto e motivato il lavoro di studio e ricerca portato avanti nel percorso dottorale.

Il triennio ha dunque visto l'avvicinarsi di periodi di studio e approfondimento personale riguardo le tematiche trattate, la partecipazione a corsi, seminari e convegni inerenti il tema dell'attività di ricerca, periodi di attività di progettazione e di sperimentazione, nonché l'attività di promozione dei risultati ottenuti.

Il percorso dottorale può essere sostanzialmente suddiviso in due rami:

- Tecniche di test con neutroni di dispositivi elettronici di potenza,
- Progettazione e caratterizzazione di facility di test con neutroni.

Per quanto concerne le tecniche di test con neutroni, il percorso di studio intrapreso ha consentito l'ampliamento della conoscenza sui modelli di interazione dei neutroni con i dispositivi elettronici di potenza, con particolare attenzione ai dispositivi Power MOSFET, e l'approfondimento delle competenze relative agli standard internazionali per il test con neutroni. Lo studio dei modelli ha garantito una migliore consapevolezza su parametri e fattori che influenzano la risposta dei dispositivi all'irraggiamento neutronico. Lo studio degli standard e la comprensione delle finalità con cui questi vengono concepiti ha invece consentito di fissare gli obiettivi ultimi delle attività sperimentali e dei test sui dispositivi. Le competenze acquisite hanno dunque portato ad una progettazione più cosciente delle attività sperimentali, garantendo l'ottenimento di risultati utili all'avanzamento della ricerca.

Sono state dunque predisposte delle sperimentazioni preliminari su dispositivi Power MOSFET destinati all'impiego in sistemi inverter per la produzione di energia da fonti rinnovabili. Le sperimentazioni sono state svolte presso l'Irradiatore Neutronico a sorgenti $^{241}\text{Am-Be}$ del Dipartimento DEIM dell'Università di Palermo. Dai risultati ottenuti è stato possibile evidenziare alcune caratteristiche salienti del comportamento dei dispositivi sotto irraggiamento neutronico, come, per esempio, l'evidente comportamento a soglia del fenomeno, rispetto alla tensione di alimentazione dei dispositivi. Tale dato è stato alla base della progettazione delle sperimentazioni svolte successivamente. Si è infatti ritenuto opportuno effettuare i test su di un campione statisticamente rilevante di dispositivi elettronici, ed inoltre di effettuare la sperimentazione su dispositivi con caratteristiche diverse al fine di studiare come gli effetti dei neutroni potessero essere correlati ad esse. Sono stati dunque individuati i target dell'attività sperimentale, che sono risultati essere lo studio delle soglie di tensione di alimentazione oltre le quali si verificano i SEEs e lo studio dell'andamento dei tassi di fallimento dei dispositivi per diversi valori della tensione di alimentazione. Fissati gli obiettivi della sperimentazione è stata individuata la facility più idonea allo svolgimento della campagna sperimentale. Nello specifico la struttura più

idonea è risultata essere la facility di irraggiamento con neutroni ChipIr, situata presso il Rutherford Appleton Laboratory (UK). L'attività sperimentale è stata dunque proposta ai responsabili della facility, Dr Christopher Frost e Dr. Carlo Cazzaniga, che hanno dimostrato il loro interesse proponendo un periodo di attività di studio e ricerca di cinque mesi. Acquisite dunque le informazioni relative alla facility è stato possibile predisporre e adeguare la strumentazione al fine di ottimizzare le procedure di test e di ottenere i risultati auspicati.

Le attività presso la facility ChipIr sono state svolte nel periodo da inizio febbraio a fine giugno 2017. Nella prima fase della sperimentazione è stata predisposta la strumentazione di test e adeguata alle condizioni operative della facility. Si è proceduto alla caratterizzazione preliminare dei dispositivi e alla prima sperimentazione con neutroni. Nella prima sperimentazione tre tipologie di dispositivi Power MOSFET sono stati sottoposti ad irraggiamento neutronico per lo studio dell'andamento delle soglie di SEEs. L'elaborazione dei dati ottenuti ha evidenziato quanto ipotizzato in precedenza mostrando l'esistenza di una correlazione diretta tra le caratteristiche del dispositivo e le soglie per l'insorgenza dei SEEs. È stata dunque predisposta una seconda campagna sperimentale su nuovi dispositivi, al fine di consolidare i dati dell'indagine riguardo la natura a soglia del fenomeno. Parallelamente sono stati programmati i test di valutazione dei tassi di guasto dei dispositivi, che hanno permesso di studiare il comportamento sotto irraggiamento dei dispositivi in diverse condizioni operative.

L'attività di progettazione e caratterizzazione di facility di test con neutroni è stata portata avanti parallelamente a quella di test. Relativamente a tale attività, è stato portato avanti uno studio preliminare sulle caratteristiche richieste dagli standard internazionali per le facility destinate al test con neutroni di dispositivi elettronici. Le competenze acquisite attraverso lo studio degli standard sono state affiancate a quelle maturate sui codici di simulazione basati su metodo Monte Carlo (MCNP). Nel corso del primo anno di dottorato è stata intrapresa una collaborazione con il Dipartimento di Fisica dell'Università di Messina. Il tema della collaborazione ha riguardato la progettazione di una schermatura per l'impiego indoor di una sorgente

di neutroni compatta. La sorgente neutronica, basata sulla reazione deuterio-deuterio, è stata acquisita per essere impiegata nell'ambito degli studi sulla biofisica e sulle interazioni dei neutroni con i dispositivi elettronici. La progettazione della schermatura ha avuto come obiettivi principali la possibilità di impiego della sorgente in laboratorio, e quindi un obiettivo primario di tipo radioprotezionistico, e la progettazione di una facility idonea allo svolgimento di attività di test sui dispositivi elettronici. Per la progettazione preliminare sono stati individuati i materiali più idonei alla realizzazione della schermatura ed è stato realizzato un modello 3D della stessa. Valutazioni preliminari sulla capacità schermante sono state effettuate a partire dalla conoscenza delle caratteristiche schermanti dei materiali scelti (Cross Section di Rimozione). Il modello 3D è stato implementato in una simulazione MCNP al fine di verificare le valutazioni preliminari. Il progetto della schermatura è stato sottoposto alla valutazione dell'esperto qualificato dell'Università di Messina, che ne dovrà valutare l'idoneità ai requisiti radioprotezionistici, prima di procedere al commissioning.

Nell'ambito della progettazione di facility per il test con neutroni è stato presentato una proposta per la realizzazione di una sorgente neutronica basata sull'interazione ${}^7\text{Li}(p,n){}^7\text{Be}$. Sorgenti di questo tipo, definite "quasi-monoenergetiche" possono essere impiegate per il test di dispositivi elettronici, come indicato dagli standard. La proposta è stata presentata nel contesto della Call for Experimental Proposals with the Tandem accelerator 2016, dei Laboratori Nazionali del Sud di Catania. L'esperimento, approvato dal comitato scientifico dei LNS, è stato svolto nel marzo 2017, in collaborazione con il Dipartimento di Fisica dell'Università di Napoli "Federico II". L'esperimento, denominato NSPP, ha visto l'utilizzo di un fascio di protoni per l'irraggiamento di un target di Litio. La produzione di neutroni è stata verificata con misure di attenuazione effettuate tramite un neutron counter. È stato parallelamente sviluppato un modello MCNP necessario ad effettuare valutazioni preliminari per il prosieguo dell'esperimento. Lo scorso 31 ottobre è stata presentata la proposta di proseguimento dell'esperimento NSPP che ha come scopo quello di caratterizzare la sorgente neutronica ottenuta nella prima fase

dell'esperimento. Al fine di conseguire tale obiettivo, sono stati coinvolti i gruppi di ricerca dell'Università di Palermo e della facility ChipIr dei Rutherford Appleton Laboratory (UK).

Il lavoro di tesi mostra i risultati ottenuti durante la campagna sperimentale e descrive le attività di progettazione svolte. Inoltre, riassume il percorso di formazione e crescita individuando e delineando le competenze acquisite e sviluppate nel corso del triennio nonché dimostrando il completamento del percorso prefissato di formazione di una figura altamente specializzata nell'ambito di ricerca degli effetti delle radiazioni sui dispositivi e sistemi elettronici.

Tale figura professionale, altamente competitiva nel panorama della ricerca industriale, rispecchia i requisiti che nel panorama internazionale sono attribuiti al ruolo del Radiation Effects Engineer.

Introduction

Nowadays, power electronic devices are widely used in systems for the energy generation, transport and transformation (PV Plants, Wind Farms, Power Systems). They are the fulcrum of modern power electronics systems and they drastically characterise their reliability. The power electronic devices, in addition to being subject to normal operational stresses, are subjected to the stresses deriving from the environment in which they operate. In recent decades the effects that atmospheric neutrons have on such devices (Single Event Effects, SEEs) has become increasingly relevant, but even how this effects can irremediably compromise the functioning of the devices and the reliability of the systems in which they are used.

In the perspective dictated by the signature of the Kyoto Protocol (1997), which highlights the question of energy efficiency in the most relevant sectors in national economies, the issue of reliability of the systems of energy generation, transformation and transport plays a fundamental role, and it has supported and motivated research carried out during the PhD course.

The doctoral path can be substantially divided into two branches:

- Neutron testing techniques of electronic power devices,
- Design and characterisation of neutrons testing facilities.

The knowledge on the models of neutron interaction with the electronic power devices, with particular attention to the Power MOSFET devices, has been enhanced, ensuring a better awareness of parameters and factors that influence the response of the devices to neutron irradiation.

Simultaneously a deep study of the standards for neutron testing has been developed in order to better define the goals of experimental activities.

The acquired skills have therefore led to a more conscious design of the experimental activities, ensuring the obtaining of results useful for the progress of the comprehension of these phenomena.

Preliminary experiments have been carried out on Power MOSFETs devices used in inverter systems for the production of energy from renewable sources. The experiments have been carried out with the ^{241}Am -Be Neutron Irradiator at the DEIM Department of the University of Palermo. Obtained results highlighted some salient characteristics of the devices behaviour under neutron irradiation, such as, for example, the threshold behaviour of the phenomenon, with respect to the supply voltage of the devices. This data has been the basis for the design of the experiments. Indeed, tests on a significant sample of electronic devices has been planned. Furthermore, it was planned to test devices with different characteristics in order to study how the effects of neutrons could be related to them. Therefore, the targets of the experimental activities have been the study of the voltage thresholds beyond which the SEEs occur and the study of the trend of the failure rates of the devices for different values of the supply voltage. Once the objectives of the experimentation have been set, the most suitable facility for the experimental campaign has been identified. Specifically, the most suitable structure has resulted to be the ChipIr neutron irradiation facility, located at the Rutherford Appleton Laboratory (UK).

The activities at the ChipIr facility has been carried out in the period from the beginning of February to the end of June 2017. In the first phase of the experimentation, the test equipment has been adapted to the operating conditions of the facility.

In the first experimentation three types of Power MOSFET devices were subjected to neutron irradiation for the study of the trends of SEEs thresholds. The obtained data highlighted the existence of a direct correlation between the characteristics of the device and the thresholds for SEEs. Therefore, a second experimental campaign on new devices has been planned.

At the same time, an experimental campaign for the evaluation of the failure rates of the devices has been programmed with the aim to study the devices behaviour under neutron irradiation in different bias condition.

The design and characterisation of neutron testing facilities has been carried out in parallel with testing experimental activities. With regard to this activity, a preliminary study has been carried out on the characteristics required by international standards for the neutron testing facilities neutrons.

In collaboration with the Department of Physics of the University of Messina, the design of a shielding for the indoor use of a compact neutron source has been developed. The neutron source, based on the deuterium-deuterium reaction, has been acquired to be used in the field of biophysics and neutron interactions with electronic devices.

For the preliminary design, the most suitable materials for the shielding have been identified and a 3D model of the shielding has been developed. Preliminary evaluations on shielding capacity have been carried out starting from the knowledge of shielding characteristics of the chosen materials (Cross Section of Removal). The 3D model has been simulated with MCNP in order to verify the preliminary shielding design.

Then, the development of neutron source based on the interaction ${}^7\text{Li} (p, n) {}^7\text{Be}$ has been approached. Sources of this type, called "quasi-monoenergetic" can be used for testing electronic devices, as indicated by the standards. The experiment, has been carried out in March 2017, in collaboration with the Physics Department of the University of Naples "Federico II". The experiment has been performed with the Tandem ion accelerator at the INFN-LNS facility in Catania (IT). A MCNP model was developed to perform preliminary evaluations for the continuation of the experiment. A second phase of the experiment has been forecasted in order to characterise the neutron source obtained in the first phase of the experiment.

The thesis shows the results obtained during the experimental campaign and describes the designing activities carried out.

Chapter 1 - Power Electronics and Reliability

1.1 Power electronics: Definition, History and Mission

Several definition of power electronics are supplied by literature:

“Power electronics is the technology associated with the efficient conversion, control and conditioning of electric power by static means from its available input form into the desired electrical output form” [18];

“Power electronics involves the study of electronic circuits intended to control the flow of electrical energy. These circuits handle power flow at levels much higher than the individual device ratings” [10];

“Power electronics refers to the use of semiconductor devices to control and convert electrical power from one form to another one to meet a specific need. In other words, power electronics enables the control of the power flow as well as its form” [12].

Taking into consideration these definitions, it is easy to understand that the first aim of power electronics is to control electric power flows taking into consideration the forms in which electrical energy is generated and the output forms in which it is required.

The evolution of power electronics follows the development of the power devices. The Mercury Arc Rectifier was the first power device developed in 1900, since then several power devices were introduced and used in power control applications. In 1948 Bardeen, Bratain, and Shockley developed the first silicon transistor, that represented the beginning of the era of solid-state electronic devices, possibly the greatest revolution in the history of electrical engineering. In 1958 the first commercial thyristor, introduced by General Electric Company, marked the

beginning of the contemporary power electronics era [3-6; 12]. In 1970's, the bipolar transistor module and the Gate Turn Off (GTO) Thyristor were developed contributing to the evolution of power semiconductor devices. Then the Metal Oxide Semiconductor Field Effect Transistor (MOSFET) represented a new step in the progress of power devices and, at the beginning of the 1990's, the best features of the Metal Oxide Semiconductors (MOS) and bipolar devices have been combined allowing the development of the Insulated Gate Bipolar Transistor (IGBT). In 1996 was introduced into the market the Integrated Gate Commutated Thyristor (IGCT), a hard-driven GTO which is generally used in direct torque and flux controlled (DTC) drives [6; 12].

In the last 10 years the wide bandgap power semiconductor devices such as SiC and GaN have been developed. With respect to silicon, SiC and GaN devices have high breakdown electric field, high electrical conductivity and high thermal conductivity. These features allow higher voltage and power capability, higher switching frequency, lower conduction drop, higher junction temperature, although processing of the materials is difficult [6; 9]. These will find widespread applications in power systems and represent the state of the art of power semiconductor technology.

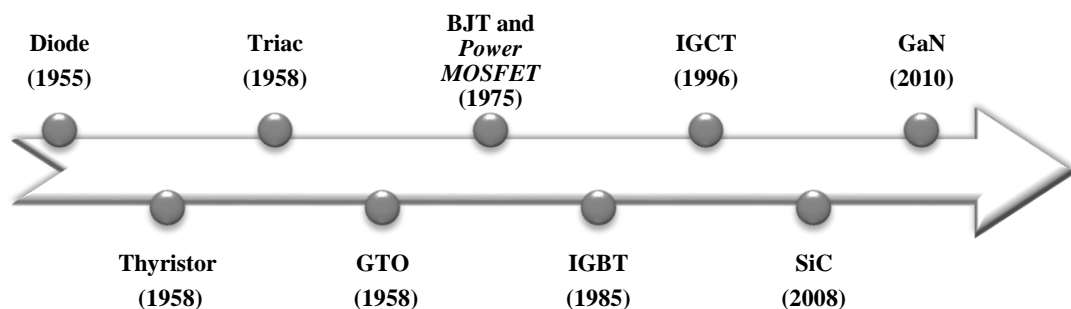


Figure 1.1: The figure represents the main milestones in power devices evolution.

In the last 20 years, power electronics have seen a relevant growth with particular regard to the applications in renewable energy field. A significant incentive to the diffusion of power electronics has come from the drafting of the *Kyoto Protocol*

(December 1997). The first objective of the Protocol regards the enhancement of the energy efficiency with the aim to reduce significantly the greenhouse gas emission and to contrast the climate changes [13]. To this end, the development of power electronics focused its target, that it is well resumed in the following sentence:

“The goal of power electronics is to control the flow of energy from an electrical source to an electrical load with high efficiency, high availability, high reliability, small size, light weight, and low cost” [18].

With this ambitious objectives, power electronics has become a multidisciplinary field that encompasses power engineering and electronic engineering, the use of electrical and electronic components and devices, the modern design techniques, the theory of linear and non-linear control and the use of analytical and numerical tools [18].

Therefore, power electronics represents a hot topic in industrial and scientific research and more attention is focused in the development of more efficient, reliable and economic power systems, able to guarantee the achievement of the objectives fixed with the Kyoto Protocol.

1.2 Power electronic systems and Power Electronic Devices

Nowadays power electronics covers even more wide areas in industrial, commercial, residential, transportation, aerospace, military and utility systems [6]. The most recent applications of power electronics can be classified in three categories:

- **Electrical applications**, to design AC and DC regulated power supplies for various electronic equipment and to design distributed power systems,
-

electric heating and lighting control, power factor correction and Static Var Compensation (SVC).

- **Electromechanical applications:** AC and DC machine tools, robotic drives, pumps, textile and paper mills, peripheral drives, rolling mill drives and induction heating.
- **Electrochemical applications:** chemical processing, electroplating, welding, metal refining, production of chemical gases and fluorescent lamp ballasts [12].

Power electronics also shows a continuous expansion due to the development of cheaper, more reliable and modular in size power electronic systems [6].

The elementary cell of a power electronic system substantially consists of an energy source, an electrical load, a power electronic circuit and a control circuit. Power electronic circuit is an assembly of power electronic devices designed to be able to receipt the energy coming from the source and to adapt this energy to the form (voltage and current) required by the load, and it is commonly called power electronic converter. The control circuit acquires information from the source and from the load and elaborates a control function that modifies the working point of the power electronic circuit with the aim to manage efficiently the energy flow between the source and the load [10].

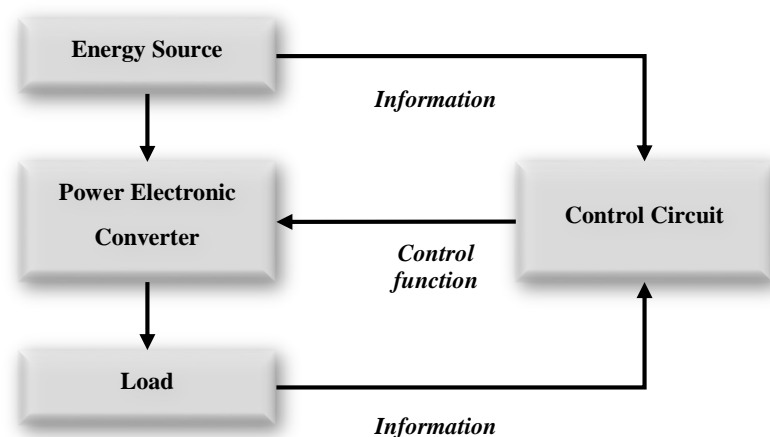


Figure 1.2: Figure shows a schematic representation of a Power Electronic System in which energy is adequately handled in order to satisfy load characteristics.

Taking into consideration the input and output power form, power electronic converter used in power systems can be classified in:

- AC to DC converters (phase-controlled rectifiers): to convert constant AC voltage to variable DC output voltage;
- DC to AC converters (Inverters): An inverter converts fixed DC voltage to a variable AC voltage. The output may be a variable voltage and variable frequency;
- AC to AC converters: to convert fixed AC input voltage into variable AC output voltage;
- DC to DC converters: to converts input DC to variable magnitude DC [12].

A power electronic converter is made up of some power semiconductor devices, as switches, storage elements, and magnetic transformers, selected with respect to their features and to the system characteristics [10]. The characteristics of power semiconductor devices allow to shape the input power, with its form, to output power in the desired form [12].

Therefore, power devices represent the inner part of the power electronic systems and the heart of the power electronics. For that reason, the evolution of power electronic systems has historically followed the evolution of power electronic devices. These have followed the evolution of semiconductor electronics. Silicon is the most widely used semiconductor material for power electronic devices, even if new semiconductor materials, as for example SiC and GaN, have been recently introduced [10; 12].

The research on semiconductor electronics has worked insistently to improve semiconductor processing, devices fabrication, and packaging, to develop the modern high-density, high-performance, high-reliability, and high yield electronic devices [3].

These improvements in semiconductor technology for power electronic devices has been guided by their two more desirable features: the time the devices use to turn-on and turn-off (Switching Speed) and their power handling capability (related to

voltage and current capabilities). As a consequence, several power electronic devices have been designed and developed with different geometries and characteristics in order to be able to operate at high off state voltages and to carry high currents in the on state with the highest switching speed [10; 12].

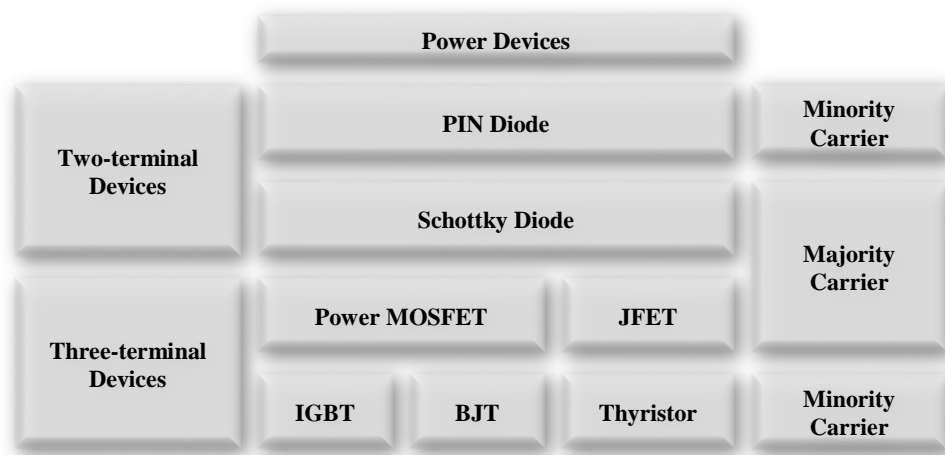


Figure 1.3: Power electronic devices groups with respect to the terminal number, on the right, and with respect to the carrier type, on the left.

1.3 Power systems in renewable applications

Several studies underline that a relevant portion of energy demand can be satisfy by promoting environmentally clean renewable energy sources and by developing adequate storage and transmission capabilities [6].

Wind and photovoltaic (PV) are particularly important in this scenario and they are strongly dependent on power electronics. Indeed, power converters are largely employed in renewable power plant to convert the starting form of energy in the form in which it is usable. In a wind generation system, a variable speed wind turbine couples to the shaft of an AC machine generates a variable voltage variable frequency power. This variable power needs to be converted to constant voltage and constant frequency through a converter system. In a PV system, PV devices as for example crystalline or amorphous Si, convert sunlight into electricity. The PV

array is connected to DC-DC converter where the DC voltage is increased. Finally, DC is converted to AC by inverter. Both in wind and PV plants, generated power can finally feed a grid or can be used for autonomous load. Furthermore, wind and PV often need back-up power source or bulk energy storage in order to compensate the availability of the energy sources [6].

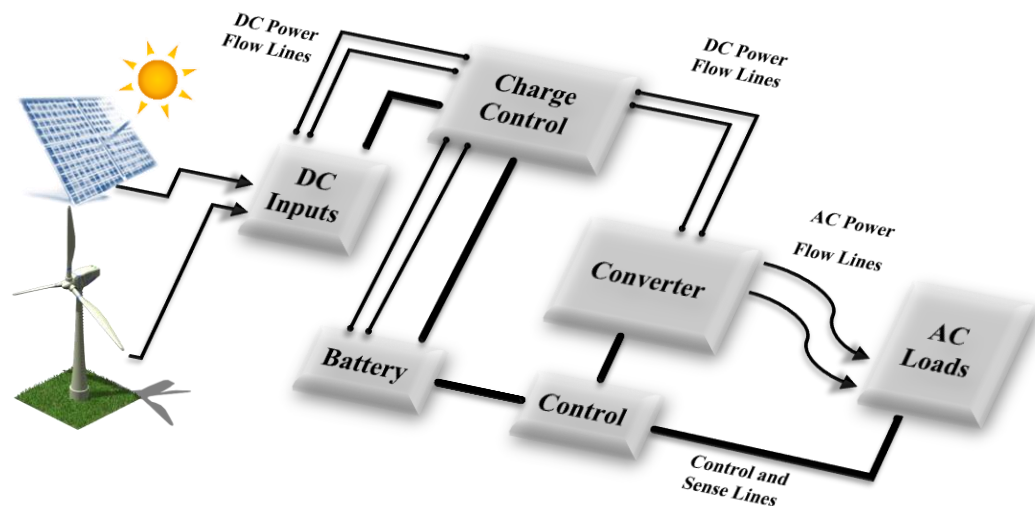


Figure 1.4: Figure shows a simplified diagram of a power system for the conversion of renewable sources of power [7].

As underlined before, renewable energy plants result strongly dependent on the power converters. These represent part of the so called Balance-of-System components and, as will be discussed, are fundamental for the reliability of the plant.

1.4 PV plant reliability

In a PV plant the components can be divided substantially in PV modules and BOS components. The BOS components include the array structure, trackers, connectors, AC and DC wiring, overcurrent protections, disconnects, interconnects, inverters, charge controllers, MPPT controllers, energy storage devices, and system controllers. Many studies, carried out on the PV plant, underline how several agents

operate on the reduction of their reliability and show how environmental and operational stresses, such as humidity, temperature, and high-voltage bias, and process limitations, such as solder bond integrity, affect PV modules and BOS components. However, these studies show that PV modules remain the more reliable component in a PV plant, while the BOS components represent a strong limitation in the plant reliability. Among the BOS components, the studies have shown that the power converters, mainly the inverters, are the most critical components in a PV plant. Data collected by the Florida Solar Energy Centre on 103 PV plants confirm that on the total of reliability events, the 65% are due to the inverters [15]. The National Renewable Energy Laboratory review on PV plant shows how the inverters need to be replaced every 5-10 years, with consequent investments for new inverters 3-5 times during the plant lifetime [20]. Moreover, information collected during the large residential PV Programs in Germany and Japan confirm that the inverters are far the most troublesome components, and that they account for about 66% of reported troubles [19].

Furthermore, in other data collected on a consistent number of PV plants in Botswana, the inverters failures represent the 77% of the total failure events, underlining the sensitivity of these components to the operating conditions. Deeper investigations on the inverters reliability have shown that the most vulnerable inverter components are the power MOSFETs, widely employed as switching devices. Indeed, Power MOSFETs operate in the inverters as switches at very high frequencies (up to kHz) and their reliability is sensitive to poor requirement definition with consequent product retrofits, immature manufacturing processes, product planning and quality control, and outdated designs that do not take into consideration the newest architectures, control schemes, packaging methods, and technologies. Furthermore, thermal management and heat extraction mechanisms for the semiconductor switches are major issues for the reliability of inverters, because switching components are highly sensitive to temperature [15].

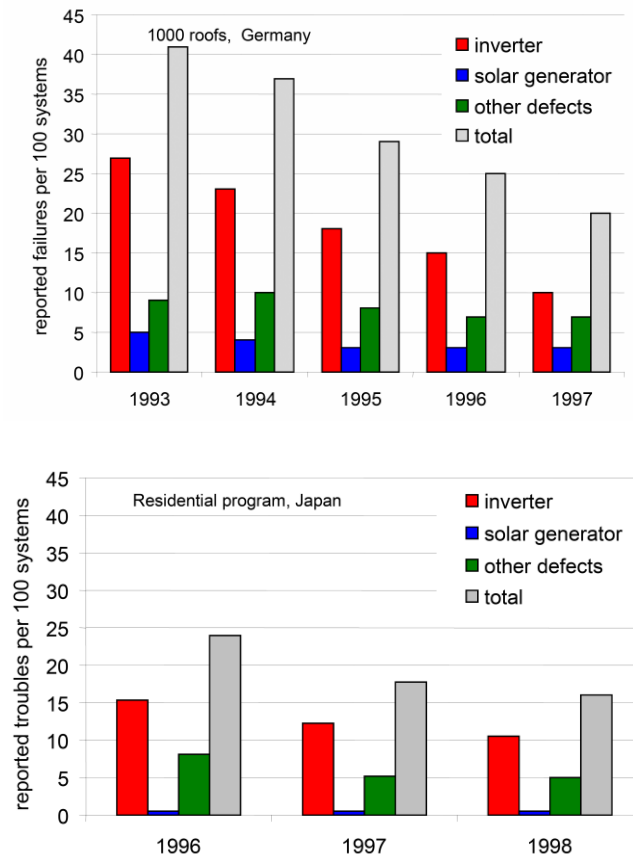


Figure 1.5: Figures show results of the large residential PV Program in Germany and Japan, presented by type of failure and failure frequency per 100 systems; data underline that the main failure source in PV plants is represented by inverter systems [19].

Therefore, the evolution of the inverters has been focused on the reliability enhancement and several strategies have been evaluated taking into consideration also economical aspects. Thank to these strategies inverters failures have diminished considerably thanks to a more mature technology and to new products less sensitive to the mentioned issues [15].

With regard to power MOSFET devices, they have been developed with the aim to reduce their impact on the inverters reliability and, consequently, their effect on the reliability of the entire PV plant. Therefore, improvement of devices reliability represents the primary target to reach in order to design even more reliable converter systems.

1.5 Power MOSFETs

The power MOSFET structure is based on the original field-effect transistor [8] but it has gone through a continuous process of development until to reach the current design. Modern power MOSFETs consist in a vertical channel structure that allows to increase the devices power rating. In the vertical structure source and drain terminals are located on the opposite side of the silicon wafer and different commercial MOSFETs exist with several type of vertical structures (V-MOSFET, D-MOSFET, U-MOSFET, etc.). The gate, located in the same side of the source terminal, allows to pilot the device, managing the channel opening. Indeed, contrary to the BJT, power MOSFETs are voltage-controlled devices that require a small amount of input current to work [10]. In a n-type power MOSFET, when a positive bias greater than the threshold voltage is applied to the gate, the inversion in the silicon surface of the channel region is induced. This generates a conductive channel allowing the current flow between source and drain, and the device is in on-state. For gate voltages of less than the threshold no surface inversion occurs in the channel and the device remains in the off-state. In on-state the current in the power MOSFET device flows at first horizontally along the inverted channel, below the gate oxide, and then vertically between drain and source [16].

The introduction of power MOSFETs allowed to go beyond the limits of the BJTs. As mentioned before, power MOSFETs are voltage-controlled devices while the BJTs are current-controlled bipolar devices that require base current to work. Moreover, MOSFETs show the highest switching speed, >MHz, because only majority carriers contribute to the current flow, reducing significantly the time necessary to turn-on and turn-off the devices. The MOSFET devices have a higher on-state resistor and its parameters are less sensitive to the junction temperature with respect to BJT devices. Furthermore, MOSFET devices do not suffer from second breakdown voltages and sharing current in parallel devices is possible [1; 10; 16].

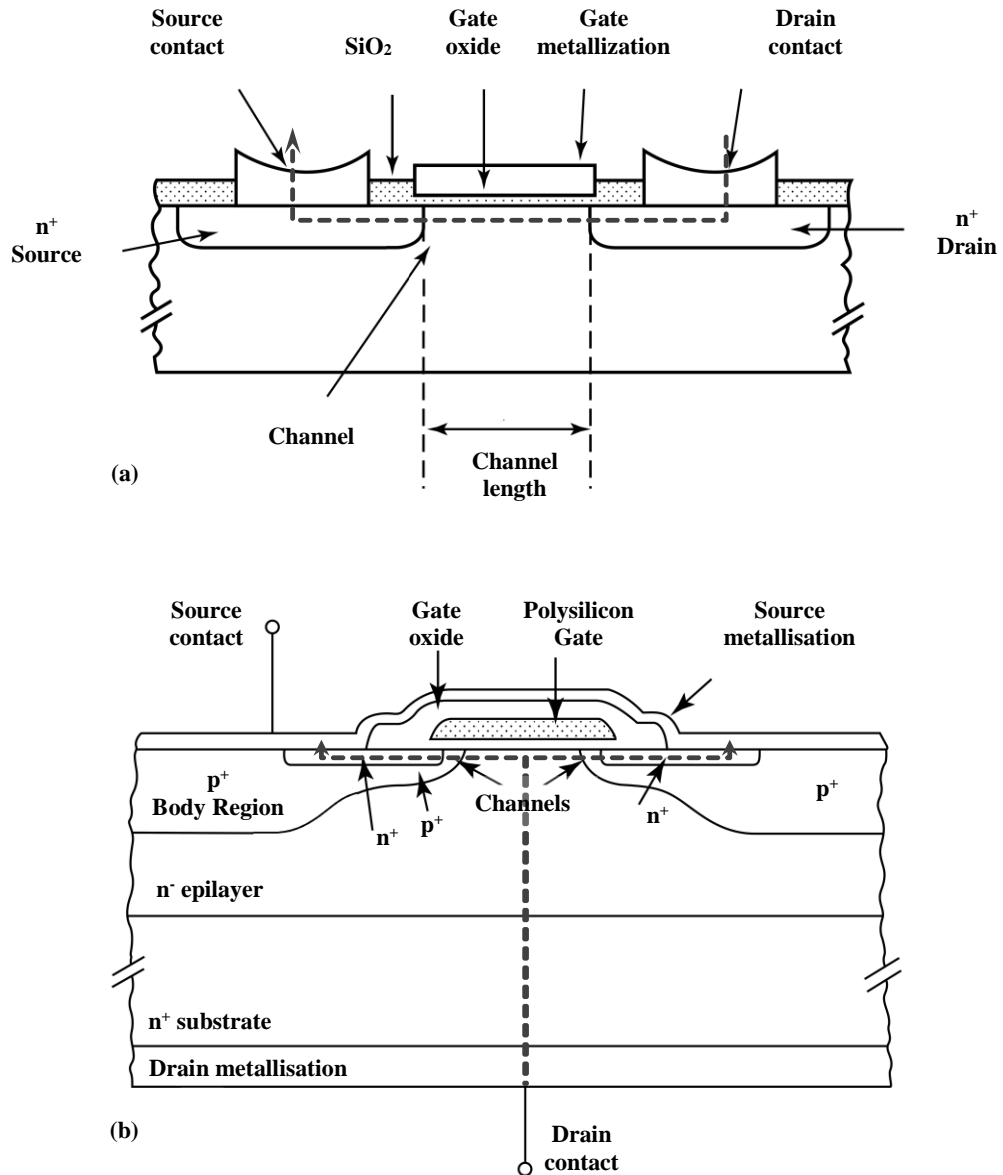


Figure 1.6: The figure illustrates Schematic diagram for (a) n-channel lateral MOSFET and (b) n-channel Power MOSFET [11; 16].

Despite the qualities of power MOSFET devices, their structure is intrinsically affected by parasitic components due to the presence of several n-p junctions inside the device. These components modify the normally behaviour of the power MOSFET and they can cause the premature device damaging.

The vertical structure of a power MOSFET shows a N+N-PN+ parasitic bipolar transistor, in which the collector, emitter and base are formed by the drain, source and P channel [14]. The BJT is the most dangerous parasitic component in a power MOSFET and it can induce unwanted device turn-on and premature breakdown, commonly called “second breakdown” [16].

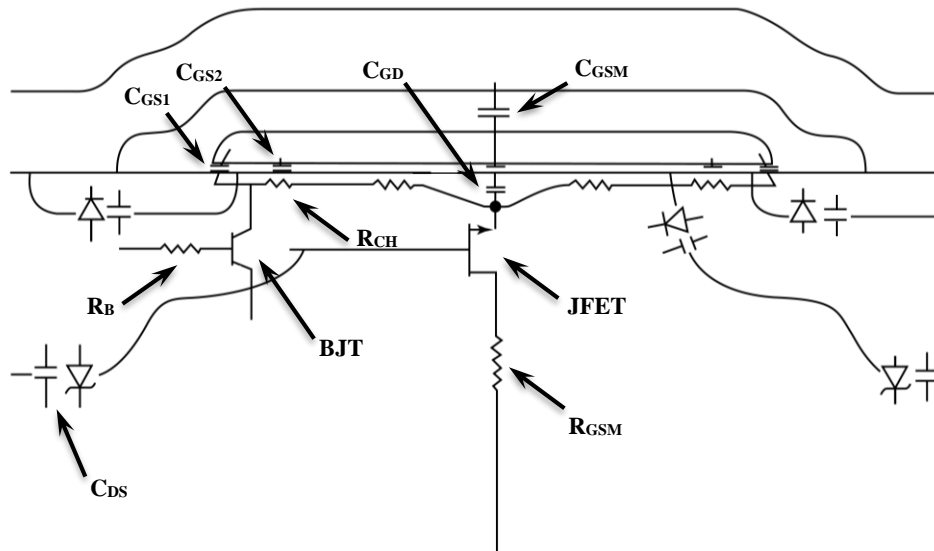


Figure 1.7: The figure shows the structure of the parasitic components in a power MOSFET device.

The second breakdown occurs when the MOSFET is in the off-state and an increasing in drain-source voltage is applied [10]. Indeed, the capacitance that appears between the base of the BJT and the drain of the MOSFET gives rise to a current which flows through the resistance R_B when a voltage ramp appears across the drain-source terminals. When the voltage developed across R_B reaches the threshold of about 0.7 V, the base-emitter junction is biased and the parasitic BJT is turned on. Under these conditions the breakdown voltage of the MOSFET will be limited to the breakdown voltage of the BJT. When the drain voltage is greater than the open-base breakdown voltage, then the MOSFET will enter avalanche and may be destroyed if the current is not limited externally [16].

In order to avoid destructive failure and to guarantee the devices lifetime is defined a Safe Operating Area (SOA). SOA provides the current and the voltage limits to

safety handle the device, preventing damages and assuring a longer lifetime both to the device and to the system in which it operates [10]. The limits traced by the SOA are due to the intrinsic device characteristics and technological aspects like current density dispersion between cells, packaging, and maximum temperature of various elements [14].

However, external stresses can reduce the device SOA limits, enhancing the probability of damages or destructive effects on the devices. Therefore, it is necessary to investigate the dominant failure mechanisms, to perform tests aimed to reproduce these mechanisms, to produce, if possible, a mathematical model that represents the phenomenon and then supply the obtained information as reliability device data. This process represents a starting point to develop new and more resistant devices and to design systems intrinsically able to reduce the effects due to external stresses.

1.6 Electronic Devices Reliability

Reliability is defined as the ability of an item to perform a required function under stated conditions for a stated period of time. In this definition the stated conditions include the total physical environment, while the stated period represents the time interval in which is requested to the item to perform its function [2; 17].

Although this definition represents a concept rich in information, the reliability is a function of the time, and more specifically, it is a function of the defined operation time of the respective item, therefore it has different values for each time interval. Thus, it is necessary to define other sizes not dependent only on the operation time [2].

The reliability can be mathematically denoted as the probability of a successful event and represented by the function $R(t)$, defined as

$$R(t) = 1 - \int_0^t f(t)dt \quad (1.1)$$

Where $f(t)$ is the failure density function. Therefore, $R(t)$ is the distribution function for the probability of success, thus the probability that a device will not fail until the time moment t .

In reliability studies other expressions that is always used are the Mean Time To Failure (MTTF), used for non-repairable systems, and the Mean Time Between Failures (MTBF), used for repairable system.

MTTF can be expressed mathematically as

$$MTTF = \int_0^{\infty} tf(t)dt \quad (1.2)$$

Furthermore, it is possible to define the instantaneous failure rate as

$$Z(t) = \frac{f(t)}{R(t)} \quad (1.3)$$

One of the most used distributions is the negative exponential distribution that allows to obtain the following reliability formulas:

$$R(t) = e^{-\lambda t} \quad (1.4)$$

$$f(t) = \lambda e^{-\lambda t} \quad (1.5)$$

$$Z(t) = \frac{f(t)}{R(t)} = \lambda \quad (1.6)$$

where λ is the failure rate and it results to be constant for this distribution. Therefore, MTTF can be evaluated for negative exponential distribution by substitution for $f(t)$:

$$MTTF = \int_0^{\infty} t\lambda e^{-\lambda t} dt = \lambda \int_0^{\infty} te^{-\lambda t} dt = \frac{1}{\lambda} \quad (1.7)$$

As a first approximation, it is very often assumed that the electronic components follow an exponential distribution [2].

MTTF can be also expressed in term of FITs (Failure In Time). FIT is the evaluation of failures considering 10^9 hours of continuous operative conditions

$$MTTF = \frac{10^9}{FIT} \quad (1.8)$$

$$FIT = \frac{10^9 \cdot N_f}{\sum t_f} \quad (1.9)$$

where N_f is the number of observed failures and t_f is the time to failure for each device in hours.

In the reliability estimation of electronic systems two methods are generally used to make reliability estimates, expressed as failure rates: *Parts count method* and *Parts stress analysis*.

In Parts counts method, the needed information regard the generic part types and quantities, the part quality levels, and the equipment environment; the expression for system failure rate for a given environment using this method is:

$$\lambda = \sum_{i=1}^n N_i (\lambda_G \pi_Q)_i \quad (1.10)$$

where λ is the total system failure rate (expressed in failures/10h), λ_G is the generic failure rate for the i th generic part (failures/ 10^6 h), π_Q is the quality factor for the i th generic part, N_i is the quantity of i th generic part and n is the number of different generic part categories. The value of the failure rate computed with this equation is valid if the entire system operates in the same environment. Otherwise, it is necessary to evaluate a failure rate for each portion of the system operating in a different environment [2; 21].

In Parts stress analysis method, the part failure models vary with different part types. However, their general form is:

$$\lambda_i = \lambda_B (\pi_A \pi_E \pi_Q \dots \pi_N) \quad (1.11)$$

Where λ_b is the base failure, π_A is the application adjustment factor and it depends on the application of the part and it accounts secondary stress and application factors, π_E is environmental adjustment factor and it takes into consideration the influence of environments, π_Q accounts for the degree of manufacturing control with which the part was fabricated and tested, π_N represents the addition adjustment factors [2; 21].

It should be noted that the prediction of the reliability of electronic equipment shows practical limitations mainly depending on data collection and technique complexity. Sufficient data must be generated to report statistically valid reliability information. Often data collection results slowly with respect the technology evolution, therefore, it is not possible to obtain valid data. Furthermore, data can be produced by different testing groups following different procedures and in different test conditions, making difficult the data correlation. In addition, data collected in particular environmental conditions may not be applied for equipment operating in other environments. A large number of other variants can affect the reliability data and, as a consequence, the derivation of reliability parameters is empirically difficult and the possibility to obtain valid confidence values is precluded. Thus, the biggest limitation on reliability evaluation is the capacity to obtain data valid for new applications [2; 21].

For electronic devices, MILITARY HANDBOOK 217 provides a basis for reliability prediction and it includes the descriptions of the two methods for the failure rates evaluation and also the failure rate models for several electronic devices.

However, as the handbook represents a good tool, it is necessary to handle carefully the models supplied taking into consideration all the limitations in the development of the failure rate models due to the difficulties mentioned before.

Furthermore, the handbook does not take into account all the possible stresses deriving from the environment, as for example none of the models in the handbook

allows to predict nuclear survivability or effects of ionising radiation on electronic devices and systems [21].

These condition make really difficult to approach the reliability prediction procedure, and often it is necessary to perform test campaigns with the aim to obtain data necessary to the evaluation of reliability parameters.

Bibliography

- [1] E. Acha, V. G. Agelidis, O. Anaya-Lara and T. J. E. Miller, *Power electronic control in electrical systems*. Oxford: Newnes, 2002.
 - [2] T. Bajenescu and M. Bazu, *Reliability of Electronic Component*. Berlin, Germany: Springer-Verlag, 1999.
 - [3] B. K. Bose, «Evaluation of modern power semiconductor devices and future trends of converters», *IEEE Transactions on Industry Applications*, vol. 28, n. 2, pagg. 403–413, 1992.
 - [4] B. K. Bose, «Power electronics-a technology review», *Proceedings of the IEEE*, vol. 80, n. 8, pagg. 1303–1334, 1992.
 - [5] B. K. Bose, «Energy, environment, and advances in power electronics», *IEEE Transactions on Power Electronics*, vol. 15, n. 4, pagg. 688–701, 2000.
 - [6] B. K. Bose, «Power Electronics, Smart Grid, and Renewable Energy Systems», *Proceedings of the IEEE*, vol. 105, n. 11, pagg. 2011–2018, nov. 2017.
 - [7] W. Bower, «Inverters—critical photovoltaic balance-of-system components: status, issues, and new-millennium opportunities», *Prog. Photovolt: Res. Appl.*, vol. 8, pagg. 113–126, 2000.
 - [8] J.-P. Colinge e C. A. Colinge, *Physics of semiconductor devices*. Springer Science & Business Media, 2005.
 - [9] J. G. Kassakian e T. M. Jahns, «Evolving and Emerging Applications of Power Electronics in Systems», *IEEE Journal of Emerging and Selected Topics in Power Electronics*, vol. 1, n. 2, pagg. 47–58, giu. 2013.
 - [10] P. Krein, «Chapter 1: Introduction» of *Power Electronics Handbook*, Academic Press, San Diego, USA, pagg. 1–12 , 2001.
 - [11] R. Locher, «Introduction to power MOSFETs and their applications», *Fairchild Semiconductor, Application Note*, vol. 558, 1998.
-

- [12] S. A. Mohammed, M. Abdel-Moamen, e B. Hasanin, «A review of the state-of-the-art of power electronics for power system applications», *Quest Journal of Electronics and Communication Engineering Research (JECER)*, vol. 1, n. 1, pagg. 43–52, 2013.
 - [13] U. Nations, «Kyoto protocol to the united nations framework convention on climate change», 1998.
 - [14] R. Perret, A c. di, *Power electronics semiconductor devices*. London: ISTE, 2009.
 - [15] G. Petrone, G. Spagnuolo, R. Teodorescu, M. Veerachary and M. Vitelli, "Reliability Issues in Photovoltaic Power Processing Systems," in *IEEE Transactions on Industrial Electronics*, vol. 55, no. 7, pp. 2569-2580, July 2008.
 - [16] T. L. Skvarenina, A c. di, *The power electronics handbook*. Boca Raton, Fla: CRC Press, 2002.
 - [17] H. Wang, M. Liserre, e F. Blaabjerg, «Toward Reliable Power Electronics: Challenges, Design Tools, and Opportunities», *IEEE Industrial Electronics Magazine*, vol. 7, n. 2, pagg. 17–26, giu. 2013.
 - [18] T. G. Wilson, «The evolution of power electronics», *IEEE Transactions on Power electronics*, vol. 15, n. 3, pagg. 439–446, 2000.
 - [19] «Reliability Study of Grid Connected PV Systems – Field Experience and Recommended Design Practice», Fraunhofer Institut für Solare Energiesysteme, Freiburg, Germany, Report IEA-PVPS T7-08, 2002.
 - [20] «A review of PV inverter technology cost and performance projections», Navigant Consulting Inc., Burlington, MA, NREL Subcontract Rep. NREL/SR-620-38771, Jan 2006.
 - [21] MIL-HDBK-217F - «Reliability prediction of electronic equipment», 1991.
-

Chapter 2 – Neutron effects on power MOSFET devices

2.1 Cosmic rays

Since the beginning of the twentieth century the term cosmic rays has been used to indicate the energetic particles that interfered with studies of radioactive materials. Nowadays cosmic rays' characteristics are well known and it is possible to classify them in four categories: *Primary cosmic rays*, *Solar cosmic rays*, *Secondary cosmic rays* and *Terrestrial cosmic rays*.

Primary cosmic rays are galactic particles which enter the solar system and they may hit the earth. They are believed to be produced and accelerated as a consequence of stellar flares, supernova explosions, pulsars, and the explosions of galactic nuclei. Cosmic rays in our galaxy have a mean lifetime of about 200 million years and they are composed mainly of protons (92%), alpha particles (6%) and heavier atomic nuclei. The galactic flux of primary cosmic rays is about $10^5 \text{ m}^{-2}\text{s}^{-1}$, while the final nucleon flux at sea level is about $360 \text{ m}^{-2}\text{s}^{-1}$, due to the little fraction of the galactic cosmic rays that has enough energy to penetrate the earth's atmosphere and due to the interactions they undergo with atmospheric atoms before to reach the ground [23].

Solar cosmic rays are the particles that constitute the solar wind, they are originated in the sun and are sometimes included in the primary cosmic rays. The flux of solar cosmic rays follows the eleven-year sun cycles and solar particles have much lower energy than galactic particles. During the period of quiet sun, in solar wind are not present particles enough energetic to penetrate to sea level on earth. During the active sun period, the number of solar particles hitting the outer atmosphere increases and some of them have sufficient energy to reach terrestrial altitudes. During periods of a large solar flare, the total intensity of cosmic rays at the earth's surface might double. However, the active sun with its large solar wind creates an

additional magnetic field about the earth able to increase the shielding against intra-galactic cosmic rays, reducing sea-level cosmic rays of about 30% during this period [23].

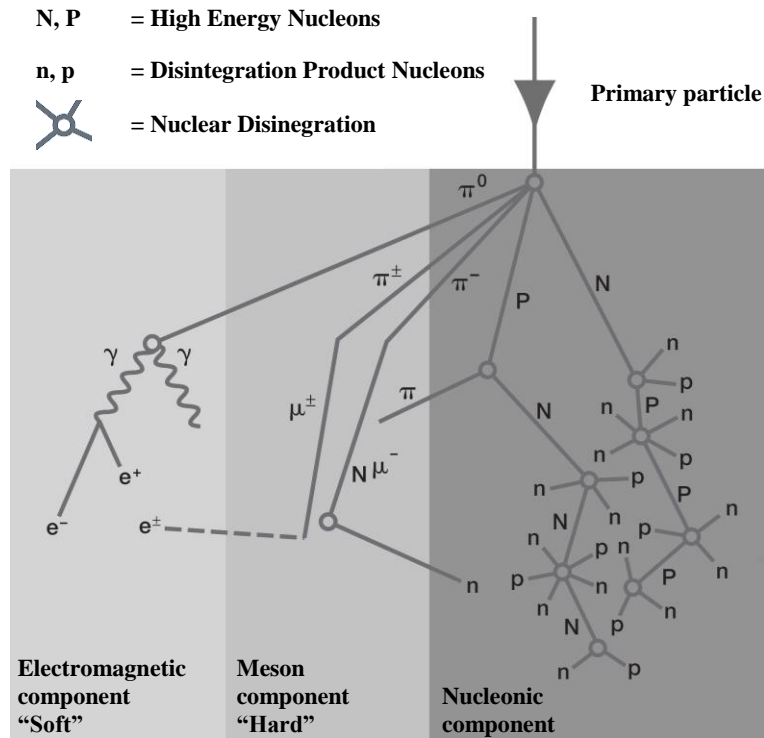


Figure 2.1: The figure shows the schematic diagram of a cosmic ray cascade, in which an incident cosmic ray particle interacts with the atoms at the top of the atmosphere producing a cascade of electromagnetic radiation, of muons and nucleons [17].

Secondary cosmic rays are the particles produced in the earth's atmosphere when primary cosmic rays hit atmospheric atoms creating a "shower" of secondary particles [23].

Indeed, when primary and solar high energetic cosmic rays enter the atmosphere they undergo nuclear spallation reactions with nuclei in the atmosphere. Spallation reactions produce a large number of light particles including neutrinos, photons, electrons, muons, pions, protons and neutrons. The secondary particles have longer ranges in the atmosphere with respect to the primary particles and, therefore, they can generate additional cascades of spallation reactions and, then, they can reach the earth surface [10].

Terrestrial cosmic rays are the particles which finally hit earth and they are composed for fewer than 1% of primary particles and mostly of third-to-seventh generation of cascade particles. Only the most penetrating particles, such as muons and neutrons, can reach sea level [23].

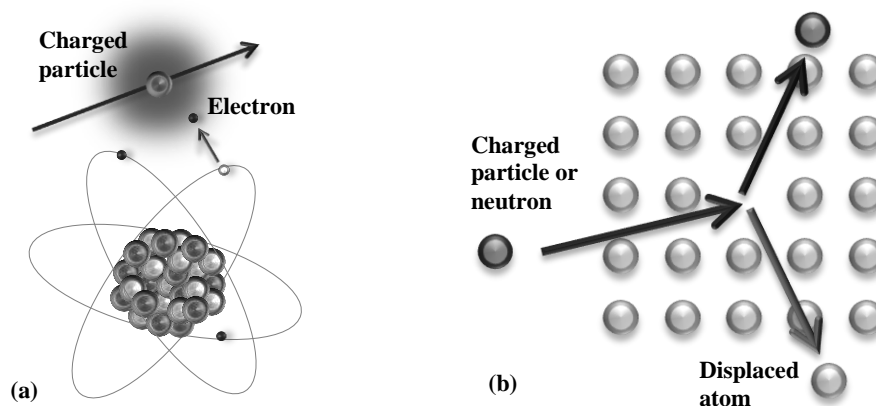


Figure 2.2: In figure are presented the mechanisms of radiation interactions; ionisation (a), in which Coulomb force due to energetic charged particles acts on the electrons surrounding atomic nuclei, and displacement (b), in which a charged particle or a neutron interact with atomic nuclei.

Cosmic rays interact with the atoms of the materials they hit with mechanisms which depend on the particles charge, on their mass, on their energy and on the characteristics of the nuclei the particles hit.

When a high energy charged particle penetrates into solid matter and it passes close to an atom, some electrons are extracted by the Coulomb force of the charged particle and electron-hole pairs are produced. The production of electron-hole pairs causes charge-up of inorganic solid materials, ionisation for gases, radiation decomposition/synthesis/polymerization for organic materials and radiation decomposition for liquid. Instead, when high energy charged particles, neutrons and photons interact through direct interaction with the atomic nucleus, the effect is the displacement of lattice atoms, that causes further defects/vacancies, dislocation loops and interstitials which result in changes in the properties of materials [10].

Therefore, cosmic rays represent a source of damage for the materials they hit and it is necessary to investigate the effects that the interactions could cause. In parallel with the development of the silicon technologies and the diffusion of semiconductor devices in several applications, relevant interest has grown on the effects that high energy cosmic rays have on electronic components.

This interest has stimulated the study on the characteristics of the neutron component of the terrestrial cosmic rays and several models on the damaging mechanisms on electronic devices due to the interactions with high energy particles has been developed.

2.2 Characteristics of neutron component of terrestrial cosmic rays

On the ground level the neutron component of terrestrial cosmic rays, shortly the terrestrial neutron field, shows three main components individuated by the neutron energies.

The first component appears around 100 MeV and it is related to the cascade component of the secondary cosmic rays. From day to day this component can fluctuate significantly (about 30%) and it shows relevant enhancements in correspondence of period of higher solar activity. The second component appears around few MeV and it is related to the evaporation component of secondary cosmic rays. Finally, the third component appears below about 1 eV and it is composed by thermal neutrons (25 meV). This component is generated by the neutron thermalisation through the atmosphere and the backscattering from the earth.

Measurements performed at different altitudes show that the neutron terrestrial spectrum substantially preserves the components individuated in ground measurements. However, in the energy below than 1 MeV, the spectrum becomes softer with increasing atmospheric depth, and the thermal component is present only at sea level. The peak values of the second and, in particular, the third components keep almost constant values of about 7.5×10^{-4} (n cm⁻² s⁻¹ lethargy⁻¹) and about 1.8×10^{-4} (n cm⁻² s⁻¹ lethargy⁻¹), respectively [7; 8; 13].

Further measurements have been performed in order to evaluate the dependency of the terrestrial neutron field intensity on the latitude [7; 8; 10; 13; 23]. Indeed, the geomagnetic field acts as a shielding on primary cosmic rays approaching the atmosphere. The geomagnetic field is stronger near the equator, where the field is nearly parallel to the ground. Here, the primary cosmic rays vertically incident to the magnetic field which have a magnetic rigidity of less than about 15 GV are rejected into space.

The magnetic rigidity that a particle vertically incident on the geomagnetic field needs to reach a point is called geomagnetic vertical cutoff rigidity for that point. In correspondence of the geomagnetic poles, the magnetic field is approximately vertical with respect to the ground and the vertical cutoff approaches zero. Here, the highest flux of primary cosmic rays can reach the atmosphere. Therefore, cosmic-ray neutron levels are highest in polar regions with respect to the equator [7].

As described, the neutron energy spectrum and flux depend on several factors. Altitude, geomagnetic field strength and sun activity can change locally the terrestrial neutron field. Literature supplies several empirical formulas obtained during studies performed on the neutron terrestrial field variability. These formulas allow to obtain the value of the neutron terrestrial field in a fixed point starting from a reference value, and taking into consideration the different factors described before. The reference value for the neutron terrestrial field has been taken as the value that it assumes in New York City [8; 10], at the sea level, during the period of mid-level solar activity.

As it is possible to understand, the intensity of the neutron terrestrial field is strongly variable on the earth surface. This variability changes from place to place the stress conditions in which electronic devices operate. Therefore, in order to study the impact of the neutron terrestrial field on devices and systems, it is necessary to evaluate the effective characteristics of the neutron field in which they will operate. The improved knowledge about the physics of the cosmic rays represents, therefore,

the best instrument to forecast the effects of terrestrial neutrons on electronic systems.

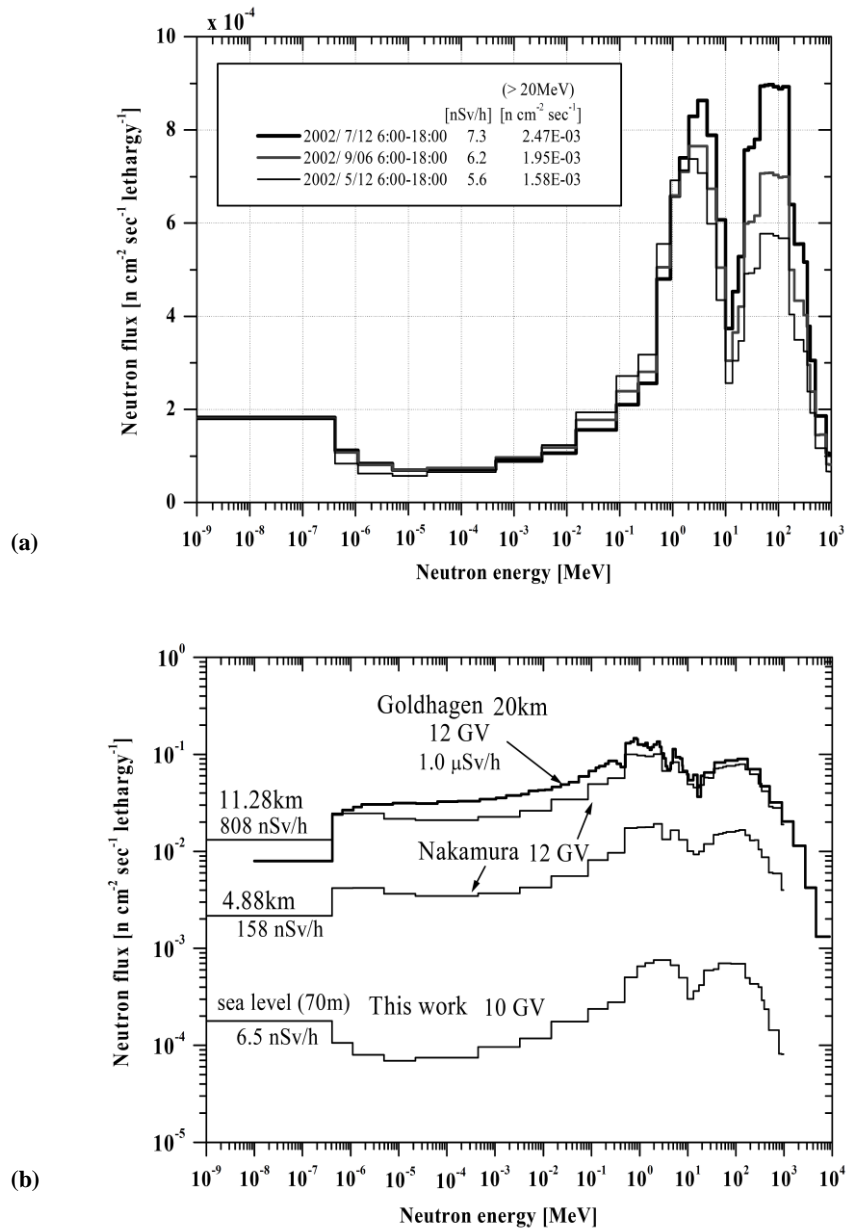


Figure 2.3: In figure (a) the comparison of neutron energy spectra in units of lethargy on three different days, July 12 (high flux), September 6 (medium flux) and May 12 (low flux) in 2002, while in figure (b) are showed cosmic-ray neutron energy spectra in units of lethargy at different atmospheric depths (altitudes) [13].

2.3 Radiation effects on electronic devices

In 1960s, the new techniques introduced for the miniaturisation of electronic devices brought to the attention of the developers the possible impacts that the cosmic rays would have had on the devices reliability [22]. Since the 1975, when unexpected anomalies in telecommunication satellites were attributed to the effects of high energy particles [2], the damaging mechanisms due to the cosmic rays' interactions with the electronic devices and systems have been studied.

The attention has been historically focused on the effects of radiation interaction on MOS materials, devices and circuits, due to their large diffusion on electronic applications [15].

The basic mechanism that induced damaging in MOS devices is the ionisation. Ionising radiations interact with the device materials releasing their energy and, if the energy locally transferred to the semiconductor is enough (about 17 eV for one pair in SiO₂), electron-hole pairs are produced along the ionisation path. The gate oxide insulators are the most sensitive parts of a MOS system to radiation. Electron-hole pairs are generated when ionising radiation passes through the gate oxide. The electrons mobility in SiO₂ is higher than the holes, therefore the electrons can easily leave the oxide in few picoseconds or less. In this time interval, some electrons-holes recombination phenomena occur. The holes that escape to the recombination remain near the point in which they have been generated, where they cause a reduction in the threshold voltage of the MOS devices. Then, the holes are transported to the Si-SiO₂ interface, where a fraction of them could be trapped. This causes a remnant negative voltage shift, which can persist for a long period. Furthermore, the holes' accumulation on the Si-SiO₂ interface causes the enhancement of the interface traps. These create states with defined energy levels in the Si band-gap. The Fermi level or the applied voltage determines the traps occupancy determining a voltage-dependent threshold shift. The described processes depend on the amount of energy that is released in the semiconductor material. Therefore, the ionisation is the basic mechanism for the *Total Ionising*

Dose (TID) effects. Indeed, the effects induced in semiconductor devices are dependent on the energy that the ionising radiation has released per unit of mass, the so called dose. Higher will be the dose higher will be the induced traps in the Si-SiO₂ interface, and higher will be the shift of the devices parameters from the nominal conditions [10; 15].

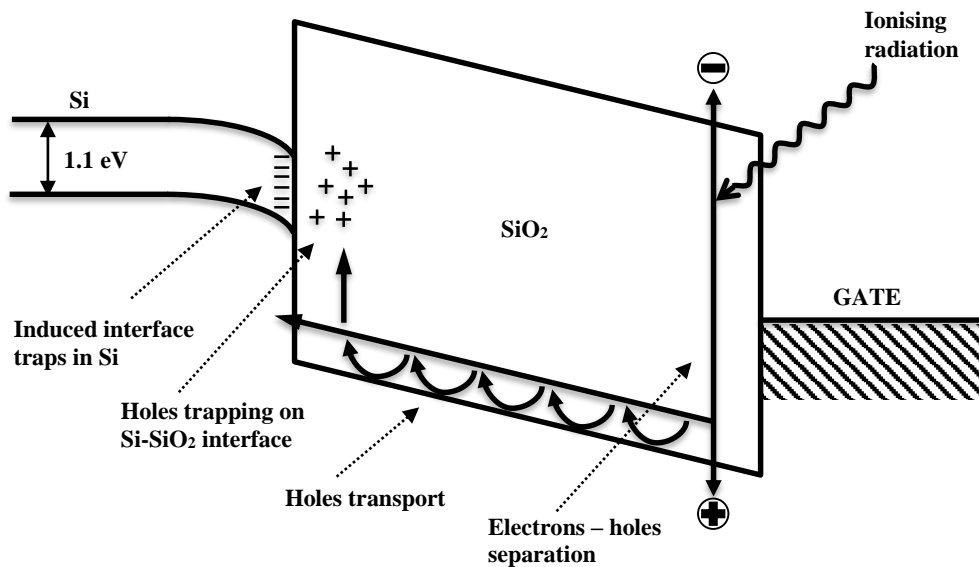


Figure 2.4: Figure shows the schematic energy band diagram for MOS structure with the major physical processes generating radiation-induced traps in Si-SiO₂ interface.

Another radiation effect starts with the displacement of lattice atoms through the direct collision of high energy particles: proton, neutron, heavy ion radiation, high energy electron and photon radiation. *Displacement Damage* (DD) occurs when an atom displaced via interaction with high energy particles leaves a vacancy in the lattice and it reaches a new position in an interstitial region, creating the so called point defect. This introduces new allowable energy states in the semiconductor band gap and, as a consequence, the electrical performances of the device can change. The metric of this type of damage is called the displacement damage dose (DDD), which is the product of the non-ionizing energy loss (NIEL) and the particle fluence. DDD shortens the carrier lifetime and reduces the carrier mobility. DDD increases the number of crystal imperfections, which increase the material's

resistance, carrier scattering, free carrier removal, trap density and overall reduction in the diffusion length. Therefore, the displacement damages can have a significant impact on the electrical properties of semiconductor materials, reducing their performances progressively during the devices exposure to high energy particles irradiation. [3; 10; 16].

As described before, the TID effects and DD are mainly due to the ionisation in the gate insulator thick of SiO₂ and to the generation of point defects inside the semiconductor material, respectively.

However, ionisation can occur in the same manner inside the device semiconductor bulk. Indeed, when an energetic particle penetrates into the depletion layer, electron-hole pairs are produced along the particle path. In a MOS devices in off-state, electrons and holes generated via ionisation will be subjected to the devices electric field. Thus, electrons will flow into the diffusion layer while the holes will flow out through the ground device terminal. As a result of the electrons-holes separation, the elongation of the electric field occurs, enhancing the charge collected in the depletion layer. Electrons collected in the diffusion layer produce a transient pulse and they can also reduce the potential of the diffusion layer. This mechanism is the basis of *Single Event Effects* (SEEs), a further class of radiation-induced damages in semiconductor devices [10].

The effects of the described process can then result in a *soft-error*, that causes reversible damage to the device and that can be corrected [18]. A typical soft-error is the Single Event Upset (SEU) that affects dynamic nMOS or static CMOS memories. In SEU, a single high-energy particle can strike a critical node of the devices, leaving an ionised track passing through the well area or storage capacitor. Depending on the node bias, the well is inverted or depleted. The electrons and the positive charge created via ionisation will flow in opposite direction due to the field present in the structure. If the well node is already filled with electrons, no change of state will occur. However, empty wells may become partially filled by SEU. If enough electrons are collected, a bit flip from “0” to “1”. This radiation-induced error can be corrected by resetting the memory [3; 5].

However, other effects are not reversible and result in permanent degradation or even destruction of the device. These are called *hard errors*. These are divided in four primary areas based on the type of effect. These are the *Single-Event Latchup* (SEL), *Single-Event SnapBack* (SESB), *Single-Event Burnout* (SEB) and *Single-Event Gate Rupture* (SEGR) [18].

These failures modes affect many different types of semiconductor devices. SEL occurs in bulk CMOS technologies or in some Silicon on Insulator (SOI) technologies. SEB affects primarily in power transistors, such as power MOSFETs, bipolar transistors, and IGFETs used both in space and in high voltage terrestrial applications. Non-volatile memories, power MOSFET, and MOS-based digital and linear ICs have showed SEGR, while SESB occurs in MOS technologies [18].

However, the interest of this dissertation is focused on the hard errors induced by terrestrial neutron field on power MOSFET devices. Therefore, a detailed description of SEB and SEGR mechanisms are proposed.

2.4 SEEs in power MOSFET devices

The power MOSFETs susceptibility to different types of irradiation is well known and SEB and SEGR are the two primary catastrophic effects that can destroy their functionality. SEB is defined as an event in which in a power MOSFET source-to-drain current suddenly increases during or following the irradiation, when the devices operate for definite drain-to-source voltages (V_{DS}) and gate-to source voltages (V_{GS}). SEGR is instead defined as an event where the gate-to-drain current suddenly increases during or following the irradiation when the devices operate for definite drain-to-source voltages (V_{DS}) and gate-to source voltages (V_{GS}). Both in SEB and in SEGR, the high current passing through the device is not acceptable in the circuit application and it can cause destructive phenomena [16].

SEB occurs when a high energy particle goes through a power MOSFET biased in the off state, generating a plasma filament of hole-electron pairs along the particle path. If a large drain bias exists, electron-hole pairs are subjected to high electric

field and a very high current density (10^4 A cm^{-2}) will flow vertically along the plasma trace and, then, flow laterally at the insulator-silicon interface to the body region. This high density current flow through the body region below the lateral channel region can cause a voltage drop. If this drop exceeds 0.7 V, then the parasitic bipolar transistor, that as explained before is an intrinsic part of the vertical power MOSFET structure, is turned on. The activation of the parasitic BJT causes the locally enhancement of the plasma current of several orders of magnitude. As a result, the high power density will induce high temperatures into the device, destroying a large volume of material and leading the device into burnout [4; 6; 9; 11; 19-21].

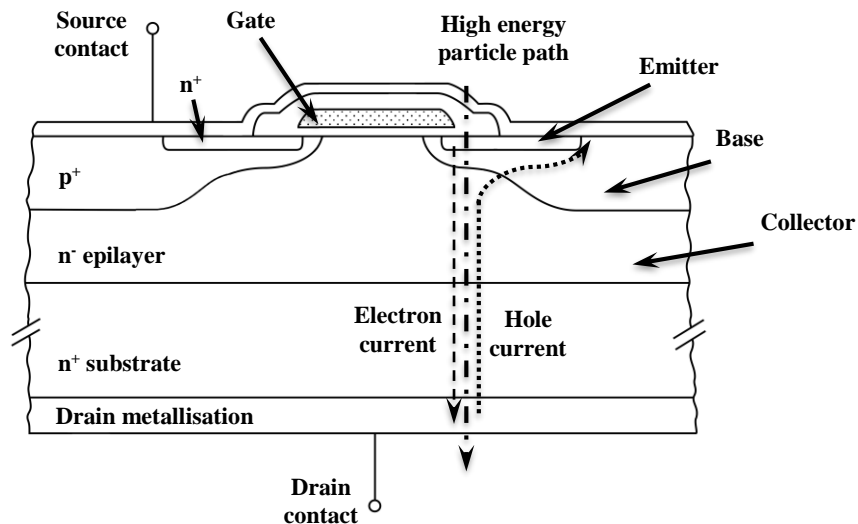


Figure 2.5: Figure describes the sequence of processes leading to the failure of the transistor due to the plasma filament generated by the passage of a heavy ion; electrons flow through the filament from the source n+ region to the substrate n+ region, while holes flow out of the plasma filament through the body p-region to the body contact; if the filament is located near the channel of the MOSFET, the voltage drop along the p-region tends to forward-bias the junction between the p-region and the source. This forward bias is highest near the filament, and there it most strongly turns on the parasitic bipolar npn transistor [9].

The SEGR basic condition is that the high energy particle goes through the gate oxide region of the MOSFET, generating the plasma filament of hole-electron pairs between the gate oxide and drain. As a consequence, the electric field between gate oxide and channel region is enhanced. Under appropriate bias conditions, accumulation of charge (generated by the heavy ion) at the Si-SiO₂ interface in the

gate-drain overlap region can result in sufficiently high electric fields across the gate oxide to cause a localized gate rupture. This rupture is manifested as a permanent short between the gate and drain [1; 11; 19-21].

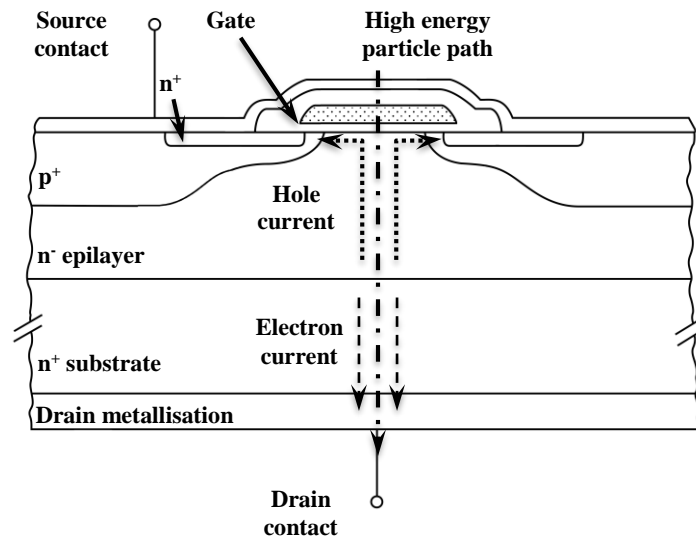
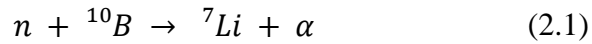


Figure 2.6: Figure describes the schematic mechanism inducing SEGR for an n-channel power MOSFET; ion strikes the device in the neck region below the gate oxide and the electric field, due to the applied positive drain bias, causes the generated holes in the silicon to move toward the interface and the electrons to move toward the drain contact. The holes diffuse toward the p-body at a slower rate than the holes drifting toward the interface resulting in a hole pile-up condition at the interface around the strike area. This hole accumulation effect at the Si-SiO₂ interface creates a pool of positive charge, which results in a transient field increase across the oxide at the track position. If this transient field increases above a critical value, oxide breakdown occurs and the collected holes discharge through the oxide, heating the structure locally; if the breakdown current lasts long enough, a permanent short-circuit through the oxide results [1].

SEB and SEGR can be induced by high energy charged particles (primary cosmic rays) in space and avionic applications, while in terrestrial applications the primary cause of SEEs in power MOSFET devices is attributable to neutron interactions (terrestrial cosmic rays) [14].

In the first condition, the high energy charged particle passing through the devices generates a large amount of electron-hole pairs along its path. Thus, the pairs production is caused by the direct ionisation operated by the charged particle.

Neutrons are neutral particles and they can generate electron-hole pairs only indirectly. They interact with atoms nuclei via elastic and inelastic reactions transferring their energy. This energy makes the nuclei instable with a consequent de-excitation that can occur via electromagnetic radiations or via charged particles emission. Both electromagnetic radiations and charged particles can induce ionisation into the devices, even if the main contribution is certainly attributable to the emitted charged particles. In an electronic device both low-energy ($E < 1$ MeV) and high-energy neutrons can induce ionisation. At thermal energy, neutrons can interact, for example, with ^{10}B included into the devices during manufacturing processes such as ion implantation, polishing and etching, etc. The interaction between thermal neutrons and ^{10}B produces an alpha particle (1.47 MeV) and a ^7Li ion (0.84 MeV) following the reaction



Li ion and alpha particle will release their energy into the semiconductor material via ionisation and therefore inducing the electron-hole pairs generation. High energy neutrons ($E > 1$ MeV) interact with atomic nuclei into the device via nuclear reactions with a probability that is function of the neutron energy (defined in terms of cross section) [10].

The most relevant interactions with high energy neutrons are the interactions able to generate secondary charged particles, as for example the following reactions involving the silicon nuclei.

Table 2.1: Q-Values and energy thresholds for neutrons interactions with silicon isotopes from literature and from Q-value Calculator of National Nuclear Data Centre

Interaction	Q- Value from [12]	Q-Value from <i>QCalc</i>	Threshold from <i>QCalc</i>
${}^{28}\text{Si} + n \rightarrow {}^{28}\text{Al} + p$	-3.87 MeV	-3.86 MeV	4 MeV
${}^{28}\text{Si} + n \rightarrow {}^{25}\text{Mg} + \alpha$	-2.60 MeV	-2.65 MeV	2.75 MeV
${}^{29}\text{Si} + n \rightarrow {}^{29}\text{Al} + p$	-3.0 MeV	-2.9 MeV	3.0 MeV
${}^{29}\text{Si} + n \rightarrow {}^{26}\text{Mg} + \alpha$	-0.04 MeV	-0.034 MeV	0.035 MeV
${}^{30}\text{Si} + n \rightarrow {}^{27}\text{Mg} + \alpha$	-4.22 MeV	-4.20 MeV	4.34 MeV

SEB and SEGR were first reported in space and avionics applications, however, in the last 20 years several studies underlined that the SEEs affect devices employed in terrestrial applications. Furthermore, the wide diffusion of the power devices, mainly the power MOSFETs, in power electronics applications enhanced the attention on SEEs induced by terrestrial neutrons and how these effects represent relevant problem for the reliability of the system they are used.

The evaluation of a complete power electronics system reliability results to be considerably difficult due the large number of electronic devices that operate into the own system and the complexity of the system structure. However, it is possible to characterise the behaviour of each device under the stress conditions in which it will operate. Accelerated test can supply the information necessary for reliability evaluation and many standards suggest the procedures to perform test campaign with the aim to evaluate the devices response to the stress due to the interaction with the terrestrial neutrons.

Bibliography

- [1] M. Allenspach, J. R. Brews, I. Mouret, R. D. Schrimpf, e K. F. Galloway, «Evaluation of SEGR threshold in power MOSFETs», IEEE transactions on nuclear science, vol. 41, n. 6, pagg. 2160–2166, 1994.
 - [2] D. Binder, E. C. Smith, e A. B. Holman, «Satellite anomalies from galactic cosmic rays», IEEE Transactions on Nuclear Science, vol. 22, n. 6, pagg. 2675–2680, 1975.
 - [3] C. Claeys and E. Simoen, «*Radiation effects in advanced semiconductor materials and devices*», Springer, 2002, pagg. 12; 28.
 - [4] C. D. Davidson, E. W. Blackmore, e J. I. Hess, «Failures of MOSFETs in terrestrial power electronics due to single event burnout», in Telecommunications Energy Conference, 2004. INTELEC 2004. 26th Annual International, 2004, pagg. 503–507.
 - [5] P. E. Dodd e L. W. Massengill, «Basic mechanisms and modeling of single-event upset in digital microelectronics», IEEE Transactions on Nuclear Science, vol. 50, n. 3, 2003, pagg. 583–602
-

-
- [6] K. F. Galloway e R. D. Schrimpf, «Research on Radiation Effects in Support of the Defense Nuclear Agency», ARIZONA UNIV TUCSON DEPT OF ELECTRICAL AND COMPUTER ENGINEERING, 1993.
- [7] P. Goldhagen, «Cosmic-Ray Neutrons on the Ground and in the Atmosphere», MRS Bulletin, vol. 28, n. 02, pagg. 131–135, feb. 2003.
- [8] M. S. Gordon et al., «Measurement of the flux and energy spectrum of cosmic-ray induced neutrons on the ground», IEEE Transactions on Nuclear Science, vol. 51, n. 6, pagg. 3427–3434, dic. 2004.
- [9] J. H. Hohl e G. H. Johnson, «Features of the triggering mechanism for single event burnout of power MOSFETs», IEEE Transactions on Nuclear Science, vol. 36, n. 6, pagg. 2260–2266, 1989.
- [10] E. H. Ibe, Terrestrial radiation effects in ULSI devices and electronic systems. Singapore: John Wiley & Sons Inc, 2015.
- [11] G. H. Johnson, J. M. Palau, C. Dachs, K. F. Galloway and R. D. Schrimpf, "A review of the techniques used for modeling single-event effects in power MOSFETs," in *IEEE Transactions on Nuclear Science*, vol. 43, no. 2, pp. 546-560, Apr 1996.
- [12] J. B. Marion, R. M. Brugger, e R. A. Chapman, «Cross Section for the Si 28 (n, p) Al 28 Reaction», Physical review, vol. 101, n. 1, pag. 247, 1956.
- [13] T. Nakamura, «Cosmic-ray neutron spectrometry and dosimetry», Journal of Nuclear Science and Technology, vol. 45, n. sup5, pagg. 1–7, 2008.
- [14] D. L. Oberg, J. L. Wert, E. Normand, P. P. Majewski and S. A. Wender, "First observations of power MOSFET burnout with high energy neutrons," in *IEEE Transactions on Nuclear Science*, vol. 43, no. 6, pp. 2913-2920, Dec 1996.
- [15] T. R. Oldham e F. B. McLean, «Total ionizing dose effects in MOS oxides and devices», IEEE Transactions on Nuclear Science, vol. 50, n. 3, pagg. 483–499, giu. 2003.
- [16] L. Scheick, «Testing Guideline for Single Event Gate Rupture (SEGR) of Power MOSFETs», Pasadena, CA: Jet Propulsion Laboratory, Feb.2008
- [17] H. Schlaepfer, "Cosmic Rays", Spatium No 11, Association Pro ISSI (International Space Science Institute), November 2003, p. 10.
- [18] F. W. Sexton, «Destructive single-event effects in semiconductor devices and ICs», IEEE Transactions on Nuclear Science, vol. 50, n. 3, pagg. 603–621, giu. 2003.
- [19] R. Sheehy, J. Dekter and N. Machin, "Sea level failures of power MOSFETs displaying characteristics of cosmic radiation effects," *2002 IEEE 33rd*
-

Annual IEEE Power Electronics Specialists Conference. Proceedings (Cat. No.02CH37289), Cairns, Qld., 2002, pp. 1741-1746 vol.4.

- [20] J. L. Titus, «An Updated Perspective of Single Event Gate Rupture and Single Event Burnout in Power MOSFETs», *IEEE Transactions on Nuclear Science*, vol. 60, n. 3, pagg. 1912–1928, giu. 2013.
 - [21] J. L. Titus e C. F. Wheatley, «Experimental studies of single-event gate rupture and burnout in vertical power MOSFETs», *IEEE Transactions on Nuclear Science*, vol. 43, n. 2, pagg. 533–545, 1996.
 - [22] J. T. Wallmark e S. M. Marcus, «Minimum size and maximum packing density of nonredundant semiconductor devices», *Proceedings of the IRE*, vol. 50, n. 3, pagg. 286–298, 1962.
 - [23] J. F. Ziegler, «Terrestrial cosmic rays», *IBM journal of research and development*, vol. 40, n. 1, pagg. 19–39, 1996.
-

Chapter 3 – Standard for accelerated neutron testing

3.1 Accelerated tests for power electronic devices

Nowadays, industries encounter an ever increasing demand to develop innovative and higher-technology products, improving the productivity, product field reliability and overall quality. The necessities of a new and evolving market have stimulated the development of methods like concurrent engineering and the use of designed experiments with the aim to improve products and processes.

The reliability has become a central point in the characterisation of materials, components and systems, in line with the modern philosophy in the producing of high-reliability products by improving the design and the manufacturing processes. However, the evaluation of reliability or long-term performance of a component is particularly difficult, because most of modern products are designed to reduce the failure rate and, therefore, to operate without failures or appreciable degradation for years or, in such case, for decades or longer.

For example, in satellite applications only eight months are allowed to test components and systems that are expected to operate for 10 or 15 years. In these applications, Accelerated Tests (ATs) are used to evaluate the components and systems reliability, to eventually detect failure mode with the aim to correct them and to proceed in a comparison of different components manufactures or systems layouts. Several factors, as for example the rapid changing technologies, the more complicated products, the high expectations for better reliability have increased the importance of ATs in the products design and development. However, accelerating the life of a product meets practical and statistical issues, due to the large number of different failure modes that can exist for a complex system [1].

Therefore, it is fundamental to properly design the ATs in order to obtain the expected information.

In electronic and ICs fields of applications, ATs are necessary to develop new electronic devices or systems, to guarantee high reliability, according to the respective application, and, therefore, to reach the target of a very low failure rates. Reliability evaluation of electronic devices or systems is not possible without ATs and information on failure-rate or long-term performances cannot be deduced.

In order to properly design ATs, it is desirable and, in such case, as for example in quality assurance purposes, necessary to refer to recognised standard test methods and procedures. Even if test methods for accelerated durability testing are not always adequate for all purposes, nevertheless, they should be used where possible, despite their limitations.

As described in the previous chapters, power electronic devices are vulnerable to cosmic radiation. Furthermore, how clarified in MIL-HDBK 217, none of the models in the handbook allows to predict nuclear survivability or effects of ionising radiation on electronic devices and systems.

Therefore, it is necessary to design ATs with the aim to evaluate the devices response under irradiation. The procedures for ATs of electronic devices are described in several recognised standards that represent the guidelines in a properly design of AT procedures.

Following in this chapter will be reported and summarised the most important standards for neutron ATs on power electronic devices.

However, the standards summarised in this chapter are not exhaustive for all the possible test conditions and for all the devices typologies. They represent the basic guidelines to properly individuate the targets of a test campaign and to design it in order to obtain the auspicated results.

Therefore, regardless to the specific device that has to be tested, it is fundamental to approach the test design with a good comprehension of the basic idea on which the standards have been developed.

The experimental test described in this thesis has been designed and performed taking inspiration from the described standard, with the aim to obtain data useful to model the response of power MOSFET devices under neutron irradiation.

3.2 JEP151 – Test Procedure for the Measurement of Terrestrial Cosmic Ray Induced Destructive Effects in Power Semiconductor Devices

Accelerated testing (AT) represents the requirement for power electronic devices for high reliability in their respective application, and, therefore, to attain very low failure rates. Furthermore, AC represents the basis of any experimental validation of such low failure rates.

In the previous chapter has been well described that power electronic devices are susceptible to terrestrial cosmic radiation. These power devices may be with or without control logic and they may be components of integrated circuit and they can be based on Si, SiC and GaN technologies. Therefore, power MOSFETs and JFETs, power diodes and IGBTs (Insulated Gate Bipolar Transistors), which are usually employed for power switching and power conversion, and also include GTOs (Gate Turn-Off Thyristors) and Thyristors are susceptible to terrestrial cosmic radiation and it results necessary to perform AC with the aim to characterise their reliability. JEP151 method, widely employed in industrial community, defines the requirements and procedures for terrestrial destructive single event effects (SEEs) as the already mentioned (SEB), (SEL) and (SEGR) testing.

This method is valid when using an accelerator as radiation source, generating a nucleon beam of either

- Mono-energetic proton or neutron beams, or
- Neutron beams with spallation energy spectrum.

The test method does not apply to beams with particles heavier than protons and the specific choice of nucleon beam energies is strictly related to the mechanism of power device failure due to terrestrial cosmic radiation.

Indeed, as explained, terrestrial cosmic rays are the result of extended air showers generated by the collision of highly energetic particles of the primary cosmic rays and consist mostly of photons and electrons, muons, pions and nucleons, i.e.,

protons and neutrons. Moreover, at sea level about 95% of the strongly interacting particles are neutrons.

For SEEs to occur in a power device a nuclear collision between a neutron or proton and a silicon nucleus has to create highly-ionizing spallation fragments which in turn will generate a dense plasma of electron-hole pairs within the semiconductor material. If the local plasma density is high enough this will initiate massive carrier multiplication which will fill and short-circuited the device, inducing device thermal destruction. This mechanism is different to the failure modes in SRAMs or DRAMs, where SEU are related to the radiation-induced charging or discharging of storage cells, and which are non-destructive. SEE process is strongly dependent on the applied voltage but also on the primary nucleon energy, that has to be significantly higher than that for SEU testing [3].

3.2.1 Beam requirements

In order to evaluate the response to SEEs of power MOSFETs and JFETs, power diodes and IGBTs, usually employed for power switching and power conversion, it is possible to use the following nucleon beams

- Mono-energetic protons or mono-energetic neutrons of at least 150 MeV energy, or
- Neutrons spallation spectrum with energy of at least 150 MeV

due to lower sensitivity of power devices to SEEs below 150 MeV for the range of typical application voltages.

Therefore, mono-energetic beams can be employed for the purpose of AT with a minimum energy of 150 MeV with the aim to ensure worst-case conditions for the terrestrial radiation environment.

However, neutron beams with adequate spallation energy spectrum are preferred with respect to mono-energetic beams due to their similarity to the natural terrestrial radiation environment. Furthermore, sources of mono-energetic neutron beams

have lower intensity than mono-energetic proton beams or neutron spallation sources. Therefore, mono-energetic neutrons can be used in order to perform AT on devices that will be used for specific applications, as for example for nuclear fusion applications.

As regard mono-energetic proton beams, they are more intense than any existing neutron spallation source. This allows to increase significantly the acceleration factors and therefore, it contributes to reach the adequate confidence in the measurement of very low failure rates. Nevertheless, proton beam of at least 150 MeV will overestimate the device failure rate due to terrestrial cosmic radiation as the low energy portion of the natural spectrum is missing.

While, as already explained, the minimum energy for mono-energetic neutrons shall be of 150 MeV, the spallation spectrum should represent the terrestrial neutron spectrum in the range from 10 MeV to maximum energy of the spectrum. The minimum energy of 10 MeV is chosen taking into consideration the threshold necessary to generate enough energetic fragments due to the interactions between the device atoms and neutrons or protons.

Furthermore, the deviation in the high energy part of the spectrum, considered as the neutron energy above the 66% of maximum beam energy, from the terrestrial neutron spectrum should be less than one order of magnitude, normalising both spectra to the 10 MeV value.

As regard the design of a testing setup, care has to be taken about the energy loss and beam scattering due to interaction of the neutrons and protons with the setup materials. The latter can be achieved by cut-outs in device holders, minimized packages or bare die test, and an adequately low number of device stacks along the beam line.

The Device Under Test (DUT) sensitive area should be covered by the beam and the flux at the DUT should be characterised by a flux-proportional beam detector and it should have a tolerance of $\pm 10\%$. Beam energy, diameter and angular spread and spatial uniformity of the beam should be characterised. In the case of spallation neutron spectrum, the flux is considered as the number of nucleons per area and per

unit time in the energy range from 10 MeV to the maximum energy of the spectrum (greater than 150 MeV). The beam provider should supply a beam monitor signal with a correspondent calibration factor necessary to calculate the fluence at the DUT.

Reliability requirements for power devices specify, depending on the applications, values between 100 FIT (traction) to 0.01 FIT (automotive) for the failure rate. These values correspond respectively to devices with a MTTF of 10^{11} hours or more than 10 million years. In order to obtain a good confidence (10-15 FIT) on these low values within reasonable time, an acceleration factor (AF) of 10^{11} - 10^9 would be required. These values of the AF correspond to an integrated beam intensity of about 10^8 - 10^6 $\text{cm}^{-2}\text{sec}^{-1}$.

The AF is evaluated assuming an average terrestrial neutron flux at sea level Φ_n of $13 \text{ cm}^{-2} \text{ h}^{-1}$ for $E_n > 10 \text{ MeV}$. The value of Φ_n varies, as explained, with respect to the global position (mainly altitude), latitude and solar activity. Therefore the actual value of Φ_n used to calculate failure rates has to be stated in the test report. The AF is then calculated as follow

$$AF = \Phi_b / \Phi_n \quad (3.1)$$

where Φ_b is the integrated beam flux between 10 MeV and maximum beam energy [3].

3. 2. 2 Test Set Up

With the aim to perform statistical evaluation of the reliability of power electronic devices with ATs, a certain number of devices has to be irradiated for sufficient statistics. Typically, up to 30-50 devices have to be inserted simultaneously into the beam path taking into consideration the following issues

- To assure that every device is subjected to the same flux by arranging the DUTs within the cross section of the beam;
- To compensate the angular spread and therefore the flux reduction along the beam by minimising the angular spread, by increasing the source distance, mounting DUTs in a single plane or entering the fluence reduction coefficient in the evaluation of the failure time;
- For protons: To compensate for energy loss, flux reduction due to electromagnetic interaction with matter by minimising the amount of matter in the beam and by placing devices in a single plane.
- To reduce radioactive activation by restricting the beam to the DUT area, using as little material as possible for test holders and choosing materials not to have long-life radioactive isotopes

The setup should be capable to detect DUTs failures during beam run, to apply voltage and temperature to the DUT during beam run and to measure the fluence to fail.

DUT failures have to be identified and recorded during irradiation, both to account for the number of failures but also for the number of devices which remain functional, excluding failures due to other mechanisms.

Failure rate has to be characterised in the voltage range guaranteed in the specification. It has to be ensured that the voltage to the DUTs remains at the required value without surges and drops. Power supplies and the detection electronics should be protected from the beam.

The fluence-to-fail is essential for calculating the failure rate. The measurement set-up should be provided with means to register flux-proportional detector signals, which are supplied by the beam provider. The monitor calibration factor is determined by the beam provider by comparison of the proportional detector signal with a calibrated beam detector system. This comparison should be made for the range of beam intensities that are put into operation during test runs. If the beam

intensity is left unchanged during a test campaign, the monitor calibration factor can be assumed to be constant [3].

3.2.3 Test Procedure

Each test has to be supported by specific test plan. This serves as guide for the procedures and for real time decisions. A test plan is crucial in tests involve a large number of devices and it is helpful to have some accelerated data to get an estimate of the expected average failure rate. This average failure rate may be used to set the stressor level, obtaining valid failure rate results with the desired confidence interval.

Beam intensity and stressors can be defined starting from previous test data. If no data exist, it is possible to set the stressors by comparing design changes with respect to technologies already analysed. However, the devices failure likely occurs for a minimum bias of about 60% of the rated voltage. If it is possible to assume a comparable sensitivity of the DUTs to terrestrial cosmic radiation, it is recommended to raise the bias voltage in order to reach as soon the number of failures required for the target confidence level.

The samples of a specific run should have comparable sensitivity to terrestrial radiation. To characterise lot to lot variation DUTs several runs have to be performed with material from an individual lot each while the sample size depends on target confidence level. Before the run, DUTs should be electrically characterised in order to ensure their electrical functioning. The position of each device in the irradiation set-up should be recorded to ensure the recording of individual fluence and voltage of failure. Calibrated equipment for voltage sources and data acquisition should be used.

After the run, irradiated DUTs and part of the test set-up will be inevitably activated. The DUTs actual activation level will depend on the fluence but also on the package material. As most of the irradiation-induced activation is short-lived, it is good

practice to wait for some 15 minutes and to check with a radiation counters before devices are handled.

The application of ALARA principle, as well as the utilisation of gloves and pincers will guarantee a sensitive reduction in the operator exposure. Test facilities will introduce their own respective standards regarding access to irradiation sites, handling and shipment of devices, test holders and setups [3].

3.3 JEDEC STANDARD – JESD89A

The standard JESD89A defines the standard requirements and procedures for terrestrial soft error rate (SER) testing of integrated circuits. However, the standard suggests relevant information with regard to the basic features that the test equipment has to show in accelerated tests with high energy neutron in spallation testing facility.

Furthermore, this standard includes a section dedicated to the terrestrial neutron field that are considered as a reference in other standard, for example into the standard JEP151, to the evaluation to the value of neutron spectrum and flux who are subjected the devices.

3.3.1 Test equipment – ATE hardware

The Automatic Test Equipment (ATE) hardware may be conventional electronic test gear or custom-built equipment. During the run the ATE could be exposed to scattered radiation and therefore it must be radiation tolerant.

In order to avoid malfunctioning due to potentially poor quality power the use of a battery-backed power supplies is recommended.

The ATE hardware must be able of exercising the DUTs over the range of operating conditions that are specified in the test plan. The operation of the ATE hardware in planned test conditions must be preliminarily verified and confirmed. Furthermore,

it is necessary to verify wire connections between the DUTs and test equipment and the power supply accuracy.

The ATE, designed for accelerated testing with a high-intensity radiation source, generally holds small number of DUTs at a time while they are irradiated.

For use at a neutron or proton beam facility, the ATE must be remote-controlled and it must allow to operators to perform the tests in a shielded control room.

ATE can be designed in two separate parts, as a holder and a separate electronic package to exercise the DUTs, designing the cabling in order to minimise the possible error during the test operations. Cabling between the control room and beam station may be provided by the beam facility or be the responsibility of the experimenter.

Test cables should be short enough to allow sufficient test speeds without electrical noise problems [4].

3.3.2 Determination of terrestrial neutron flux

The *Annex A* in JESD89A standard provides the value for terrestrial neutron differential flux above 1 MeV for a reference location and conditions and it also supplies formulas and tables to scale the reference spectrum to other locations and conditions.

The neutron flux intensity is variable with respect to altitude, cutoff, or solar modulation while its shape, the neutron spectrum, does not change significantly above few MeV respect to the sea-level.

The location and conditions for the reference terrestrial neutron differential flux have been chosen to be New York City outdoors at sea level at a time of average solar activity. Values of the neutron flux are expressed in units of $\text{cm}^{-2} \text{MeV}^{-1} \text{s}^{-1}$ at 46 energies above 1 MeV [4].

Table 3.1: Cosmic ray induced neutron differential flux for reference conditions (sea level, New York City, mid-level solar activity, outdoors) [4]

Neutron Energy (MeV)	Differential Flux (cm ⁻² s ⁻¹ MeV ⁻¹)	Neutron Energy (MeV)	Differential Flux (cm ⁻² s ⁻¹ MeV ⁻¹)	Neutron Energy (MeV)	Differential Flux (cm ⁻² s ⁻¹ MeV ⁻¹)
1.054	6.83×10 ⁻⁴	5.220	1.53×10 ⁻⁴	130.7	9.64×10 ⁻⁶
1.165	8.19×10 ⁻⁴	5.769	1.25×10 ⁻⁴	224.6	4.30×10 ⁻⁶
1.287	7.61×10 ⁻⁴	6.376	1.16×10 ⁻⁴	386.3	1.33×10 ⁻⁶
1.423	7.02×10 ⁻⁴	7.047	8.90×10 ⁻⁵	664.2	3.99×10 ⁻⁷
1.572	6.00×10 ⁻⁴	7.788	7.16×10 ⁻⁵	1.142×10 ³	1.02×10 ⁻⁷
1.738	5.72×10 ⁻⁴	8.607	6.73×10 ⁻⁵	1.964×10 ³	2.24×10 ⁻⁸
1.920	5.06×10 ⁻⁴	9.512	5.53×10 ⁻⁵	3.376×10 ³	3.36×10 ⁻⁹
2.122	5.02×10 ⁻⁴	10.51	4.58×10 ⁻⁵	5.805×10 ³	4.71×10 ⁻¹⁰
2.346	5.44×10 ⁻⁴	11.62	4.09×10 ⁻⁵	9.982×10 ³	9.87×10 ⁻¹¹
2.592	4.30×10 ⁻⁴	12.84	3.80×10 ⁻⁵	1.716×10 ⁴	3.83×10 ⁻¹¹
2.865	3.34×10 ⁻⁴	14.19	3.44×10 ⁻⁵	2.951×10 ⁴	8.60×10 ⁻¹²
3.166	2.65×10 ⁻⁴	16.16	3.02×10 ⁻⁵	5.074×10 ⁴	2.17×10 ⁻¹²
3.499	1.86×10 ⁻⁴	18.52	3.22×10 ⁻⁵	8.725×10 ⁴	6.97×10 ⁻¹³
3.867	1.64×10 ⁻⁴	25.70	2.59×10 ⁻⁵	1.500×10 ⁵	1.88×10 ⁻¹³
4.274	1.73×10 ⁻⁴	44.19	2.09×10 ⁻⁵		
4.724	1.88×10 ⁻⁴	75.98	1.53×10 ⁻⁵		

The following analytical expression provides the values between those given in the *Table 3.1*

$$\frac{d\dot{\Phi}_0(E)}{dE} = 1.006 \cdot 10^{-6} \cdot \exp \left[-0.35(\ln(E))^2 + 2.1451 \cdot \ln(E) \right] + \quad (3.2)$$

$$+ 1.011 \cdot 10^{-3} \cdot \exp \left[-0.4106(\ln(E))^2 - 0.667 \cdot \ln(E) \right]$$

where E is neutron energy and $d\dot{\Phi}_0(E)/dE$ is the reference neutron differential flux. The total neutron flux of the measured reference spectrum above 10 MeV is $3.596 \times 10^{-3} \text{ cm}^{-2} \text{ s}^{-1}$ ($12.9 \text{ cm}^{-2} \text{ h}^{-1}$). The total neutron flux of the analytic fit above 10 MeV is $3.585 \times 10^{-3} \text{ cm}^{-2} \text{ s}^{-1}$, within 0.3% of the measurement. The estimated uncertainty in the measured value of the neutron flux above 10 MeV is over 10%. However, it is possible to consider a rounded value of the total neutron flux of the reference spectrum above 10 MeV of $3.6 \times 10^{-3} \text{ cm}^{-2} \text{ s}^{-1}$ or equivalently $13 \text{ cm}^{-2} \text{ h}^{-1}$. The reference neutron spectrum does not include protons, even if high-energy secondary protons are also present in the cosmic-ray-induced particle showers and such protons can also cause single-event effects in electronics. The terrestrial cosmic-ray proton flux is roughly 5% to 20% of the neutron flux above 10 MeV,

depending on altitude and cutoff, with the higher fraction of protons at high altitude and high cutoff [4].

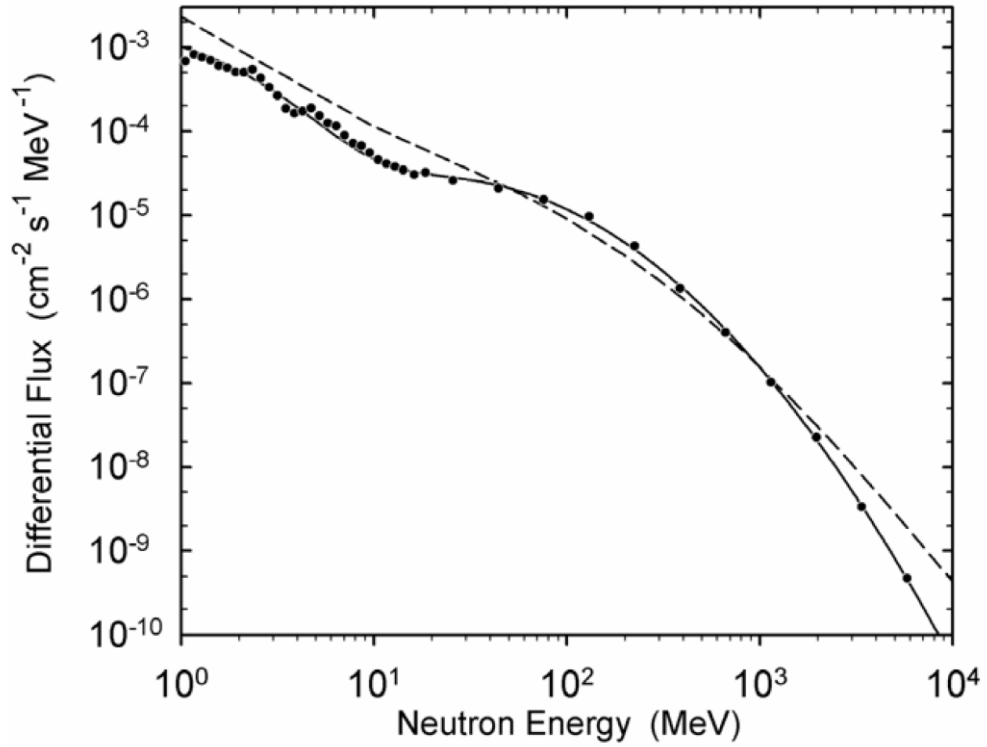


Figure 3.1: The differential flux of cosmic-ray-induced neutrons under reference conditions (sea level, New York City, mid-level solar activity, outdoors); the data points are the reference spectrum, the solid curve is the analytic fit to the reference spectrum, and the dashed curve is the model from the previous version of this standard [4].

In order to obtain the value of differential neutron spectrum in other locations taking into account the effects of altitude, cutoff, and solar modulation, the neutron spectrum can be expressed as follows:

$$\frac{d\dot{\Phi}(E)}{dE} = \frac{d\dot{\Phi}_0(E)}{dE} \cdot F_A(d) \cdot F_B(R_c, I, d) \quad (3.3)$$

where $d\dot{\Phi}_0(E)/dE$ is the reference spectrum, d is the atmospheric depth, R_c is the vertical geomagnetic cutoff rigidity, I is the relative count rate of a neutron monitor measuring solar modulation, $F_A(d)$ is a function describing the dependence on

altitude and $F_B(R_c, I, d)$ is a function describing the dependence on geomagnetic location and solar modulation, that also has a dependence on depth.

The standard supplies the analytical formula to evaluate F_A and F_B scaling factors. For a faster evaluation of the differential neutron spectrum at sea-level for different vertical cutoff rigidity, standard supplies a table of F_B factors for several cutoff rigidity values [4].

Table 3.2: Relative neutron flux at sea level vs. geomagnetic vertical cutoff rigidity [4].

Cutoff Rigidity (GV)	Relative Neutron Flux			Cutoff Rigidity (GV)	Relative Neutron Flux		
	Active Sun Minimum	Quiet Sun Peak	Average		Active Sun Minimum	Quiet Sun Peak	Average
0	0.939	1.098	1.019	9	0.686	0.737	0.712
1	0.938	1.097	1.018	10	0.657	0.702	0.679
2	0.929	1.076	1.002	11	0.630	0.670	0.650
3	0.902	1.030	0.966	12	0.606	0.640	0.623
4	0.866	0.975	0.920	13	0.583	0.614	0.598
5	0.827	0.919	0.873	14	0.562	0.589	0.576
6	0.789	0.867	0.828	15	0.542	0.567	0.555
7	0.752	0.819	0.786	16	0.524	0.547	0.535
8	0.718	0.776	0.747	17	0.508	0.528	0.518

Furthermore, the standard supplies a list of cities and some high-elevation research locations with the latitude, longitude, and altitude of each, and the corresponding geomagnetic vertical cutoff rigidity, typical atmospheric depth, and F_A and F_B for active sun, quiet sun, and average solar modulation. Therefore, it is possible to evaluate the long-term average neutron differential flux of the listed locations, multiplying the reference spectrum by the cumulative scaling factor supplied in the table.

For different locations the shape of the terrestrial neutron spectrum above a few MeV is similar. However, at lower energies the shape of the spectrum strongly depends on how local materials scatter neutrons. Indeed, at lower energies, the spectra vary by up to 66% and the relative flux at thermal energies (<0.4 eV) does not correlate well with the relative flux at higher energies. The reference value for the flux of cosmic-ray-induced terrestrial neutrons at thermal energies (<0.4 eV) at

New York City outdoors at sea level at a time of average solar activity is $1.8 \times 10^{-3} \text{ cm}^{-2} \text{ s}^{-1}$ ($6.5 \text{ cm}^{-2} \text{ h}^{-1}$).

The standard also takes into consideration the shielding effect due to building or other materials. For concrete, in a large building it was found that two 15 cm slabs (plus associated roofing, ceiling, and flooring material, ductwork, etc. in an industrial building) reduced the high-energy portion ($E > 10 \text{ MeV}$) of the neutron spectrum by a factor of 2.3, while the total neutron flux was reduced by a factor of only 1.6. Indeed, low-energy neutrons are scattered, thermalized, and absorbed, but the high-energy neutrons are attenuated by interactions with the nuclei in the shielding, regenerating the low-energy portion of the neutron spectrum.

Above 10 MeV, the attenuation by horizontal concrete layers may be estimated using exponential attenuation with an attenuation length of 0.37 m:

$$\dot{\Phi} = \dot{\Phi}_0 \exp(-x/0.37) \quad (3.4)$$

Where x is the concrete thickness expressed in meters. The lower energy portion of the neutron spectrum does not decrease as fast; the attenuation length for the total flux is about 0.65 m [3].

3.4 MIL-STD-750E - Test Methods for Semiconductor Devices

The standard provides uniform methods for testing semiconductor devices, including basic environmental tests to determine resistance to deleterious effects of natural elements and conditions surrounding military operations, and physical and electrical tests.

Among them, some methods can be used as guidelines to design and perform accelerated test on power MOSFET devices under neutron irradiation and are described below.

3. 4. 1 METHOD 1017.1 – Neutron Irradiation

Destructive neutron irradiation test is performed to evaluate the susceptibility of discrete semiconductor devices to degradation due to neutron environment. Objectives of the test are to detect and measure the degradation of semiconductor device electrical characteristics as a function of neutron fluence and to determine if specified semiconductor device electrical characteristics are within specified limits after exposure to a specified level of neutron fluence.

Test instrumentation shall be standard laboratory electronic test instruments such as power supplies, digital voltmeters, and picoammeters, capable of measuring the electrical parameters required. Parameter test methods and calibration shall be in accordance with this general specification.

The test sample shall be randomly selected and consist of a minimum of ten parts which shall have met all the requirements of the governing specification. Each part shall be serialised to enable pre and post-test identification and comparison.

Pre-exposure electrical tests shall be performed on each part as required and pre-exposure data and delta parameter limits shall be recorded.

Each device shall be mounted unbiased with their terminal leads either all shorted or all open. For MOS devices all leads shall be shorted. An appropriate mounting fixture which will accommodate both the sample and the required shall be used. Test devices shall be mounted such that the total variation of fluence over the entire sample does not exceed 20%.

In reporting the results of radiation tests on discrete devices, adequate identification of the devices is essential. The report shall include the device type number, serial number, the manufacturer, controlling specification, the date code, and other Part or Identifying Numbers (PINs) eventually provided by the manufacturer.

Each data sheet shall include radiation test date, electrical test conditions, radiation test levels, and ambient conditions, as well as the test data. When other than specified electrical test circuits are employed, the parameter measurement circuits

shall accompany the data. Any anomalous incidents during the test shall be fully explained in footnotes to the data [2].

3.4.2 METHOD 1080 – SEB and SEGR

This method describes the procedure for conducting heavy ion irradiation of power MOSFETs. This method establishes the procedure for characterisation and for verification of discrete power MOSFETs for SEB and SEGR. This test method may be applicable to testing where neutrons, protons, or other light particles are used.

It shall be ensured that the devices are not damaged before testing. Otherwise, devices shall be handled in accordance with standard operating procedures to protect against damage and electrostatic discharge.

Power MOSFETs that require voltages in excess of 32 volts can present a safety hazard, therefore safety precautions shall be taken to ensure safe operation of all equipment and personnel.

The test instrumentation can be made with standard electrical instruments able to supply the required test conditions and to measure the required electrical parameters.

The test circuit board contains the test socket, DUT, wiring, and any auxiliary components. The test board provides a mounting surface and interface between the test instrumentation and the DUT.

Two testing circuit can be used: the basic SEB/SEGR test circuit and SEB circumvention test circuit.

Auxiliary components, such as the resistors, capacitors, or current probes, shall be included in the final test circuit. Any accepted SEB circumvention and monitoring technique is acceptable. The test board can have multiple test sockets in which the DUT is inserted.

Cables are typically used to connect the test circuit board to the test instrumentation. The cable length shall be minimised to prevent interference with the desired measurement.

However, the actual cable length is dictated by the spatial location of the test board with respect to the cabling feed-throughs, and the minimum distance from the cabling feed-throughs to the DUT test instrumentation.

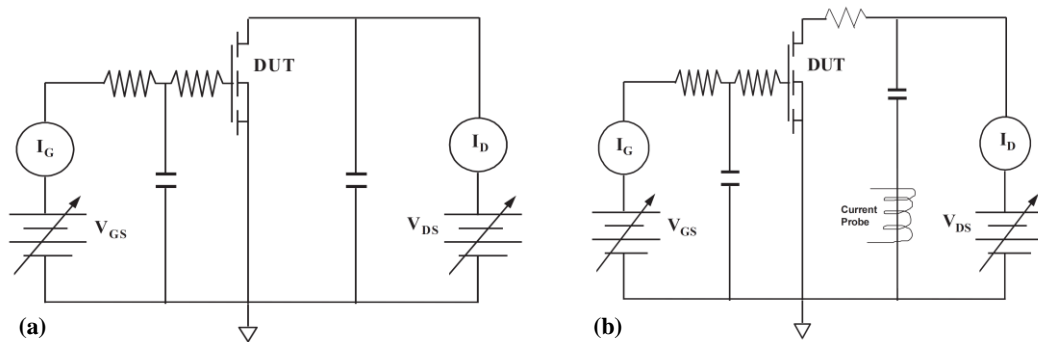


Figure 3.2: Figure shows the SEB/SEGR test circuit (a) and SEB circumvention and monitoring circuit (b) supplied by Method 1080 of MIL-STD-750E [2].

An appropriate SEB/SEGR prediction method may be utilized to prepare the test plan and the select initial bias conditions. The SEB/SEGR failure thresholds should be predicted preferable using previous measurements on similar device types. The predicted failure thresholds can be used to verify that the SEGR and SEB test measurements are valid. If a difference greater than $\pm 30\%$ with respect to the predicted response is observed, the test setup should be verified.

Currently, there are not any accurate prediction models available for SEB. Predictions based upon previously obtained SEB data are helpful, but, due to the nature of the failure mechanism, cannot be used to accurately predict SEB.

Predictions of SEGR can be made from previous SEGR data or calculated using currently accepted models. If previous test results are unavailable or the device layout, design, or process has been modified, then SEGR failure thresholds can be predicted using an empirical prediction method or an analytical prediction method. SEB and SEGR both can result in catastrophic failure due to large leakage currents that can destroy the device. In SEB testing, a capacitance sufficient to hold the bias voltage within $\pm 10\%$ may be required to induce damage during a SEB event [2].

3. 4. 3 Method 3407.1 – Breakdown Voltage, Drain-To-Source

This method supplies information on test circuit configuration and procedure to use to characterise the field-effect transistor or IGBT breakdown voltage, under the specified conditions.

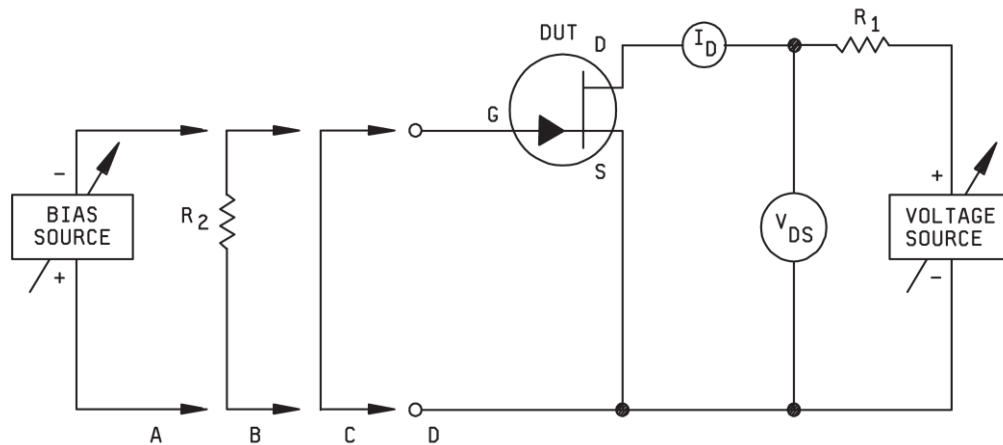


Figure 3.3: Figure represents the test circuit configurations for breakdown voltage characterisation suggested by Method 3407.1 of MIL-STD-750E [2].

The method suggests four possible test configurations:

- A. Gate-to-source: Reverse bias.
- B. Gate-to-source: Resistance return.
- C. Gate-to-source: Short-circuit.
- D. Gate-to-source: Open-circuit.

The resistor R_1 is a current-limiting resistor and it should be of sufficiently high resistance to avoid excessive current flowing through the device and current meter. The voltage shall be gradually increased from zero, with the specified bias condition applied, until either the minimum limit for $V_{(BR)DSX}$ or the specified test current is reached [2].

Bibliography

- [1] R. P. Brown, D. Kockott, P. Trubiroha, W. Ketola, e J. Shorthouse, «A Review of Accelerated Durability Tests», n. 18, pag. 44.
 - [2] MIL-STD-750F, Department Of Defense Test Method Standard: Test Methods For Semiconductor Devices, 2016.
 - [3] JEP151 – Test Procedure for the Measurement of Terrestrial Cosmic Ray Induced Destructive Effects in Power Semiconductor Devices, JEDEC Solid State Technology Association 2015, 2015.
 - [4] JESD89A – Measurement and Reporting of Alpha Particle and Terrestrial Cosmic Ray-Induced Soft Errors in Semiconductor Devices, JEDEC Solid State Technology Association 2001, 2006.
-

Chapter 4 – Investigation on the Single Event Burnout of Power MOSFETs under atmospheric-like neutron spectrum irradiation

As described in the previous chapters, neutron-induced SEEs on power electronic devices could reduce considerably their reliability and, consequently, the reliability of the systems they are employed in. Nowadays, Power MOSFETs are largely employed in several applications (avionics, inverters, power conversion systems, power AC/DC systems, automotive, etc.). Many of the fields of application of power MOSFETs need high levels of reliability and it is therefore necessary to evaluate the failure parameters of the devices in order to undertake the adequate strategies to guarantee the correct operations of the systems in which power MOSFETs operate.

Several studies demonstrated that neutrons induce SEEs in power MOSFETs and different physical models regarding those phenomena have been proposed in literature. However, no models have been proposed with regard to the failure analysis of these devices and with regard to the physical parameters that influence the behaviour of the devices under neutron irradiation.

Therefore, our attention has been focused on the response of power MOSFETs devices under neutron irradiation with atmospheric-like energy spectrum. Furthermore, our interest has been to investigate the relationship between the failure parameters and the devices characteristics.

The study on SEEs physical models and preliminary experimental test allowed to individuate the parameters that influence the devices response under neutron irradiation. The standards have guided the test facility selection, the design and development of the test equipment, and the definition of test procedures.

This chapter describes the different phases that have characterised the test campaign and it shows the results obtained.

4.1 Test Facility

ChipIr is a beamline of the ISIS spallation source at the Rutherford Appleton Laboratory (UK) dedicated to the irradiation of electronic devices with atmospheric-like neutron spectrum [4]. ChipIr has the characteristics suggested in Jedec Publication *JEP151* and in Jedec Standard *JESD89A*, necessary to perform test on power electronic devices. ChipIr shows energies of neutrons up to 800 MeV with a good match with the atmospheric neutron spectrum above 10 MeV, it has a high neutron flux ($>10^6$ n/cm²/s) and an acceleration factor up to 10^9 [1].

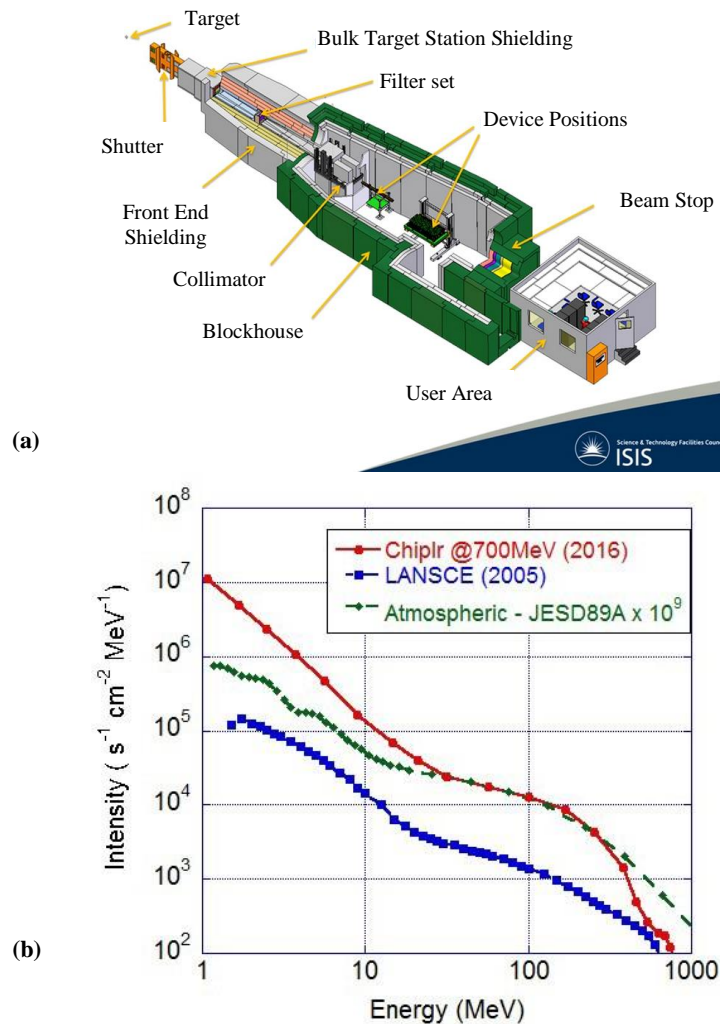


Figure 4.1: Figures shows ChipIr Neutron Irradiation Facility layout (a) and the ChipIr neutron spectrum in units of energy in comparison with the JESD89A atmospheric and LANSCE spectra (b) [1].

In ChipIr a Single-crystal Diamond Detector (SDD), in which neutrons detection is based on the electrons-holes pairs generation due to secondary charged particles produced by neutron reactions with carbon nuclei, is used as proportional detector during the experiments and to perform beam uniformity mapping. The SDD electronic chain generates a NIM signal that could be modified in order to be used by the users as beam monitor in their acquisition system. The SDD signal is acquired with a cumulative counter during the irradiation and the neutron flux on the DUTs can be obtained multiplying the SDD registered counts during the irradiation with a conversion factor 5.736×10^5 n/cm²/count [2].

SDD is arranged on a remote positioning system that allows to perform the flux mapping with variable spatial resolution. Therefore, the beam uniformity can be evaluated accordingly to the JEP151 standard. ChipIr facility has a square beam with a good uniformity in a region of 7x7 cm², as shown below. Uniformity map has been obtained sampling the beam size with the SDD with a spatial resolution of 2 mm both on x and y axis [3].

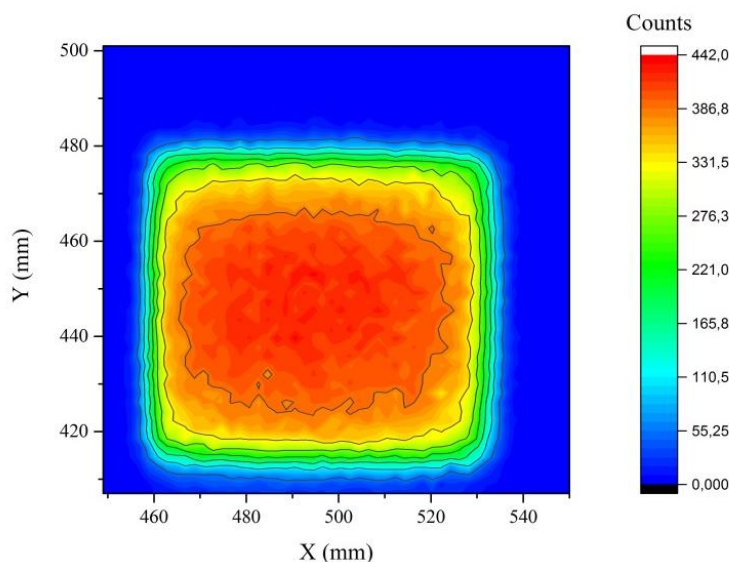


Figure 4.2: Figure shows a map of the neutron beam measured with a diamond detector [3].

The evaluation of the neutron flux tolerance on DUTs has been performed taking as references the beam maps, the DUTs board characteristics and the devices size.

Interpreting the JEP151 tolerance definition as the maximum deviation in the flux with respect to the average flux value on the DUTs, the tolerance has been evaluated. The flux on each DUT has been evaluated as the average flux value on the device package surface. In this condition the maximum tolerance evaluated is of about the 9.5%, falling inside the range suggested in the standard ($\pm 10\%$).

4.2 Test equipment

Test equipment (TE) [5] has been developed with the aim to perform destructive tests on power MOSFET devices under neutron irradiation. Taking into consideration the Method 1080 of the MIL-STD 750E, TE has been designed to perform measurements and to obtain information about the following failure parameters

- SEEs thresholds
- SEEs failure rate vs. Drain-Source Voltage (V_{DS})

Furthermore, in order to obtain significant statistics, the TE has been designed to be able to test 8 DUTs per run. In order to allow to the operator to perform tests in a shielded room, TE has been developed to be remotely controlled.

TE is constitute by

- a core block, the host PC,
- a Data Acquisition board (DAQ),
- a Source Measure Unit (SMU),
- a capacitor board,
- a DUTs board.

The host PC, running the control and acquisition software, developed with the National Instruments Labwindows C Virtual Instrument (CVI) suite. The PC acquires data from a DAQ through an Ethernet connection. DAQ board consists of 2 elements:

- the National Instruments Compact DAQ 9184, which is a 4 slot Gigabit ethernet chassis,
- the National Instruments 9205 C-Series analog input module, 32 (in single ended mode) or 16 (in differential mode) multiplexed voltage channels, 16 bit Analog to Digital Converter (ADC) resolution, 250 kS s^{-1} sampling rate, $\pm 10 \text{ V}$, $\pm 5 \text{ V}$, $\pm 1 \text{ V}$ and $\pm 0.2 \text{ V}$ signal input range, isolation.

The host PC also manages a SMU that is controlled via GPIB interface and has to operate far to the experimental room, because it also consists of power switching circuits and it may be subject to SEEs due to neutron irradiation.

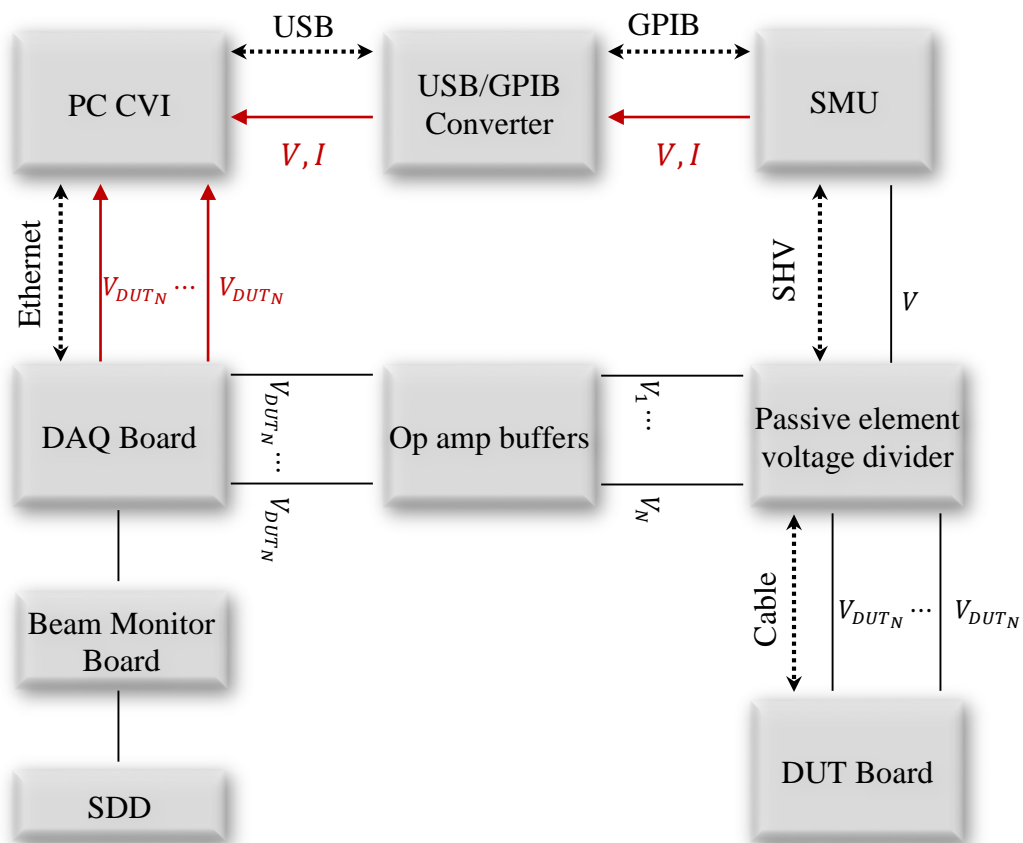


Figure 4.3: In figure are presented the block diagram of the experimental apparatus used during SEEs investigation.

The SMU provides the supply voltage to the test circuit and it measures the output current. A Keithley 2410-C has been used as SMU in the test equipment.

The capacitor board is powered by the SMU through a cable that extends up to the control room. Furthermore, the capacitor board is constituted by a module with different passive components and by a series of voltage follower for the appropriate signal conditioning (attenuation and impedance matching) of the drain voltages upstream of the ADCs.

Test equipment, previously developed for preliminary test performed in the ^{241}Am -Be Neutron Irradiator at the University of Palermo, has been upgraded in order to perform destructive tests at ChipIr. With respect to the previous test equipment a neutron beam monitor acquisition system able to acquire data from SDD has been developed and the software has been modified for a better management of the test.

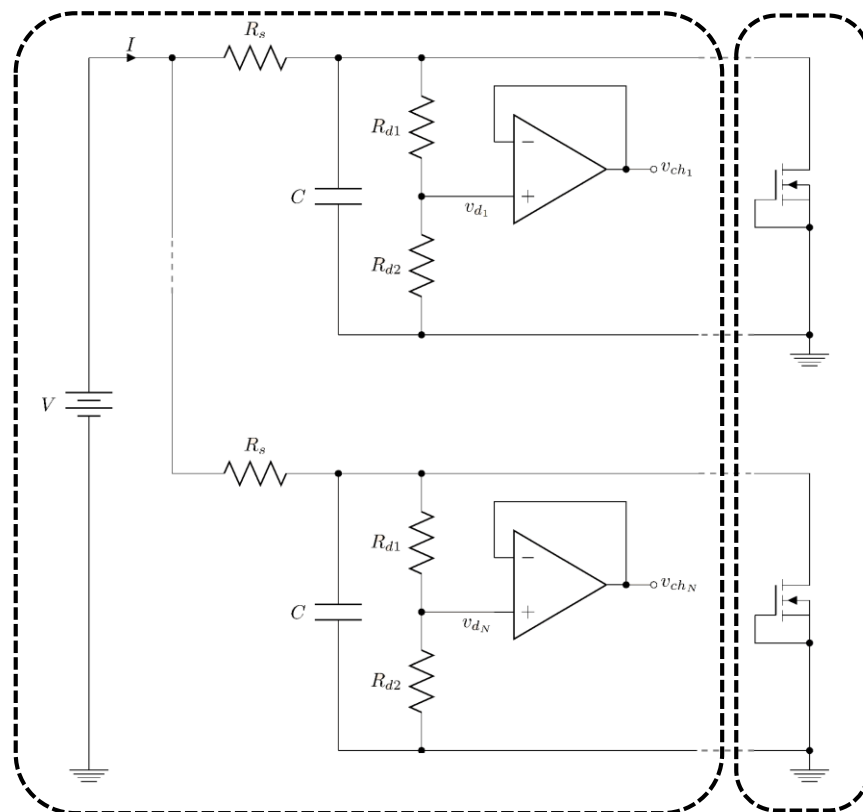


Figure 4.4: The figure represents the electronic layout of the capacitor board and op amp buffers (on left) and DUTs Board (on right).

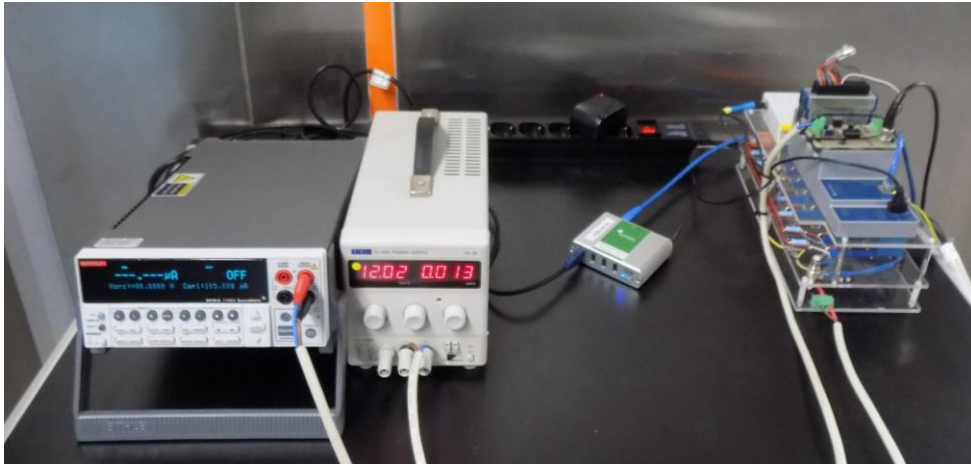


Figure 4.5: In figure the test equipment, from left, SMU, Beam monitor Board DC Supply and Capacitor Board.

The DUTs board has been designed taking into consideration the facility characteristics. In particular, we took into consideration the beam shape and size and the experimental setup. Particular attention has been done to the procedure necessary to perform each test, taking into account the possibility that the procedures could be longer than the own experiment. In order to reduce the time necessary for each experiment, we decided to maximise the number of DUTs the board is able to hold and we thought to use a remote sample control to move the board positioning the devices in the beam line. Therefore, the board has been designed to be able to hold at least 32 DUTs in 4 sets. The board has been made with two square layers of compact polycarbonate with 300 mm of side dimension and 3 mm of thickness. On each layer 4 square windows with 70 mm of side dimension have been realised. The DUTs holders (PCB 3-ways terminal blocks) have been positioned around each window, in order to keep the DUTs into the beam line. For each DUTs set a 10-ways connector (PCB 10-ways terminal block) has been arranged on the board. Adequate connections have been realised between the 3-ways PCB and the 10-ways PCB. Below the preliminary design of the board and the preliminary assembly, in which it is possible to observe the 4 windows, the DUTs holder and the connection. The DUTs board has subsequently been modified

to be arranged on a holder able to move the board both in x and y axis and to position the DUTs board adequately on the neutron beam.

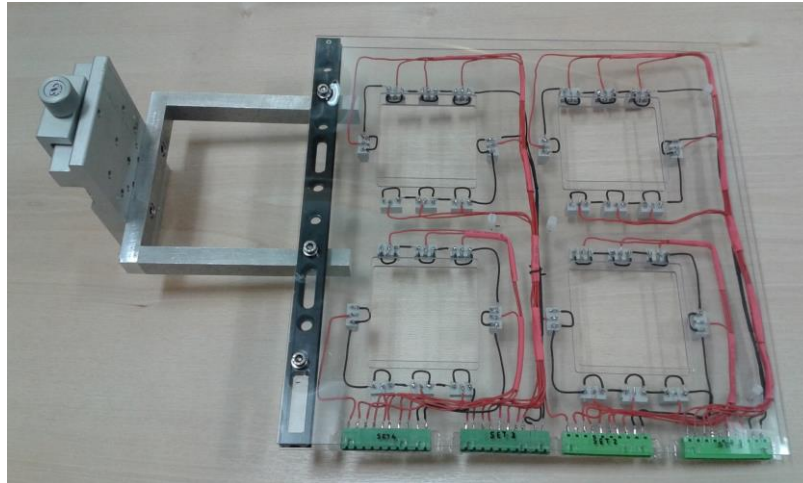


Figure 4.6: Figure shows the structure of DUTs Board.

4.3 Devices characterisation procedures

Six commercial types of Power MOSFETs employed in switching applications with different values of rated $V_{(BR)DSS}$ have been selected:

- STW20N95K5 – N-channel 950 V, 0.275 Ω , 17.5 A, MDmesh™ K5,
- STW15N80K5 – N-channel 800 V, 0.375 Ω , 14 A, SuperMESH™ 5,
- STW55NM60N – N-channel 600 V, 0.047 Ω , 51 A, MDmesh™ II,
- STW18NM60ND – N-channel 600 V, 0.25 Ω , 13 A, FDmesh™ II,
- STW60NM50N – N-channel 500 V, 0.035 Ω , 68 A, MDmesh™ II,
- STW19NM50N – N-channel 500 V, 0.2 Ω , 14 A, MDmesh™ II.

Power MOSFETs have been preliminary characterised following the suggestion for test procedures specified in JEP151. Devices characterisation has been performed with reference to METHOD 3407.1 of MIL-STD-750E, to determine the $V_{(BR)DSS}$ of the field-effect transistor. Between the bias configurations mentioned in the METHOD 3407.1, the gate-to-source short-circuit condition has been used to characterise the $V_{(BR)DSS}$ for each device. With this aim a characterisation board has been realised and a characterisation software has been developed.

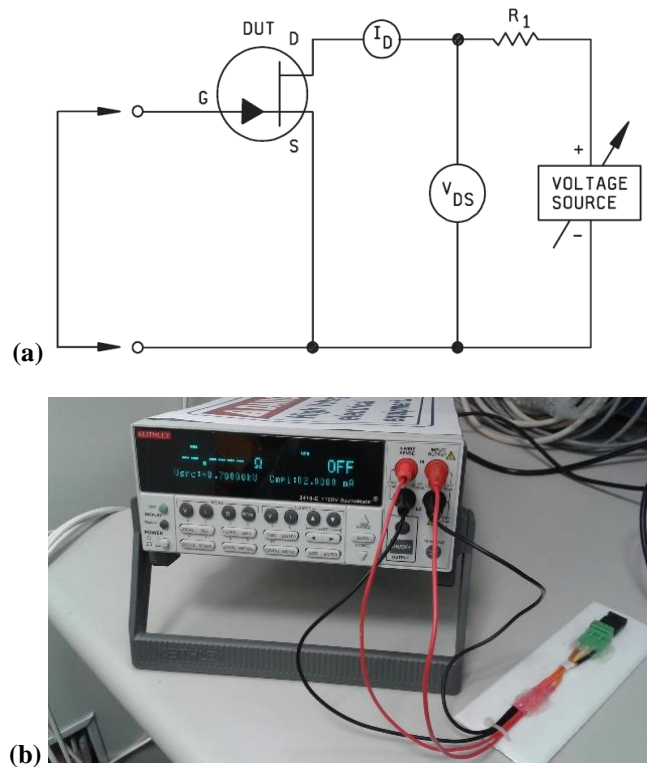


Figure 4.7: Figures show the gate-to-source short-circuit configuration used in DUTs characterisation (a) and the corresponding setup (b).

The devices have been numbered and then the characterisation has been performed. For each device three measurements have been executed and, then, the $V_{(BR)DSS}$ for each device has been evaluated as the mean value on the three measurements. The devices have been characterised and the $V_{(BR)DSS}$ value has been calculated as the mean value of the breakdown voltage for each device type.

Table 4.1: Summary of devices characterisation results

Device Type	Rated $V_{(BR)DSS}$ [V]	Measured Mean $V_{(BR)DSS}$ [V]	Correct Standard Deviation [%]	Standard Error on the Mean $V_{(BR)DSS}$ [%]
STW20N95K5	950	1092.3	1.2	0.3
STW15N80K5	800	925.6	1.1	0.1
STW55NM60N	600	703.5	2.0	0.4
STW18NM60ND	600	664.3	2.5	0.2
STW19NM50N	500	570.2	0.5	0.04
STW60NM50N	500	555.1	0.9	0.2

4.4 SEE threshold evaluation

After the devices have been electrically characterised, it was possible to proceed with the SEB threshold evaluation. This procedure is suggested in the MIL-STD-750E – METHOD 1080, as an appropriate prediction method that may be utilised to predict the SEE failure thresholds before the failure test campaign. In this work the procedure has been instead performed to study the relationship between the SEE threshold and the devices $V_{(BR)DSS}$.

Test setup has been arranged inside the experimental room and the characterised devices have been arranged on DUTs board in 3 sets of 8 devices for each type. DUTs board has been fixed on a holder able to slide the board with respect to the beam along x and y axis, with beam axis as the z one.

The board and consequently the DUTs have been aligned with respect to the beam centre with the help of a laser alignment system.

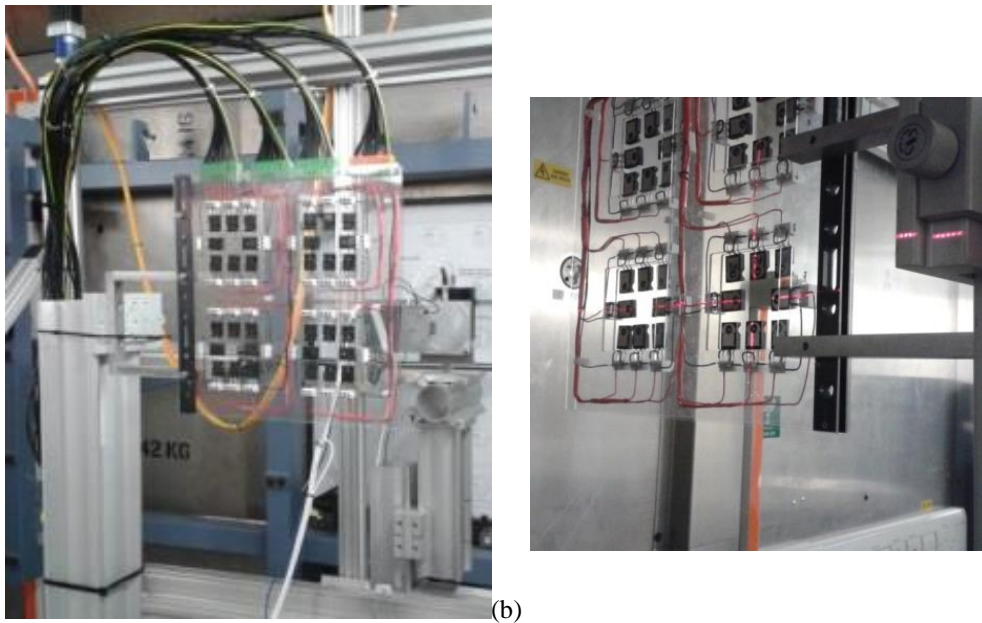


Figure 4.8: Figures shows the DUTs board fixed on the sliding holder inside the experimental room (a) and a detail of the laser alignment system (b).

The starting bias voltage has been set at 10 V and the procedures to activate the neutron beam started contemporarily with the data acquisition on the DUTs. The first signal from the beam neutron monitor has been taken as the start signal for the test. The bias voltage has been progressively increased until to reach the burnout of all the DUTs. For each voltage step the DUTs have been irradiated for 60 seconds. Taking into consideration the acceleration factor, devices have been irradiated for the equivalent of about 6700 years, a time much longer than their average lifetime. Furthermore, taking into consideration the definition of Failure In Time, as the number of failures in 10^9 operative hours, 60 seconds of irradiation give a minimum detectable value of about 17 FITs. This value results to be close to the reasonable confidence level suggested by JEP151 and largely acceptable considering a higher expected values of the FITs for these devices.

At the end of each test, with all the DUTs of a set gone into burnout, the acquisition has been stopped and the data have been stored. The beam has been interrupted allowing the access to the experimental room and the DUTs board positioning for the successive DUTs irradiation.

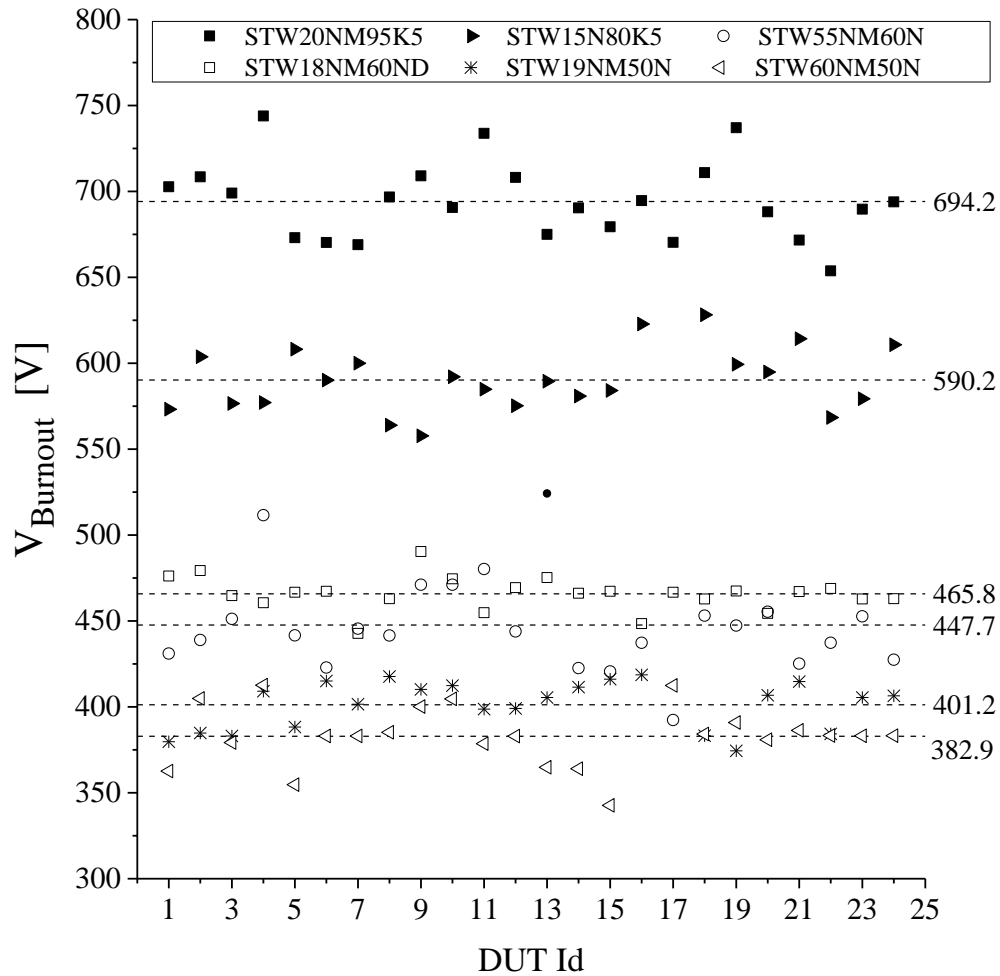


Figure 4.9: Figure summarises the SEEs thresholds evaluation in which symbols represent the devices V_{Burnout} while dashed lines represent the mean V_{Burnout} obtained for each type of device.

The procedure described has been performed for 18 sets of DUTs (3 sets for each device type) for a total of 144 DUTs tested. Acquired data have been evaluated in order to obtain information on the failure voltage threshold (V_{Burnout}). This has been evaluated as the mean value of the threshold values distribution. Obtained data show a low standard deviation (lower than 7%) and a low standard error on the mean value V_{Burnout} (lower than 2%). Results obtained show a V_{Burnout} significantly lower than the breakdown voltage, as expectable for this type of devices.

The relationship between the V_{Burnout} and the device breakdown voltage, both with regard to the rated $V_{(\text{BR})\text{DSS}}$ both with regard to the measured $V_{(\text{BR})\text{DSS}}$, has been

investigated. Data underline how the burnout voltage threshold of the devices is dependent on their breakdown voltage. V_{Burnout} resulted growing exponentially with $V_{(\text{BR})\text{DSS}}$. Fitting curves have been obtained using the following fitting formula, where A and B are the two fitting parameters.

$$V_{\text{Burnout}} = A \cdot \exp(B \cdot V_{(\text{BR})\text{DSS}}) \quad (4.1)$$

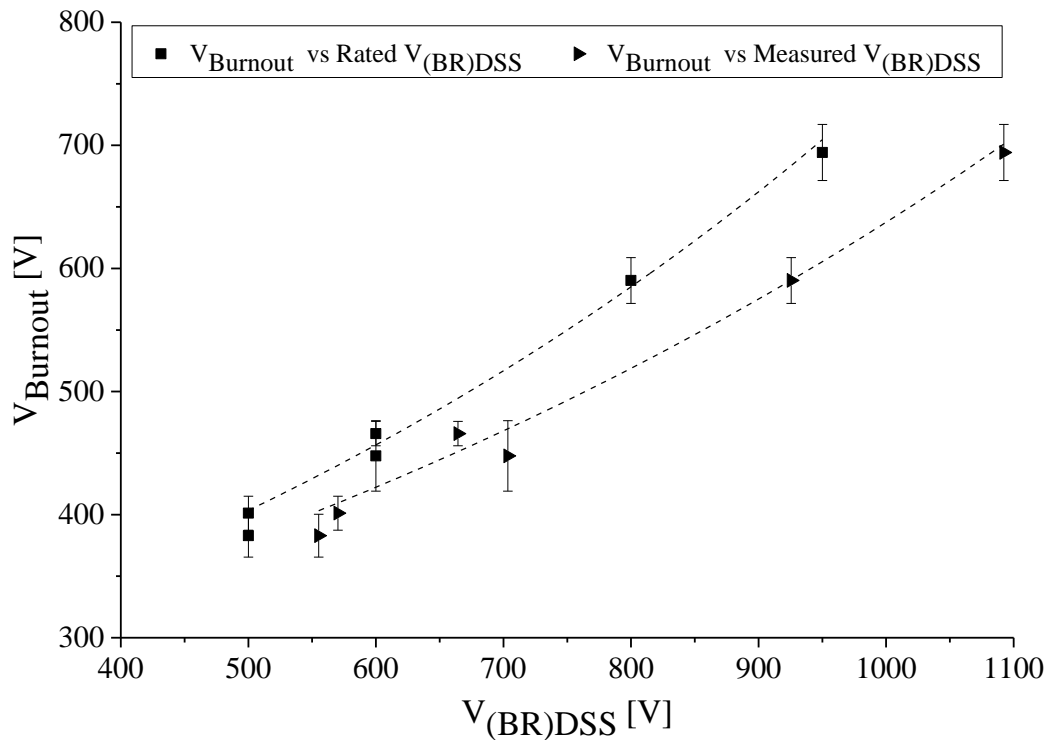


Figure 4.10: In figure is showed the correlation between the V_{Burnout} and the Rated and Measured values of $V_{(\text{BR})\text{DSS}}$ for each type of tested device and relative fit curves that underline the exponential trend.

Table 4.2: Summary of V_{Burnout} Fitting Parameters

Parameter	V_{Burnout} vs. Rated $V_{(\text{BR})\text{DSS}}$	Standard Error [%]	V_{Burnout} vs. Measured Mean $V_{(\text{BR})\text{DSS}}$	Standard Error [%]
A [V]	217.12415	4.7	227.61215	5.8
B [V⁻¹]	0.00124	5.5	0.00103	7.2

A comparison with a linear fitting has been carried out in order to evaluate the best fitting formula. The comparison between the Adjusted R^2 parameters shown that the linear fit is slightly better than the exponential fitting. However, the reduced χ^2 resulted to be closer to the value 1 for exponential fitting than the linear fitting. Furthermore, the standard error on the A and B parameters for linear fitting resulted to be greater than for the A and B parameters for exponential fitting. Taking this comparison into account, the exponential fitting has been considered the best in representing data.

The tests described have been performed taking into consideration the procedures suggested in the standards for neutron testing on power electronic devices. Experimental evaluation of the SEE thresholds for different power MOSFETs has allowed to study the relationship with the devices breakdown voltage. It is evident that SEE threshold grows up exponentially with the $V_{(BR)DSS}$. As a consequence of a non-linear trend, the ratio between $V_{Burnout}$ and $V_{(BR)DSS}$ decreases and the power MOSFETs sensitivity to SEE results to be higher in the devices with higher rated breakdown voltage.

Results show also a difference in the values of $V_{Burnout}$ for devices with the same rated $V_{(BR)DSS}$ but with different rated maximum current. Taking into consideration that the maximum current depends on the device channel size, it is possible to suppose a relationship between the SEE threshold and the channel size. Therefore, the proposed method could represent a valid prevision instrument of the SEE thresholds for power MOSFET devices with different breakdown characteristics and it allows to individuate the other devices features that could influence the behaviour of Power MOSFETs under neutron irradiation.

4.5 Failure parameters evaluation

After the evaluation of the burnout thresholds, the relationship between device failure parameters and bias conditions under neutron irradiation has been

investigated. To perform the experiment, four device types have been selected among the six previously characterised in term of threshold voltage

- STW20N95K5 – N-channel 950 V, 0.275 Ω , 17.5 A, MDmesh™ K5,
- STW15N80K5 – N-channel 800 V, 0.375 Ω , 14 A, SuperMESH™ 5,
- STW18NM60ND – N-channel 600 V, 0.25 Ω , 13 A, FDmesh™ II,
- STW19NM50N – N-channel 500 V, 0.2 Ω , 14 A, MDmesh™ II.

The preliminary procedures for devices characterisation have been carried out in the same manner that in the previous experiment. For each device type the test bias conditions have been individuated taking into consideration the results of threshold experiment. Indeed, as bias values for failure test have been chosen the maximum, minimum and mean values of the threshold values distribution for each device type.

Table 4.3: Summary of bias conditions for failure rate evaluation procedures

Device Type	Rated $V_{(BR)DSS}$ [V]	Measured Mean $V_{(BR)DSS}$ [V]	Minimum threshold value [V]	Mean threshold value [V]	Maximum threshold value [V]
STW20N95K5	950	1092.3	650	695	745
STW15N80K5	800	925.6	560	590	630
STW18NM60ND	600	664.3	445	465	490
STW19NM50N	500	570.2	375	400	420

In order to evaluate the failure parameters, the DUTs have been irradiated until to reach their failure. 24 devices have been tested for each type and for each bias condition and SDD has been used as time trigger to evaluate the failure time for each device. Obtained data have been handled to obtain the devices MTTF, FIT and failure rate λ_N , that it was assumed to be constant, in the different bias conditions

for each device. Data underlined how the devices failure parameters are dependent on the V_{DS} . MTTF resulted decreasing exponentially with V_{DS} . Fitting curves have been obtained using the following fitting formula, where A and B are the two fitting parameters

$$\mathbf{MTTF} = \mathbf{A}_{MTTF} \cdot \mathbf{exp}(\mathbf{B}_{MTTF} \cdot \mathbf{V}_{DS}) \quad \mathbf{B}_{MTTF} < \mathbf{0} \quad (4.2)$$

$$\mathbf{FIT} = \mathbf{A}_{FIT} \cdot \mathbf{exp}(\mathbf{B}_{FIT} \cdot \mathbf{V}_{DS}) \quad \mathbf{B}_{FIT} > \mathbf{0} \quad (4.3)$$

The failure rate λ_N can be evaluated as $1/MTTF$ and used in *Parts count method* and *Parts stress analysis*, for the evaluation of the total failure rate.

Data on failure parameters have shown a greater error with respect to the data obtained in the previous experiment, especially for the device STW20N95K5 and for the lower values of V_{DS} , due to the low number of DUTs on which the data have been evaluated. Therefore, in order to improve the statistics for lower V_{DS} values it will be necessary to test a greater number of devices.

However, despite the poor statistics, it has been possible to underline the trend in the failure parameters and the relationship with the bias conditions. Below the fitting parameters are summarised and the fitting curves are shown.

Table 4.4: Summary of fitting parameters

Parameter	STW20N95K5	STW15N80K5	STW18NM60ND	STW19NM50N
A_{MTTF} [V]	1.65175×10^{20}	7.41907×10^{23}	1.16197×10^{24}	3.07347×10^{20}
B_{MTTF} [V ⁻¹]	-0.04335	-0.06237	-0.08071	-0.07438
A_{FIT} [V]	2.09213×10^{-4}	2.47469×10^{-15}	1.99296×10^{-15}	2.70202×10^{-9}
B_{FIT} [V ⁻¹]	0.01854	0.0614	0.07896	0.05774

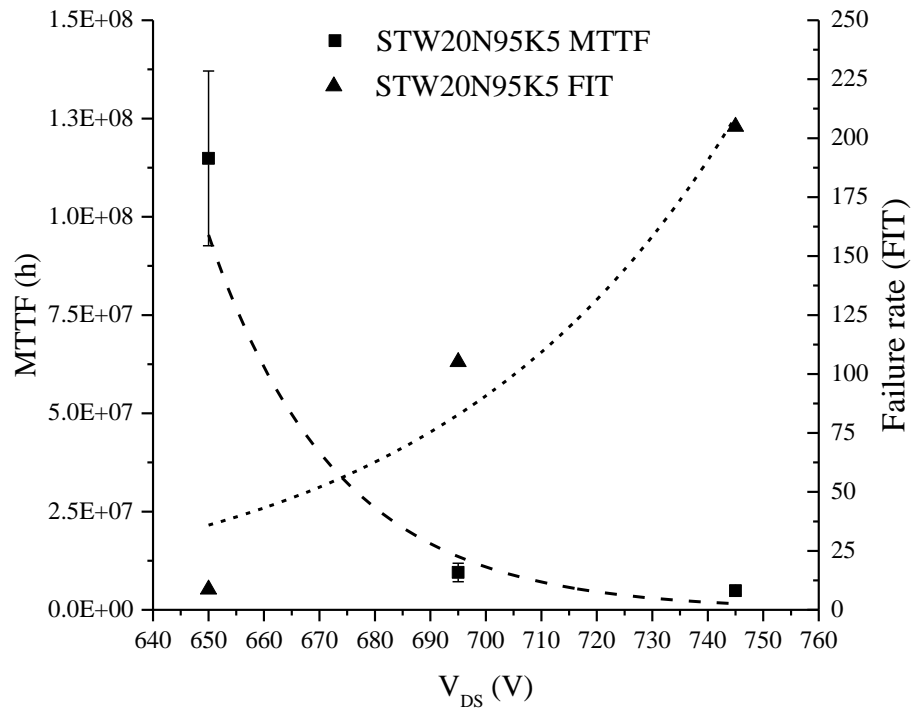


Figure 4.11: Failure parameters trend for a STW20N95K5 power MOSFET.

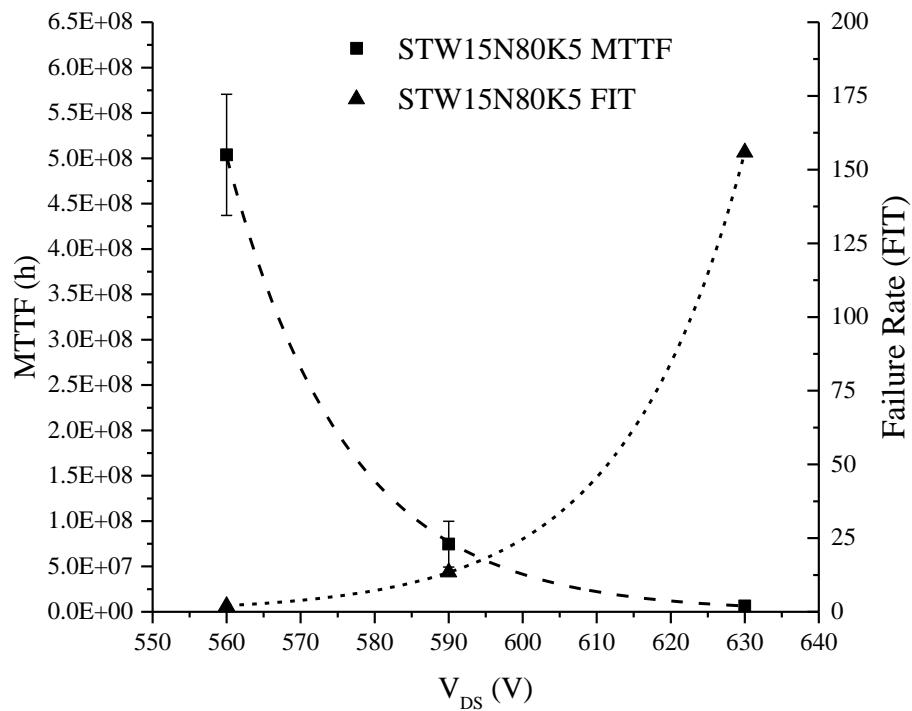


Figure 4.12: Failure parameters trend for a STW15N80K5 power MOSFET.

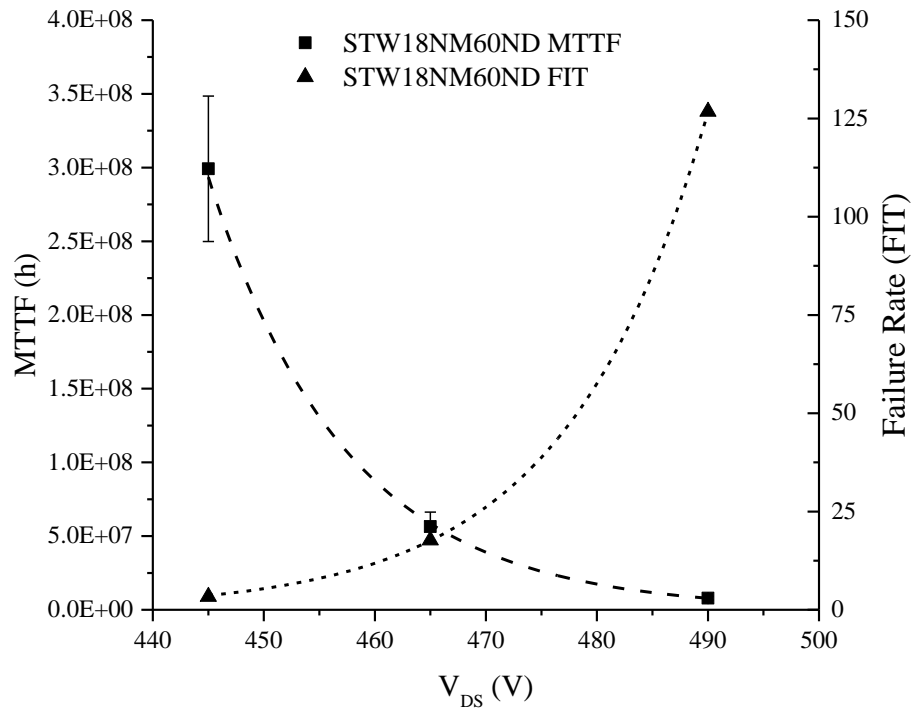


Figure 4.13: Failure parameters trend for a STW18NM60ND power MOSFET.

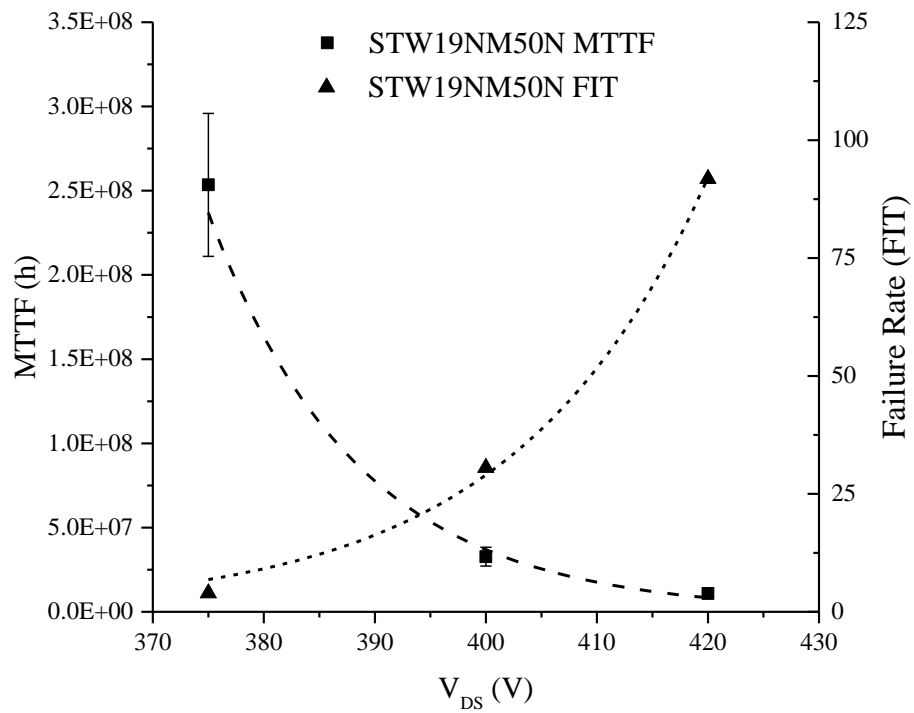


Figure 4.14: Failure parameters trend for a STW19NM50N power MOSFET.

Bibliography

- [1] C. Cazzaniga e C. D. Frost, «Progress of the Scientific Commissioning of a fast neutron beamline for Chip Irradiation», *Journal of Physics: Conference Series*, vol. 1021, pag. 012037, mag. 2018.
 - [2] C. Cazzaniga, C. D. Frost, T. Minniti, E. Schooneveld, E. P. Cippo, M. Tardocchi, M. Rebai, G. Gorini, «Characterization of the high-energy neutron beam of the PRISMA beamline using a diamond detector», *Journal of Instrumentation*, vol. 11, n. 7, pagg. P07012–P07012, lug. 2016.
 - [3] C. Cazzaniga, Simon P. Platt and Christopher D. Frost, “Preliminary Results of ChipIr, a new Atmospheric-like Neutron Beamline for the Irradiation of Microelectronics”, proceeding of the SELSE-13: “The 13th Workshop on Silicon Errors in Logic – System Effects”, 21-22 March 2017, Northeastern University, Boston, Massachusetts (USA).
 - [4] C. D. Frost, S. Ansell, e G. Gorini, «A new dedicated neutron facility for accelerated SEE testing at the ISIS facility», in *Reliability Physics Symposium, 2009 IEEE International*, 2009, pagg. 952–955.
 - [5] G. Consentino et al., «Dangerous effects induced on power MOSFETs by terrestrial neutrons: A theoretical study and an empirical approach based on accelerated experimental analysis», in *AEIT Annual Conference*, 2013, 2013, pagg. 1–6.
-

Chapter 5 – Neutron irradiation facilities

Parallel with the investigation on the effects that neutron irradiation induces in power MOSFET devices, the design and characterisation of neutron irradiation facilities for electronic device testing have been conducted.

The aim of these activities has been the development of instruments that could be used in the research on the neutron-induced effects on electronic devices.

Nowadays three primary sources can be employed for industrial applications that require neutrons: nuclear reactors, radioisotopes, and accelerator-based neutron sources.

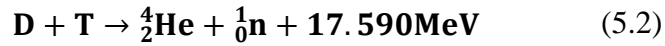
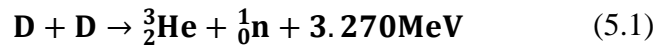
Nuclear reactors are clearly the largest and most prolific sources of neutrons. Radioisotope neutron sources are used in a myriad of industrial applications, including thickness gauging and petroleum exploration, and they are ideal for fixed installations that run continuously. Particle accelerators are the third source of neutrons for industry. These systems vary in size and diversity, and they include large installations such as the Spallation Neutron Source, photoneutron sources or compact neutron generators.

The development of new instrumentations, that can be used parallel with the recognised tools for neutron testing, represents a valid contribution in the field of neutron applications.

This chapter summarises the design and characterisation of neutron irradiation facilities carried out in collaboration with the University of Palermo, the University of Messina and INFN - South National Laboratory.

5.1 D-D Neutron Generator for accelerated test on power devices

Among the various light-ion accelerators, compact devices designed as hermetic, sealed tubes that use deuterium–deuterium (D–D) and deuterium–tritium (D–T) reactions have found the most widespread use in industry:



These accelerators generate neutrons of ~ 2.5 and ~ 14.1 MeV, respectively. The most common ion source used in neutron generators is a cold-cathode, or Penning ion source, which is a derivative of the Penning trap used in Penning ion gauges [2].

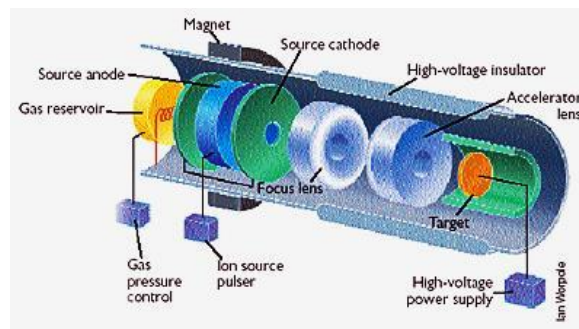


Figure 5.1: Figure shows the schematic design of a sealed-tube neutron generator with a Penning ion source.

In collaboration with the Department of Physics of the University of Messina, the shielding of a compact neutron source based on the deuterium-deuterium reaction has been designed. The source is a ThermoScientific MP 320 a very lightweight portable neutron generator. It can be used in different applications like explosive or weapon detection or drug detection. It is possible to operate with either a Deuterium-Tritium (DT) or a Deuterium-Deuterium (DD) neutron tube, simply changing the target inside the neutron tube. In “DT mode” the source generates a neutron yield of 1.0×10^8 n/s with energy of ~ 14.1 MeV. In “DD mode” will be generated a neutron yield of 2.0×10^6 n/s with energy of ~ 2.5 MeV. The neutron generator can be modulated varying the pulse rate from 250 Hz to 20 kHz, varying respectively from 5% to 100% the duty factor [1].

For indoor application, such as research activities, the neutron generator needs the realization of a specific bunker necessary to avoid damage from radiation exposition for users and instrumentation.



Figure 5.2: In figure the ThermoScientific MP 320 Neutron Generator.

For the calculation of the shielding the following methods have been used: *Method of Removal Cross Section* and *Monte Carlo Method simulations*.

The *Method of Removal Cross Section* takes into account the ability of materials to "remove" the neutrons of different energies from the primary beam. The interactions that slow neutrons down and cause their eventual removal from a beam are probabilistic: they either occur or they do not. Consequently, a flux of neutrons of intensity I will be diminished in a thickness x of absorber proportionally to the intensity of the neutron source and the neutron removal coefficient Σ_{nr} , of the absorbing material:

$$-\frac{dI}{dx} = \Sigma_{nr}I \quad (5.3)$$

which has the solution

$$I(x) = I_0 e^{-\Sigma_{nr}x} \quad (5.4)$$

where I_0 is the initial intensity and $I(x)$ refers to those neutrons that penetrate a distance x in the absorber without a collision; therefore, $e^{-\Sigma_{nr}x}$ represents the probability that a given neutron travels a distance x without an interaction.

Conceptually, Σ_{nr} can be thought of as the probability per unit path length that a neutron will undergo an interaction as it moves through an absorber and be removed from the beam either by absorption or scattering. Then, in this context, it very much resembles the attenuation coefficient for photons in “good (or narrow-beam) geometry,” and it can be similarly developed and used for neutron shielding and dosimetry [6].

Monte Carlo Method simulations obtain answers by simulating individual particles and by recording some aspects (tallies) of their average behaviour. The particles tally values in the physical system is then inferred from the average behaviour of the simulated particles. Monte Carlo can be used to duplicate theoretically a statistical process (such as the interaction of nuclear particles with materials) and it is particularly useful for complex problems that cannot be modelled by computer codes that use deterministic methods [14].

For the design of the Neutron Generator MP320 shielding, has been considered the D-D source configuration with a maximum neutron energy of 2.45 MeV and a neutron yield of 2×10^6 neutron s^{-1} .

The method of Removal Cross Section has been used in order to perform a preliminary evaluation of the shielding thicknesses. Then, MCNP Monte Carlo simulations have been performed with the aims to verify preliminary data and to preliminary characterise the neutron spectrum. The removal cross sections for different materials are available in several handbooks for shielding dimensioning. Some materials used in neutron shielding and their Σ_r are reported below.

Table 5.1: Removal cross section for some shielding materials

Material	ρ [g cm ⁻³]	Σ_r [cm ⁻¹]
Borated Silicone [3]	1.59	0.1007
30% Borated PE [3]	1.19	0.1191
Iron [7]	7.86	0.168
Lead [7]	11.35	0.116
Barite Concrete [4]	3.491	0.0945

In order to optimise the shielding size, both from the point of view of the “weight” and cost, have been select materials that offer a good shielding power (high Σ_r).

The shielding has been designed with successive layers of different materials (lead, iron, hydrogenated materials).

The neutron generator can be assimilated to a "point source", therefore the neutron flux spatial attenuation has been considered, obtaining the following attenuation law

$$\phi = \frac{\varphi_0 e^{-\Sigma_r \cdot t}}{4\pi d^2} \quad (5.5)$$

Where φ_0 is the initial neutron yield ($n \text{ s}^{-1}$), d is the distance at which neutron flux is calculated respect to the source position, ϕ is the neutron flux at distance d from the source and t is the thickness of shielding material.

With the aim to reduce the neutron flux up to make the dose rate lower than the project limit, the shielding should consist in 15 cm of Borated PE (30% of boron) and 15 of Barite Concrete. The interest of using borated PE is due to the boron high capture cross section for thermal neutron. Therefore, the use of Borated PE allows to reduce considerably the shielding thickness. Furthermore, Barite Concrete, with its higher average atomic weight with respect to common concrete, represent a good shielding both for high energy neutrons and for γ rays generated inside the shielding due to the neutron interactions.

A preliminary design of the shielding has been developed in order to evaluate the geometry and, therefore, the parameter d in the attenuation law. The shielding has a window for the samples irradiation in the lower part of the shielding.

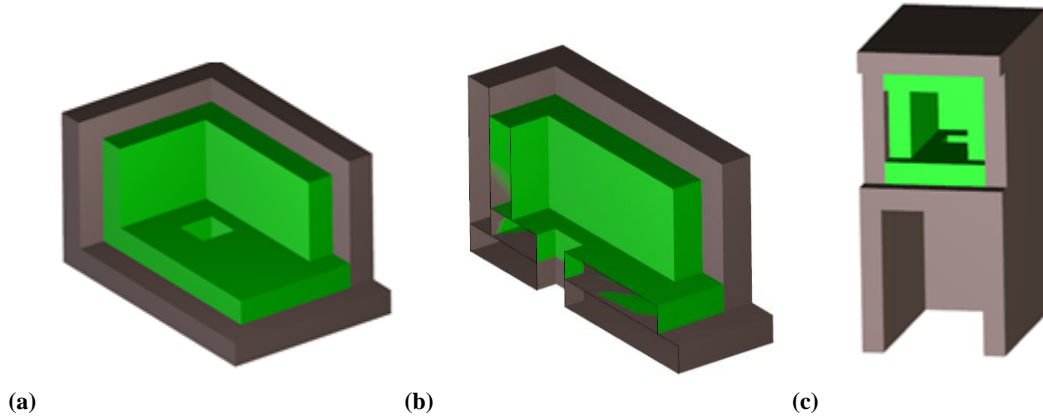


Figure 5.3: Figures represent the shielding thicknesses (a), the shielding section view (b) and the shielding whole structure (c); green is the 30% Borated PE, while grey is the Barite Concrete.

Table 5.2: Neutron flux attenuation due to the different materials

Shielding								
Material	Up		Lateral		Back		Front	
	t [cm]	ϕ [n cm ⁻² s ⁻¹]	t [cm]	ϕ [n cm ⁻² s ⁻¹]	t [cm]	ϕ [n cm ⁻² s ⁻¹]	t [cm]	ϕ [n cm ⁻² s ⁻¹]
Air	33	146.15	15	397.89	23	300.86	57	48.99
30% Borated PE	15	11.57	15	21.77	15	18.47	30	0.59
Barite Concrete	15	1.63	15	2.59	15	2.30	0	0.59

After the preliminary evaluation of the shielding attenuation capability, several simulations have been performed in order to verify the values obtained with the application of removal cross section. The shielding geometry and materials have been translated in MCNP and the neutron source features have been defined. The neutron flux evaluation cells have been specified. For neutron flux evaluation has been chosen the Track Length Estimate of Cell Flux (F4), that allows to obtain the average neutron flux in a volume V , as described in following formulation.

$$\overline{\phi}_V = \frac{1}{V} \int dE \int dV \int ds N(\vec{r}, E, t) \quad (5.6)$$

Where $N(\vec{r}, E, t)$ is the density of particles, regardless of their trajectories, at a point [14].

Simulations have been performed considering the “life” of $2 \cdot 10^9$ neutrons and the obtained values have been handled in order to obtain the value of the mean neutron flux.

Table 5.3: Summary of neutron flux values obtained via Monte Carlo simulation.

Energy [MeV]	Shielding			
	Up ϕ [n cm ⁻² s ⁻¹]	Lateral ϕ [n cm ⁻² s ⁻¹]	Back ϕ [n cm ⁻² s ⁻¹]	Front ϕ [n cm ⁻² s ⁻¹]
2.45	0.349	0.103	0.252	0.009
Total	3.75	1.61	2.63	0.145

The values obtained with simulations and with the method of removal cross section have resulted similar, showing also how the method of removal cross section could be used in the preliminary evaluation of shielding thickness for high energy neutrons.

Then, the neutron dose rate outside the shielding has been evaluated, taken into account as references for the dose rate limits evaluation the project equivalent Dose of 0.5 [mSv/y] and 1200 annual duty hours.

Taking into account these parameters, the reference value for the dose rate is equal to

$$\frac{0.5 \left[\frac{\text{mSv}}{\text{y}} \right]}{1,200 \left[\frac{\text{h}}{\text{y}} \right]} = 4.2 \cdot 10^{-4} \left[\frac{\text{mSv}}{\text{h}} \right] \quad (5.7)$$

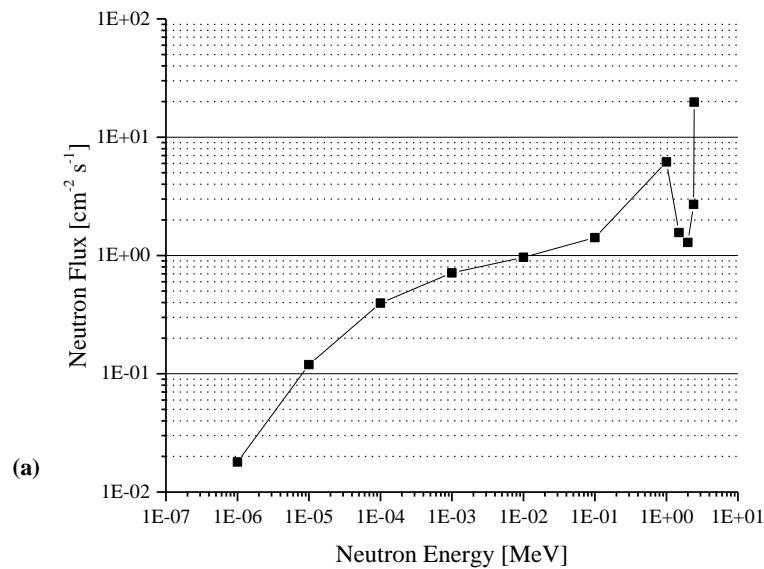
The dose rate has been evaluated applying the flow-to-dose rate energy-dependent conversion factors [5; 8]. The obtained values of neutron dose rate are over the limit of $4.2 \cdot 10^{-4} [\text{mSv}/\text{h}]$, however, taking into account the geometric attenuation it is possible to evaluate that the neutron dose rate goes down rapidly below the limit. Therefore, it is possible to define a restricted zone outside of which the neutron dose rate is surely below the limit considered.

For a complete evaluation of the dose rate it should be necessary to evaluate the contribution of γ -rays to the dose rate and then, to take this contribution into account in the design of the gamma shielding.

Table 5.4: Neutron dose rate values outside the shielding

	Shielding			
	Up	Lateral	Back	Front
Equivalent Dose Rate [mSv/h]	1.51×10^{-3}	2.81×10^{-2}	4.0×10^{-2}	1.62×10^{-2}
Equivalent Dose Rate @ 0.1 m from the shielding [mSv/h]	1.20×10^{-8}	2.23×10^{-7}	3.18×10^{-7}	1.29×10^{-7}

However, the shielding or other structural materials cause the modification of the energy spectrum of a neutron source and, hence, “seen” by the exposed samples. Therefore, several simulations have been performed to preliminary characterise the neutron spectrum in correspondence to the “window” for samples irradiation. The simulations were performed both for the D-D mode and D-T mode in order to evaluate the effect of shielding on the two different energy neutron beams.



Following the International Standards guidelines, LNS Tandem accelerator in Catania has been selected with the aim to design a quasi-monoenergetic neutron beam to perform tests on electronic devices and to study devices reliability under neutron irradiation.

The quasi-monoenergetic neutron source is based on ${}^7\text{Li}(p,n){}^7\text{Be}$ reaction [9]. In the preliminary design of the neutron source the use of a 24 MeV protons beam generated with the Tandem accelerator has been taken into consideration. Preliminary evaluations of the neutron yield have been performed taking into consideration the literature and performing numerical simulations. In order to verify the forecasted data experimental procedures have been planned and it has been chosen to use a siloxane organic scintillator used as neutron counter [13].

A lithium target has been designed to be made with 1 mm lithium layer, a 0.5 mm iron backing and a 1 mm lead layer with the function of protons absorber.

The experiment has been carried out with accelerated protons extracted in air in 80° beamline of Tandem LNS. The protons beam has been set to 24 MeV energy and 3.6 nA current and it has been employed to irradiate the lithium target, that has been arranged at 12.5 cm to the beam extraction window. The Li-Fe-Pb target has been fixed on an aluminum frame by means of two Plexiglas supports. The frame was placed in protons beam line on a mobile support plane that allows the alignment with the protons beam.

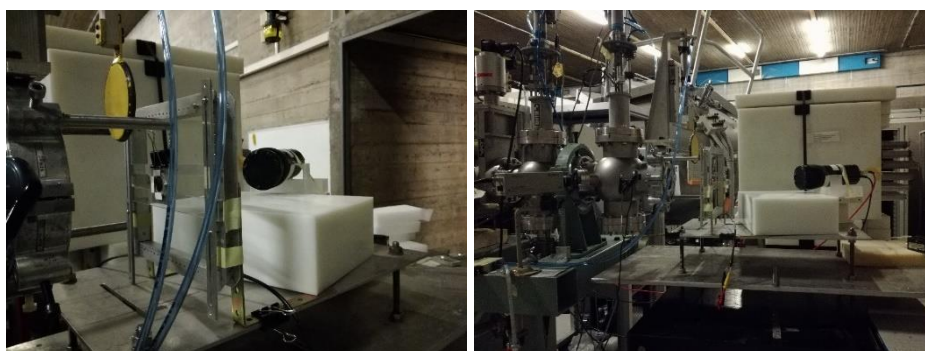


Figure 5.5: Figure shows the experimental setup with Li target and siloxane organic scintillator positioned at 26° with respect to the protons beam line; yellow disk is the beam stopper.

A beam stopper, made up of a thick lead disk and driven by an actuator, has been arranged in correspondence of the beam extraction window in order to stop immediately the protons beam.

The siloxane organic scintillator was placed on the mobile support plane at 26° with respect to the protons beamline and at 30 cm to the target position.

Neutron measurement has been performed with siloxane scintillator inserting progressively lead bricks with different thickness between the target and the neutron counter, in order to evaluate the neutron beam attenuation. Therefore, measurements have been performed with 0.8 cm, 5 cm, 5.8 cm, 10 cm, 12.5 cm, 15 cm of lead thicknesses.



Figure 5.6: Figures shows experimental setup with lead bricks placed between the target and the neutron counter.

Numerical evaluation has been performed with MCNP code to reproduce the experimental setup. Simulations have been run according to different experimental configurations in which the lead thickness was progressively increased. The neutron attenuation due to lead bricks has been evaluated.

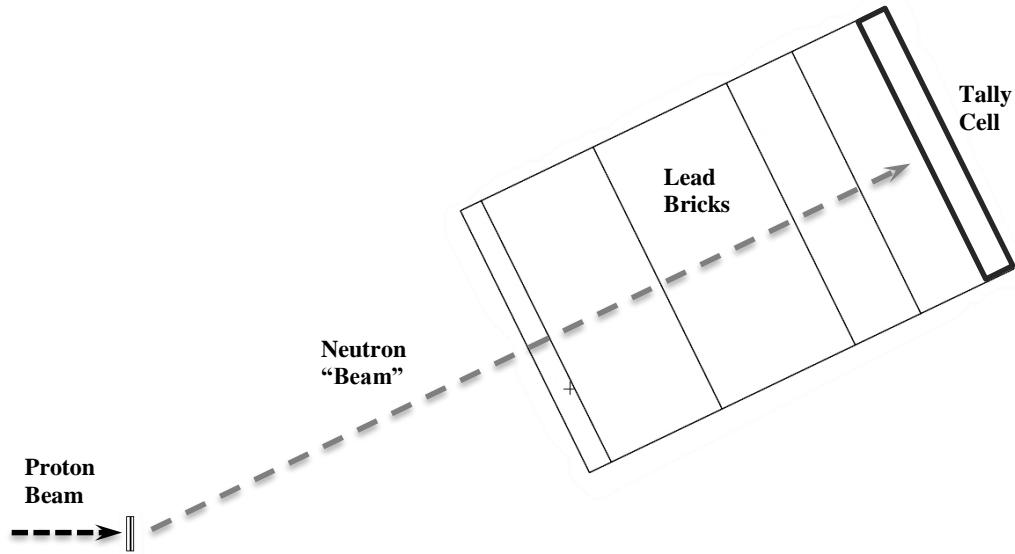


Figure 5.7: Figure represents the MCNP preliminary model of the experimental setup.

Starting from the experimental data the lead neutron attenuation coefficient, also known as removal cross section has been evaluated, taking into consideration the following formula

$$\dot{\Phi} = \dot{\Phi}_0 e^{-\Sigma_r t} \quad (5.8)$$

where $\dot{\Phi}_0$ is the primary neutron flux, Σ_r is the removal neutron cross section, t is the lead thickness and $\dot{\Phi}$ is the neutron flux beyond the lead thickness. This equation, as mentioned before in this chapter, is valid for neutron with energy above 2 MeV. Taking into consideration the emission spectra for different proton incident energies supplied by literature [9], it is possible to use the formula to describe the neutron attenuation due to the interaction with lead bricks. Data from siloxane scintillator have been normalised with respect to the integrate proton current and then data have been handled to evaluate the removal cross section.

Neutron attenuation data has been fitted by an exponential function according to the follow relationship:

$$y = A \cdot e^{-Bx} \quad (5.9)$$

where B is the neutron attenuation coefficient (Σ_{rem}) that results 0.103 cm^{-1} , that taking into consideration that no information were available about the real neutron spectrum, represents a not bad results compared with the lead removal cross section supplied by the literature that is 0.116 cm^{-1} [4]. Therefore, numerical simulations have been carried out in order to evaluate the neutrons attenuation in function of the energy range and lead thickness.

Data have been plotted and the fitting curve have been used to obtain the neutron attenuation coefficient (Σ_{rem}), taking into consideration the following formula

$$\text{Tally} = A \cdot e^{-Bx} \quad (5.10)$$

$$B = \Sigma_{rem} \quad (5.11)$$

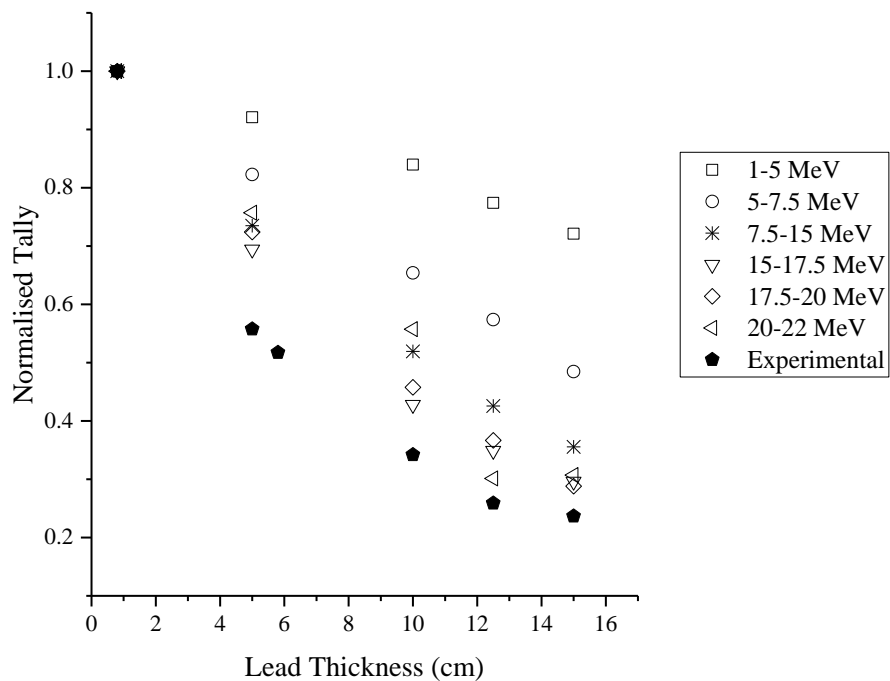


Figure 5.8: In figure is summarised the neutrons attenuation profile in function of lead thickness for different energy ranges.

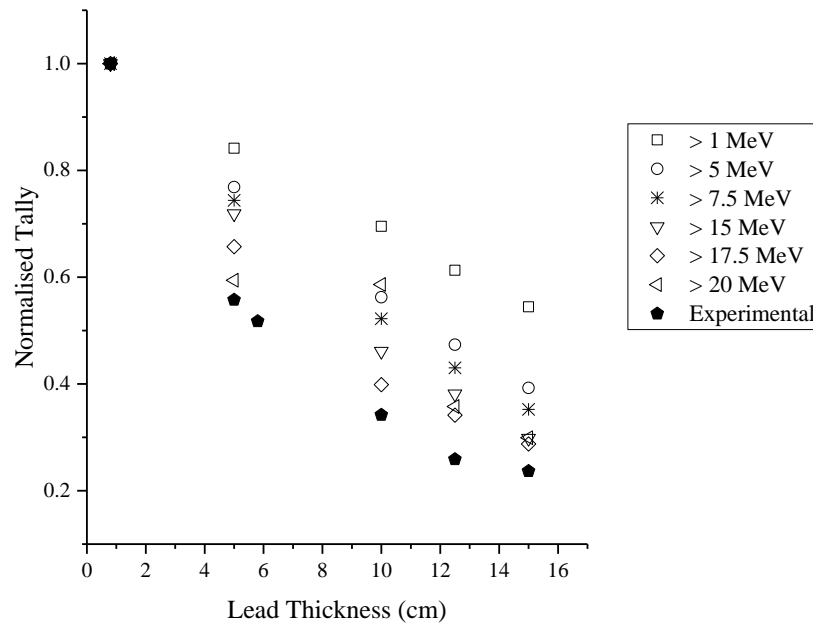


Figure 5.9: In figure is summarised the neutrons attenuation profile in function of lead thickness for different energy threshold.

The comparison shows a good agreement between the preliminary MCNP model and experimental data. The attenuation coefficients, evaluated for different energy ranges and for different energy thresholds, have been compared with the experimental values, showing the best agreement in the energy range 17.5 – 20 MeV).

Table 5.5: Summary of neutron attenuation coefficients from MCNP simulations.

Neutron Energy Attenuation Coefficient		Neutron Energy Threshold Attenuation Coefficient	
1-5 MeV	0.02375	E > 1 MeV	0.0416
5-7.5 MeV	0.04894	E > 5 MeV	0.06422
7.5-15 MeV	0.07013	E > 7.5 MeV	0.07199
15-17.5 MeV	0.08261	E > 15 MeV	0.08324
17.5-20 MeV	0.09421	E > 17.5 MeV	0.09073
20-22 MeV	0.07931	E > 20 MeV	0.07931
Experimental Attenuation Coefficient [cm⁻¹]		0.103	

This experiment has been the first attempt to develop a quasi-monoenergetic neutron beam based on ${}^7\text{Li}(p,n){}^7\text{Be}$. In the second phase of the experiment the neutron beam should be characterised as suggested in International Standards for power devices testing. The neutron beam characterisation should be performed using different neutron detectors with the aim to obtain information on neutron flux, angular distribution and energy spectrum [10-12].

A second proposal has been developed in order to perform the neutron beam spectrum characterisation with different neutron detectors with the aim to obtain information on neutron flux, angular distribution and energy spectrum. The proposal has been submitted for a second call for experiment but it has not been accepted.

Bibliography

- [1] M.T. Caccamo, S. Magazù, F. Migliardo, «Elemental Analysis by Portable Neutron Source», Società Italiana Fisica XCIX Congresso Nazionale - Trieste 2013. p. 199, BOLOGNA: SIF, ISBN: 9788874380817 (2013).
 - [2] L. Chichester, J. D. Simpson, «Compact Accelerator Neutron Generators», The Industrial Physicist, American Institute of Physics, Vol. 9, Issue 6, pp. 22, Dec2003-Jan2004.
 - [3] Y. Elmahroug, B. Tellili, C.Souga, «Calculation of fast neutron removal cross-sections for different shielding materials», International Journal of Physics and Research (IJPR), ISSN 2250-0030, Vol. 3, Issue 2, pp. 11, Table 6, Jun 2013.
 - [4] G.W.C. Kaye, T.H. Laby, «Tables of Physical & Chemical Constants (16th edition 1995)», 4.7.3 Attenuation of fast neutrons: neutron moderation and diffusion, Kaye & Laby Online. Version 1.0 (2005) www.kayelaby.npl.co.uk
 - [5] S.G. Kwon, K. E. Kim, C. W. Ha, P. S. Moon, & C.C. Yook, (1981). «Calculation of Neutron and Gamma-Ray Flux-to-Dose-Rate Conversion Factors», Journal of the Korean Nuclear Society, Vol. 12., No. 3, pp. 173, Table 1, September 1980.
 - [6] J. R. Lamarsh, «Introduction to Nuclear Reactor Theory», Addison-Wesley Publishing Company, pp.17-118-132-152, June 1966.
-

- [7] National Bureau of Standards, «Protection against neutron radiation up to 30 Million electron Volts», Handbook 63, Issue 22, pp. 81, Table 8, 1957.
 - [8] D. C. Ward, «Impact of Switching To The ICRP-74 Neutron Flux-To-Dose Equivalent Rate Conversion Factors At The Sandia National Laboratory Building 818 Neutron Source Range», SAND2009-1144, Appendix G, March 2009.
 - [9] S. G. Mashnik et al., « ${}^7\text{Li}$ (p, n) Nuclear Data Library for Incident Proton Energies to 150 MeV», arXiv preprint nucl-th/0011066, 2000.
 - [10] M. Rebai et al., «Response of a single-crystal diamond detector to fast neutrons», Journal of Instrumentation, vol. 8, n. 10, pag. P10007, 2013.
 - [11] C. Cazzaniga et al., «A diamond based neutron spectrometer for diagnostics of deuterium-tritium fusion plasmas», Review of Scientific Instruments, vol. 85, n. 11, pag. 11E101, 2014.
 - [12] N. P. Zaitseva et al., «Neutron detection with single crystal organic scintillators», in Hard X-Ray, Gamma-Ray, and Neutron Detector Physics XI, 2009, vol. 7449, pag. 744911.
 - [13] Quaranta et al., «Characterization of polysiloxane organic scintillators produced with different phenyl containing blends», Materials Chemistry and Physics, vol. 137, n. 3, 2013, pagg. 951–958.
 - [14] X-5 Monte Carlo Team MCNP, «A General Monte Carlo N-Particle Transport Code, Version 5», LA-UR-03-1987, Volume I, Chapter 1, pp. 2, January 2008.
-

Conclusions

SEEs represent a significant limit in the reliability of systems in which the power devices are employed. Power MOSFETs are widely used in several applications and in the last decades they have had a considerable diffusion in energy converter systems and in renewable applications.

Their recognised sensitivity to the neutron effects represents an important issue for the systems in which power MOSFETs are employed in, due to the reduction of the systems reliability. Despite to the great relevance that the SEEs have, no failure models able to forecast the devices response under neutron irradiation exist. Therefore, the study of the devices behaviour under neutron irradiation becomes fundamental in order to forecast and to mitigate the neutron-induced effects. Due to its great relevance, our interest has been focused on the effects that neutrons induce in power MOSFETs.

We designed the experimental activities taking into consideration the mechanisms of SEEs in power MOSFETs. The knowledge about these mechanisms allowed to correctly address the experimental activities and to focus the interest principally on the correlation between the failure parameters and the devices characteristics. Meanwhile, the standards for neutron testing of electronic devices have been taken as basis and support to design the experimental apparatus and to define the testing procedures.

The first objective of the experimental campaign has been the evaluation of the SEEs thresholds for several power MOSFETs in correlation with their breakdown voltage. The second objective has been the calculation of the devices failure parameters (MTTF, FIT, λ) with respect to the operating conditions.

The experimental campaign has been developed at ChipIr Neutron Irradiation facility, STFC-ISIS (UK), where a neutron beam with atmospheric like neutron spectrum has been used to irradiate the devices, following the suggestions of the JESD89A standard. The experimental apparatus has been developed in order to reach the fixed objectives, following the procedures suggested in JEP151 standard.

First of all, the testing apparatus has been arranged and preliminary tests have been performed to check the apparatus and to consolidate the procedures. Then, the experiments have been performed. In order to evaluate the SEEs thresholds, 6 types of power MOSFETs with different features have been tested. 24 devices for each type have been irradiated with growing V_{DS} until to reach the failure of all the devices in the sample. The V_{DS} has been monitored during the test in order to identify the failure of each tested device. Data obtained during the tests confirmed the SEEs threshold behaviour and underlined the relationship between the device threshold and its characteristics. In particular, data have shown that the SEEs threshold grows exponentially with the devices breakdown voltage $V_{(BR)DSS}$. As a consequence, devices with higher $V_{(BR)DSS}$ result to be more sensitive to the neutron irradiation.

Thus, the failure parameters have been studied performing destructive tests on 4 types of power MOSFETs. Each type has been irradiated at three different V_{DS} , respectively below, in correspondence and above the SEEs threshold previously evaluated for each device. 24 devices for each V_{DS} have been irradiated until to obtain the failure of each device in the sample. The failure times have been monitored with the experimental apparatus and evaluated taking into consideration the SDD beam monitor as trigger for the beginning of the irradiation. Failure data obtained during the tests have been handled according to the MILITARY HANDBOOK 217 and the failure parameters MTTF, FIT and λ have been evaluated for each device and for each V_{DS} . Failure parameters result to be dependent on V_{DS} , in particular MTTF decreases exponentially with V_{DS} and, therefore, both FIT and λ increase exponentially with V_{DS} .

The proposed method could represent a valid prevision instrument of the SEEs thresholds for power MOSFET devices with different breakdown characteristics and it allows to identify the other devices features that could influence the behaviour of power MOSFETs under neutron irradiation.

Furthermore, the developed apparatus can be used to correlate the devices responses to different irradiation conditions. For example, it will be possible to evaluate the

SEEs thresholds and the failure parameters dependence with respect to the neutron spectrum. In this case the same procedures could be performed in different facilities, accordingly with the standards, to improve the failure model.

For this reason, our interest in developing, designing and characterising new neutron sources, as showed in the last chapter. The development of new neutron sources has an important role in the diffusion of neutron testing and investigation techniques. These neutron sources, more compact with respect to nuclear reactors or spallation facilities could represent a useful starting point for several investigations and experimental activities and, furthermore, a good instrument to compare the material or devices responses under different irradiation conditions.

Anyway, this thesis represents the end of my academic adventure and of my research activity. I decided to change my perspective, after two really difficult years, during which I lost my PhD supervisor due to a brain cancer, and in which I had to carry out my research activity alone, without a guide, and without any help from people from my PhD course.

Therefore, I decided to interrupt my research activity. I think I will never more try to start again to perform research activity but I want to conclude my PhD, with the aim to close definitely this chapter of my life and to take a new road and a new project.
